EcoSal Plus
Cellular and Molecular Biology of
E. coli, Salmonella, and the *Enterobacteriaceae*

DOMAIN 8 PATHOGENESIS

Pathogenesis of *Proteus mirabilis* Infection

CHELSIE E. ARMBRUSTER,[1,2] HARRY L. T. MOBLEY,[1] AND MELANIE M. PEARSON[1]

[1]Department of Microbiology and Immunology, University of Michigan Medical School, Ann Arbor, MI 48109

[2]Department of Microbiology and Immunology, Jacobs School of Medicine and Biomedical Sciences, State University of New York at Buffalo, Buffalo, NY 14263

ABSTRACT *Proteus mirabilis*, a Gram-negative rod-shaped bacterium most noted for its swarming motility and urease activity, frequently causes catheter-associated urinary tract infections (CAUTIs) that are often polymicrobial. These infections may be accompanied by urolithiasis, the development of bladder or kidney stones due to alkalinization of urine from urease-catalyzed urea hydrolysis. Adherence of the bacterium to epithelial and catheter surfaces is mediated by 17 different fimbriae, most notably MR/P fimbriae. Repressors of motility are often encoded by these fimbrial operons. Motility is mediated by flagella encoded on a single contiguous 54-kb chromosomal sequence. On agar plates, *P. mirabilis* undergoes a morphological conversion to a filamentous swarmer cell expressing hundreds of flagella. When swarms from different strains meet, a line of demarcation, a "Dienes line," develops due to the killing action of each strain's type VI secretion system. During infection, histological damage is caused by cytotoxins including hemolysin and a variety of proteases, some autotransported. The pathogenesis of infection, including assessment of individual genes or global screens for virulence or fitness factors has been assessed in murine models of ascending urinary tract infections or CAUTIs using both single-species and polymicrobial models. Global gene expression studies performed in culture and in the murine model have revealed the unique metabolism of this bacterium. Vaccines, using MR/P fimbria and its adhesin, MrpH, have been shown to be efficacious in the murine model. A comprehensive review of factors associated with urinary tract infection is presented, encompassing both historical perspectives and current advances.

Received: 29 September 2017
Accepted: 21 November 2017
Posted: 08 February 2018
Editor: Michael S. Donnenberg, Virginia Commonwealth University School of Medicine, Richmond, VA
Citation: EcoSal Plus 2018; doi:10.1128/ecosalplus.ESP-0009-2017.
Correspondence: Melanie M. Pearson, mpears@med.umich.edu

doi:10.1128/ecosalplus.ESP-0009-2017

INTRODUCTION

Proteus mirabilis, a Gram-negative rod-shaped bacterium, is well-known for its urease production and distinctive ability to differentiate into elongated swarm cells and characteristic bull's-eye pattern of motility on agar plates. *P. mirabilis* belongs to the class *Gammaproteobacteria*, and has long been recognized as a member of the order *Enterobacteriales*, family *Enterobacteriaceae*. However, one group recently created a reconstructed phylogenetic tree based on shared core proteins, ribosomal proteins, and four multilocus sequence analysis proteins, and has proposed that the order *Enterobacteriales* be reclassified, placing *Proteus* within a new *Morganellaceae* family (1).

P. mirabilis can be found in a wide variety of environments, including soil, water sources, and sewage, but it is predominantly a commensal of the gastrointestinal tracts of humans and animals (2, 3). While the bacterium is capable of causing a variety of human infections, including those of wounds, the eye, the gastrointestinal tract, and the urinary tract, it is most noted for infections of the catheterized urinary tract, known as catheter-associated urinary tract infections (CAUTI) (4–9). These infections are common in long-term catheterized patients, such as those who reside in nursing homes and chronic care facilities, and may be of particular danger to spinal cord injury patients (10). Urinary tract infections (UTIs) and CAUTIs involving *P. mirabilis* are typically complicated by the formation of bladder and kidney stones (urolithiasis) and permanent renal damage (11–13), and may progress to bacteremia and sepsis (14, 15). Indeed, CAUTI is the most common source of bacteremia in nursing homes, bacteremia involving *P. mirabilis* most frequently occurs following UTI or CAUTI compared to other sources of infection, and bacteremia and sepsis due to *P. mirabilis* carry a high mortality rate (14–17). CAUTIs are also often polymicrobial (8, 17), and *P. mirabilis* is one of the most common organisms present during polymicrobial urine colonization and infection (4, 9) (Table 1).

P. mirabilis is an agent of catheter biofilm formation, quickly fouling the surface of a newly inserted urinary catheter. Surface organelles such as fimbriae and other adhesins appear to play a significant role in this process. The enzyme urease also contributes dramatically to this process. Urea, our means of eliminating excess nitrogen, is present in high concentrations in urine (~400 mM), is the substrate of urease, and is hydrolyzed to CO_2 and NH_3. The liberated ammonia raises the pH of the urine and initiates the precipitation of otherwise soluble polyvalent anions and cations present in urine. The result is urolithiasis, the formation of struvite ($MgNH_3PO_4$) or apatite ($CaPO_4$) stones. These crystals can form on and within the lumen of catheters, blocking urine flow and necessitating catheter removal and replacement. Stones

Table 1 Epidemiology of single-species and dual-species clinically diagnosed catheter-associated urinary tract infection in nursing home residents

		Single species		Dual species	
Microorganism	**Total urine cultures[a]**	**Urine cultures[b]**	**%[c]**	**Urine cultures[d]**	**%[e]**
Proteus mirabilis	48	28	22	20	35
Enterococcus spp.	38	15	12	23	40
Escherichia coli	37	23	18	14	25
Pseudomonas aeruginosa	34	18	14	16	28
Staphylococcus aureus	20	11	9	9	16
Klebsiella pneumoniae	14	6	5	8	14
Citrobacter spp.	9	3	2	6	11
Morganella morganii	7	2	2	5	9
Providencia stuartii	7	3	2	4	7
Yeast	6	3	2	3	5
Acinetobacter baumannii	4	2	2	2	3
Enterobacter spp.	5	5	4	0	0
Serratia marcescens	1	1	1	0	0
Corynebacterium spp.	1	1	1	0	0
Other	8	4	3	4	7
Total	182	125	100	57	100

[a]Number of urine cultures containing each microorganism.
[b]Number of single-species urine cultures containing each microorganism.
[c]Percent of all single-species cultures represented by each microorganism.
[d]Number of dual-species urine cultures containing each microorganism.
[e]Percent of all dual-species cultures represented by each microorganism.
Reproduced, with permission, from reference 9.

may also form in the renal tubules or renal pelvis, causing inflammation and often requiring surgical removal. This bacterium is capable of invading bladder epithelial cells, and produces a variety of cytotoxins that damage the epithelium, leading to significant histopathology.

Over the past four decades, our laboratory and others have developed a variety of approaches to study the virulence of *P. mirabilis*. Importantly, two primary models of ascending urinary tract infections have been developed in mice, in which organisms are transurethrally delivered to the bladder and bacteria can be enumerated in the urine, bladder, and kidneys following a suitable interval, depending on the experimental question asked. One model requires no manipulation of the murine host, yet it still represents a model of complicated urinary tract infection for *P. mirabilis* as urolithiasis quickly occurs, offering a substrate for bacterial colonization and sometimes blockage of proper urine flow along with significant pathology. In a more recent modification of this model, a small silicone catheter segment is introduced into the bladder, providing an immediate substrate for bacterial colonization. This latter model may more closely reflect the catheterized urinary tract and CAUTI in humans. It has also been demonstrated as an excellent model for polymicrobial bacteriuria, a common feature of CAUTI.

The advent of straightforward genome sequencing and comparative genomics studies has provided a view of the heterogeneity of the species, and has allowed for a more global understanding of metabolic pathways, regulatory schemes, and virulence determinants present in the bacterium. The importance of individual genes and operons must be addressed experimentally. Nevertheless, sequencing information allows for the generation of testable hypotheses. This information has also opened the door for transcriptomic studies, both under *in vitro* conditions and during experimental infection. While not as facile as in other genera, allelic exchange methods for specific gene mutation may be routinely conducted in *P. mirabilis* strains. In addition, genome-wide transposon mutagenesis is also straightforward and has facilitated a variety of screens, including signature-tagged mutagenesis (STM) and transposon insertion-site sequencing (Tn-Seq).

Clearly, *P. mirabilis* possesses an impressive arsenal of virulence factors (Fig. 1). Urease is a critical feature of this species, but the bacterium also expresses a startling number of fimbriae and other adhesins. The most well-studied fimbria is the mannose-resistant *Proteus*-like (MR/P) fimbria, whose expression is phase variable. The *mrp* operon also encodes a nonstructural protein, MrpJ, which directly represses flagella synthesis, thus shutting down motility while the bacterium adheres, and flagella themselves contribute to pathogenesis. As well, a variety of potent toxins and proteases compound virulence. Similar to other members of the *Enterobacteriaceae*, *P. mirabilis* carries numerous secretion systems, including types I, III, IV, V, and VI. To provide cofactors and regulate intracellular metabolism, *P. mirabilis* also carries a myriad of ion importers and exporters. Last, the bacterium carries an integrative and conjugative element named ICE*Pm1* that can self-replicate and self-transfer to other strains and species, transferring virulence genes and antibiotic resistance.

There are no currently licensed vaccines available for this organism, and multidrug-resistant isolates are becoming increasingly common. Thus, efforts to generate effective vaccines or therapeutic treatments are warranted. The majority of experimental vaccine studies have targeted *P. mirabilis* fimbriae, and successes have been described in the murine model for the MR/P fimbriae themselves, as well as the tip adhesin of the fimbria, MrpH. However, none of the experimental vaccines have provided complete protection against infection, and additional targets remain to be explored.

In this review, we will focus on the current state of knowledge regarding how this fascinating bacterium is capable of infecting the urinary tract and causing disease. We will summarize studies that have made a clear connection between specific genes, gene clusters, and operons and their role in pathogenesis. While there is an enormous literature on the fascinating phenotype of swarming motility, this has been extensively summarized elsewhere (3, 18–20). We will therefore address only those studies that relate to flagellum-mediated motility and virulence in the murine model.

HOST INTERACTIONS

The Catheterized Urinary Tract

Numerous bacteria colonize the periurethral area, but are generally prevented from establishing an infection of the urinary tract by the regular flushing of the urethra during micturition (the passing of urine). Urothelial cells lining the bladder also provide a barrier against bacterial

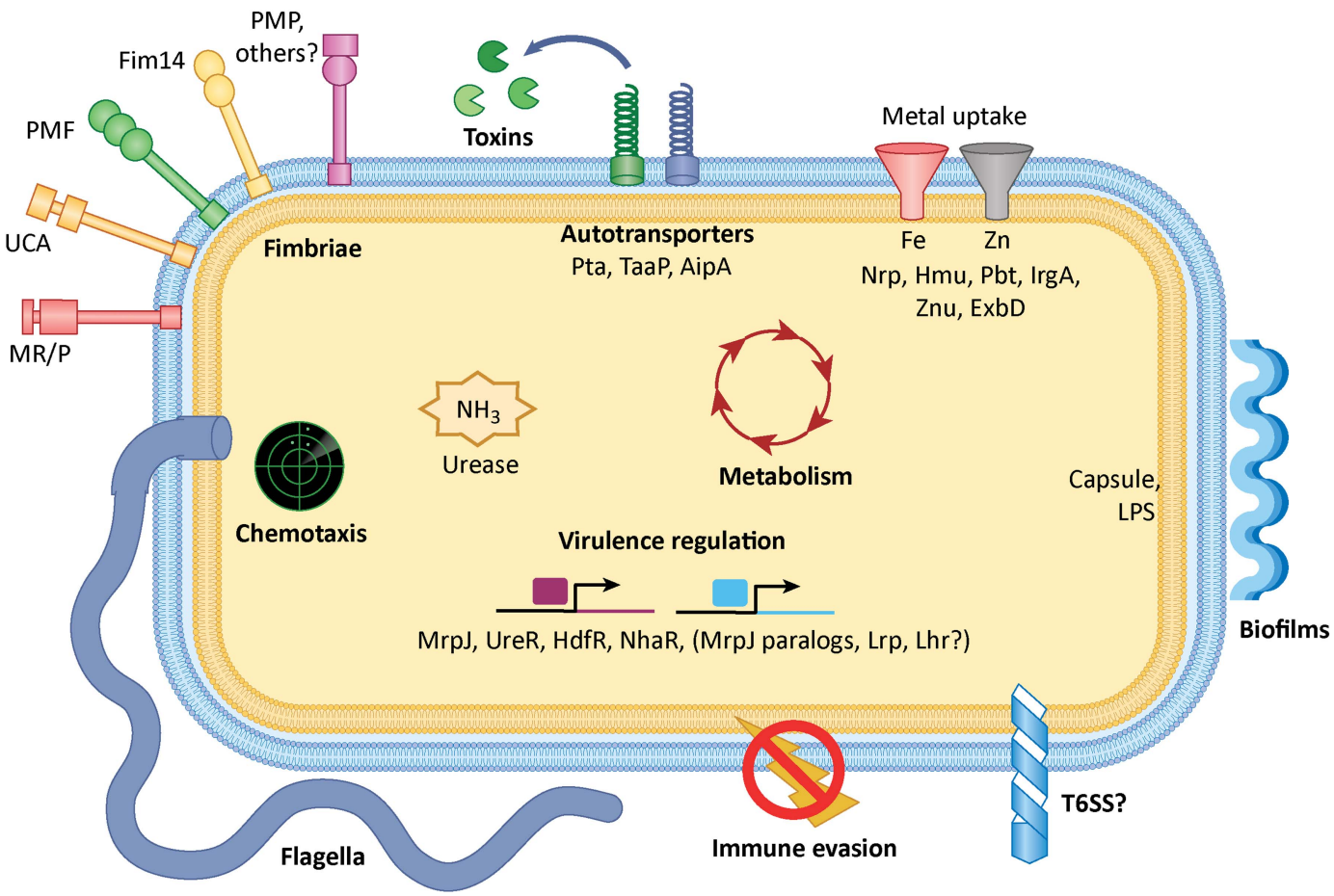

Figure 1 Concepts of *Proteus mirabilis* pathogenesis during urinary tract infection (UTI). Adherence: binding catheters, host tissues, and neighboring bacteria may all contribute to disease. Adherence is mediated by chaperone-usher fimbriae and autotransporter adhesins. Urease: involved in stones, crystalline biofilms, and possibly nutrition or host sensing. Motility: *P. mirabilis* swarms across catheters and may ascend to the kidneys using swimming motility. Both forms of motion are mediated by flagella. Chemotaxis proteins allow the bacteria to follow chemical gradients. Metabolism: likely permits establishment of a nutritional niche, competition with other species, and response to host cues. Metal scavenging: iron and zinc uptake are essential for growth, but are sequestered by the host; therefore, specialized proteins are required for bacteria to scavenge these metals. Toxins: proteins such as HpmA and Pta may aid in nutrient accessibility, immune evasion, or provision of surfaces to colonize. Biofilm formation: Crystalline biofilms readily form on catheters, and bacterial clusters in the bladder may be a biofilm-mediated process. Immune evasion: this can include antibody and antimicrobial peptide degradation, polymyxin resistance, lipopolysaccharide (LPS) variation, and physical obstruction of phagocytosis. Virulence regulation: required to coordinate all steps of infection. Type 6 secretion system (T6SS): involved in self-recognition; unknown role during UTI. MrpJ-controlled systems in this figure are bolded. Figure adapted, with permission, from reference 20.

adhesion and invasion, partly due to a coating of glycosaminoglycan mucin as well as their role in the innate immune response.

When an indwelling urinary catheter is inserted, it bypasses many of the natural host defenses against urinary tract infection. In contrast to normal micturition and flushing of the urethra at regular intervals, the catheter allows for continuous bladder drainage as urine accumulates, which is not of sufficient volume or force to effectively flush the urinary tract. The design of the traditional Foley catheter and draining tubing also causes retention of 10 to 100 ml of urine within the bladder, providing a reservoir for bacteria to replicate (21). The urothelium is only 3 to 4 cell layers thick, and is easily damaged during rushed or multiple attempts to place a catheter (22). Any rough surfaces on the catheter can also facilitate bacterial biofilm formation or cause damage to the urethral lining and bleeding during insertion or withdrawal. Furthermore, improper insertion of the catheter or inflation of the balloon can create mucosal and submucosal tears (22). All these potential complications of catheter insertion provide *P. mirabilis* with additional sites of attachment, nutrients, and routes for establishing more severe

infection. The presence of an indwelling urinary catheter also elicits a robust inflammatory response, both in humans and in experimental animal models, and the resulting accumulation of fibrinogen on the catheter surface can provide bacteria with an ideal substrate for attachment (23–25).

Approximately 50% of individuals with long-term catheterization (>28 days) experience catheter blockage from crystalline deposits, and the urease activity of *P. mirabilis* is the most common cause of this blockage (5, 26, 27) (*see* **Urease** section) (Fig. 2). Urease catalyzes the hydrolysis of urea to ammonia and carbon dioxide, thereby raising urinary pH. As urine pH increases, calcium and magnesium phosphates begin to precipitate out of solution, leading to the formation of struvite (magnesium ammonium phosphate) and apatite (calcium phosphate) crystals (11, 28). The urinary pH at which precipitation occurs is referred to as the nucleation pH (pH_n), and if the pH of voided urine (pH_v) falls within the range of the pH_n (common during colonization with urease-positive organisms), crystallization and catheter blockage are likely to occur (29).

The struvite and apatite crystals that form during *P. mirabilis* colonization deposit on the catheter surface, facilitating the formation of crystalline biofilms (*see* **Biofilms** section). Indeed, it has been experimentally determined that *P. mirabilis* typically begins establishing crystalline biofilms on a urine-bathed catheter when urinary pH reaches pH_n (30). Adherence to the catheter and the formation of crystalline biofilms provide protection from the action of host cells recruited to the site of infection, particularly neutrophils. Crystalline biofilms formed by *P. mirabilis* can also result in blockage of the catheter lumen, which obstructs urine flow and may cause reflux of infected urine to the kidneys (31, 32). The lifestyle of *P. mirabilis* within the catheterized urinary tract is depicted in Fig. 3.

Urolithiasis

The urease of *P. mirabilis* is unambiguously associated with the development of infection-induced stone formation, known as urolithiasis (5, 11, 33–36) (Fig. 4). Indeed, *Proteus* species have been isolated in 70% of cases of bacteria-induced stone formation (37). The cytoplasmic enzyme urease catalyzes the hydrolysis of urea, the nitrogenous waste product of mammals, which is maintained normally at 400 to 500 mM in human urine. Ammonia, generated from the breakdown of urea, results in a dramatic elevation of the pH of urine, and normally

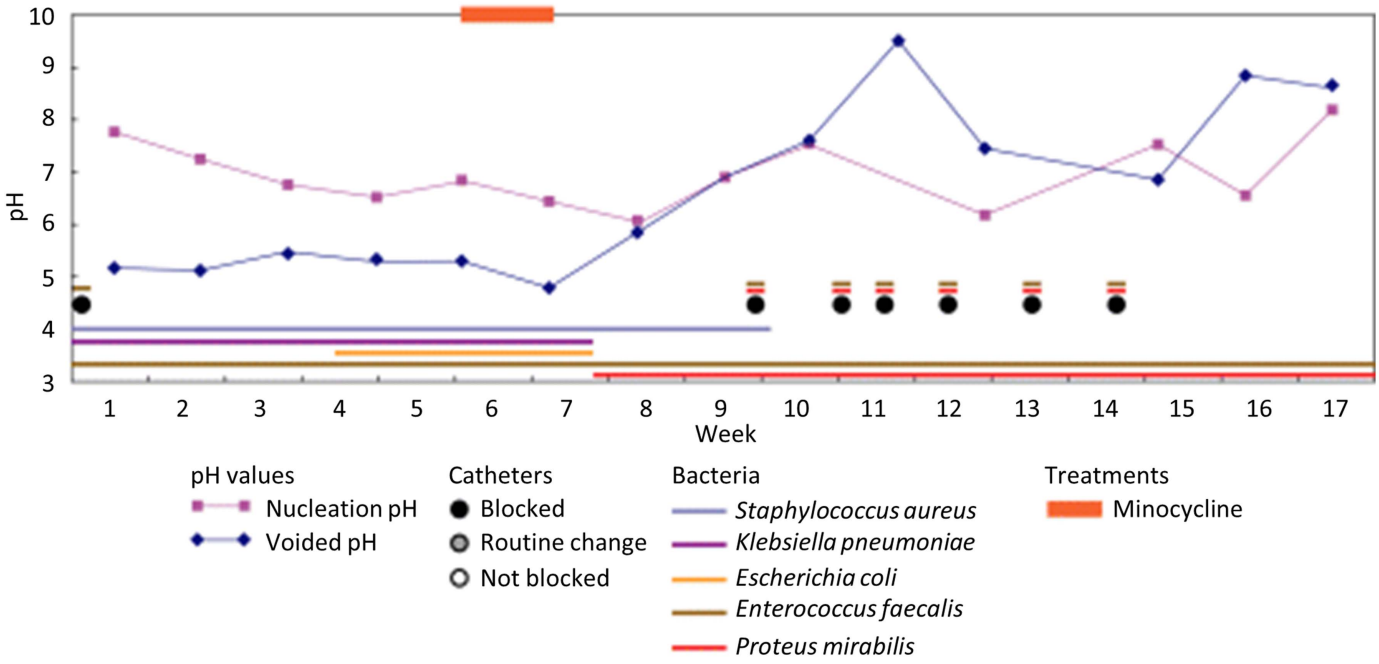

Figure 2 Treatments, nucleation pH, voided pH, catheter changes, and bacterial isolates in a patient undergoing long-term urinary catheterization. Colonization occurred with multiple species, but *P. mirabilis* colonization specifically led to an increase in urinary pH and repeated catheter blockage. Figure adapted, with permission, from reference 344.

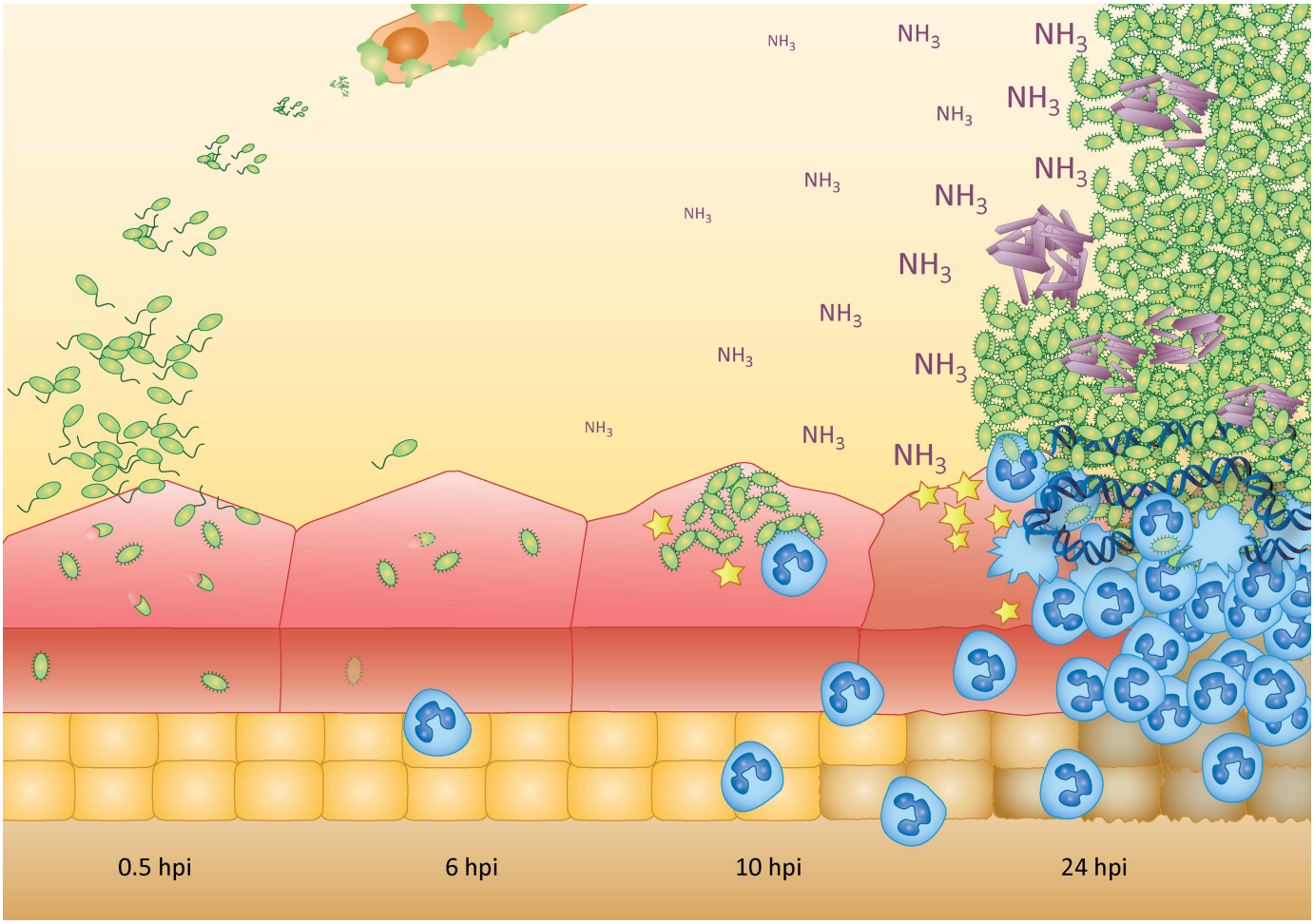

Figure 3 Lifestyle of *Proteus mirabilis*. *P. mirabilis* bacteria (green) form crystalline biofilms on the surface of catheters (Top). Once inside the bladder (0.5–6 h postinfection [hpi]), this organism can invade urothelial cells of the bladder. As early as 10 to 24 hpi, *P. mirabilis* forms intraluminal clusters that can extend the length of the bladder and are associated with urothelial cell destruction (perhaps through the production of toxins [yellow stars] or an increase in urine pH) and mineral deposition (purple rods). Host innate immune cells such as neutrophils (blue) are recruited to the site of infection and can form NETs (neutrophil extracellular traps). Figure adapted, with permission, from reference 20.

soluble polyvalent anions and cations precipitate at high pH to form struvite ($MgNH_4PO_4{\cdot}6H_2O$) and carbonate apatite [$Ca_{10}(PO_4)_6{\cdot}CO_3$]. *In vitro* studies inoculating urine with *P. mirabilis* demonstrated that increasing the concentration of Mg^{2+}, Ca^{2+}, or PO_4^{3-} ions intensified the magnitude of crystallization (38).

Experimental evidence for the involvement of urease in *P. mirabilis* pathogenicity was provided by infection of mice via transurethral inoculation into the bladder (39, 40). Separate groups of mice were inoculated with the wild-type strain or a urease-negative mutant of *P. mirabilis*, and struvite stones were found in the renal pelvis of mice infected with the wild-type strain one week after inoculation. Quantitatively, 12 of 39 mice (31%) developed stones after 1 week and 8 of 20 mice (40%) developed stones after 2 weeks, while no stones were found in the 38 mice infected with the urease-negative mutant. A caveat to the study was that the urease-negative mutant did not colonize the mouse urinary tract to the same extent as the wild-type strain. However, follow-up studies with higher inocula of the urease-negative mutant construct still failed to result in development of urolithiasis.

Because *P. mirabilis* is often part of a polymicrobial infection, the impact of polymicrobial colonization on urease activity and urolithiasis in a murine CAUTI model has been examined for coinfection of *P. mirabilis* and its common CAUTI partner *Providencia stuartii* (25, 41). Coinfection resulted in bacterial loads that were similar to monoinfections with either pathogen. However, there was a significantly increased incidence of urolithiasis and bac-

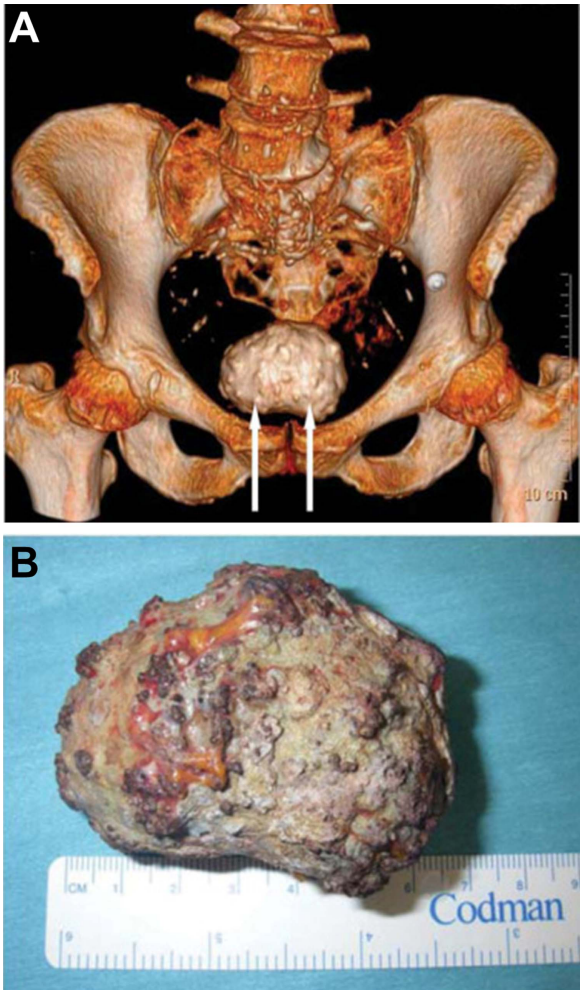

Figure 4 A particularly large urolith. (A) Reconstructed computed tomography image, showing the location and relative size of the urate cystolith (indicated by arrows). (B) Photograph of the urate cystolith, showing its absolute size. Reproduced from reference 345 with permission.

teremia during coinfection. Coinfection was also accompanied by a significant increase in urease activity that was manifested in a synergistic manner (*see* **Urease** section).

Adding to the mechanism of stone formation, it has been noted that green fluorescent protein (GFP)-expressing *P. mirabilis* could be observed within the matrix of urinary stones in mice experimentally infected with *P. mirabilis* (12). Genome sequences of *P. mirabilis* have also been detected in urinary calculi by PCR (42). Furthermore, Schaffer and colleagues (43) found, using confocal microscopy, that *P. mirabilis* formed extracellular clusters in the bladder lumen that served as the basis for focused mineral deposition, consistent with nascent stone formation (Fig. 5).

Internalization, Cytotoxicity, and Histopathology

The ability of *P. mirabilis* to invade and lyse host cells has been explored for decades, and has been demonstrated to contribute to infection progression and severity of disease in animal models. The level of host cell invasion and cytotoxicity achieved by *P. mirabilis in vitro* varies dramatically by the bacterial strain being tested, growth phase, and morphology of the bacteria (for instance, log phase growth versus stationary phase and vegetative cells versus differentiated swarm cells), host cell line, multiplicity of infection, pH of the medium, and the duration of the experiment. Similarly, pathological changes in the bladder and kidneys of infected animals vary to some extent based on the bacterial strain, inoculating dose, and infection model. However, *P. mirabilis* has been demonstrated to be more invasive than *Salmonella enterica* serovar Typhimurium (Table 2) (44). Although not an exhaustive list, the invasion and cytotoxic properties of various *P. mirabilis* isolates are summarized in Table 3.

While it is clear that *P. mirabilis* invades host tissues during infection, it does not appear to establish a significant intracellular niche as observed for uropathogenic *Escherichia coli* (43). Several virulence factors have been implicated in contributing to cell invasion and cytotoxicity *in vitro*, as well as histopathological changes *in vivo*. For instance, flagella contribute to invasion in part by allowing the bacterial cells to come into close proximity to the host cells, and mutants lacking flagella are unable to invade cells unless centrifuged directly onto the host cell monolayer (44, 45). The specifics of *P. mirabilis* invasion of bladder and kidney cells and the contributions of select virulence factors are detailed further below.

Bladder invasion and histopathology

Internalization of *P. mirabilis* by bladder epithelial cells has been directly demonstrated *in vitro* using a hemolysin (*hpmA*) mutant to avoid confounding from the effects of the cytolytic toxin. In these experiments, it was determined that *P. mirabilis* utilizes the AipA autotransporter for internalization into bladder cells (46). In addition to internalization, *P. mirabilis* is capable of lysing bladder epithelial cells using a combination of the *Proteus* toxic agglutinin (Pta) and hemolysin (47).

In the murine model of ascending UTI, *P. mirabilis* invades bladder epithelial cells as early as 30 min postinoculation, which may provide transient protection

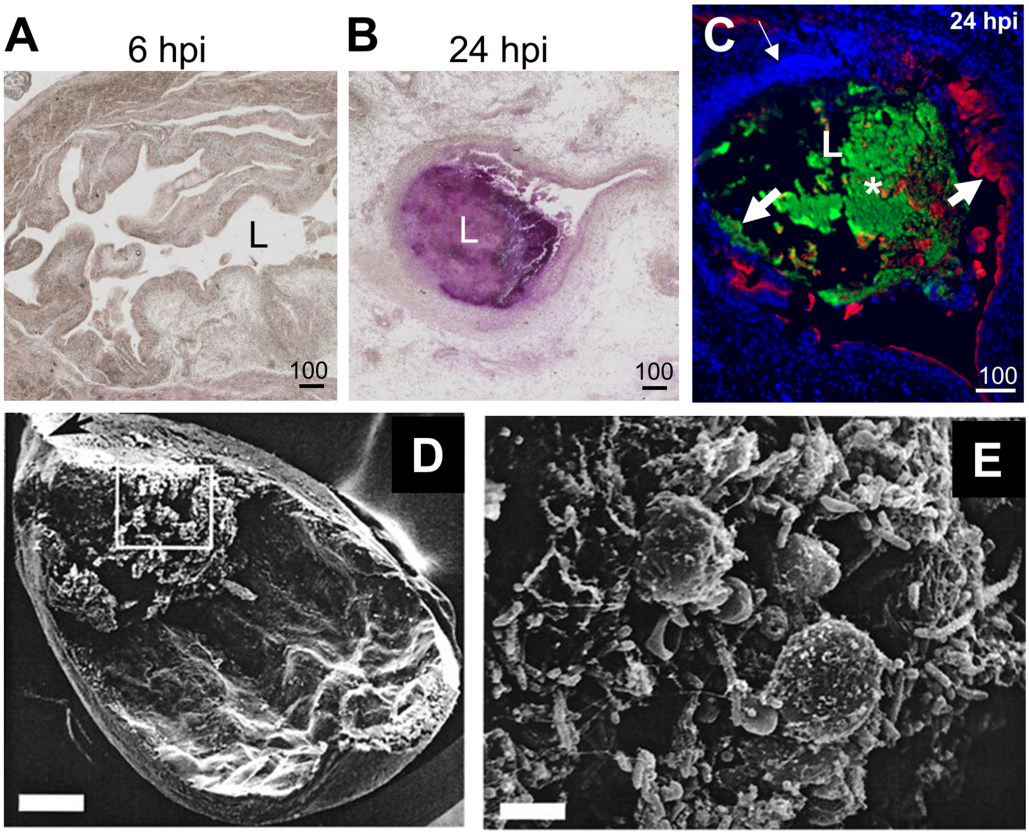

Figure 5 ***P. mirabilis*** **extracellular clusters are precursors to stone formation.** (A and B) Detection of mineral deposition using Alizarin Red staining of *P. mirabilis*-infected bladder sections at 6 (A) and 24 hpi (B) (scale bars, 100 μm). L, bladder lumen; purple staining indicates extracellular cluster. (C) A representative image of a *P. mirabilis* cluster at 24 hpi (scale bar, 100 μm). Staining of bacteria (green), UPIIIa (red), and DNA (blue) shows accumulation of bacterial clusters at the bacteria-bladder interface. An asterisk indicates an extracellular cluster; L, bladder lumen. The thin arrow indicates a region with increased 4′,6-diamidino-2-phenylindole (DAPI) signal, whereas thick arrows indicate areas of extensive urothelial damage. (D and E) Scanning electron micrographs of *P. mirabilis* urease-induced bladder stone (7 dpi). (D) One-quarter of the bladder viewed at a low magnification (bar, 500 μm). The orientation of the bladder is indicated by an arrow pointing to the inferior end of the bladder (the end leading to the urethra). (E) Higher magnification (bar, 5 μm) of the area enclosed in a box in panel D. Figure adapted, with permission, from reference 43 (A–C) and reference 12 (D and E).

from the immune response and an intracellular niche for initial replication and survival (43, 45, 48–51). However, intracellular bacteria are uncommonly observed at later times postinoculation, and *P. mirabilis* appears to instead form large, extracellular clusters within the bladder lumen and adjacent to the urothelium after this initial invasion phase rather than establishing the intracellular communities that are characteristic of uropathogenic *E. coli* (43) (Fig. 6). Formation of these clusters requires urease activity and the mannose-resistant *Proteus*-like (MR/P) fimbriae, and provides protection from infiltrating neutrophils (43).

Bladder colonization by *P. mirabilis* most often results in mild to moderate cystitis in murine models of UTI, including transmural neutrophilic inflammation, epithelial transcytosis of neutrophils, and submucosal edema (25, 47). The pathology of *P. mirabilis* bladder colonization during ascending UTI is largely due to a combination of urease activity, Pta, and hemolysin (25, 47). In the murine model of CAUTI, infection with *P. mirabilis*

Table 2 Internalization of *P. mirabilis* strains by cultured human renal epithelial cells

Strain	Growth condition	Internalized bacteria (CFU/ml)[a]
P. mirabilis WPM111	Broth; aerated; 18 h	22,420
E. coli HB101	Broth; aerated; 18 h	67
S. Typhimurium	Broth; aerated; 18 h	18,130

Modified from reference 44.
[a]Values are means of three independent determinations.

Table 3 Invasive and cytotoxic properties of human *P. mirabilis* isolates

		Invasion		Cytotoxicity	
Strain source	**Strain name**	**Cell line**	**Ref**	**Cell line**	**Ref**
Catheterized urinary tract	HI4320	Human embryonic kidney (HEK293), monkey kidney (Vero), human urothelial (UMUC-3)	(46)	Human primary renal proximal tubular epithelial cells (HRPTEC), human embryonic kidney (HEK293)	(25, 53)
	BA6163	ND		Human primary renal proximal tubular epithelial cells (HRPTEC), human bladder epithelial (T24), human B-cell lymphoma (Daudi and Raji), human monocyte (U-937), monkey kidney (Vero)	(53, 192)
	CFT295 HU2450 CFT106 SA1387 MI159 EL1131 CFT37 MA2489 DR3282 CFT403	ND		Human primary renal proximal tubular epithelial cells (HRPTEC)	(53)
	C6 C7 C11 C31	Human ureter (Hu 609), and human bladder epithelium (HCV 29)	(349)	ND	
UTI	T1 31	Monkey kidney (Vero)	(51)	Monkey kidney (Vero)	(51)
Urinary stone	PM7002	Human urothelial (UMUC-3)	(350)	ND	
	K8 K608	Human ureter (Hu 609)	(349)	ND	
	U6450	ND		Human urothelial (EJ/28)	(45)
Wound	KR37 KW28	Human ureter (Hu 609) and human bladder epithelium (HCV 29)	349	ND	
Unspecified	N2 P19	Human urothelial (NTUB1)	269, 351	ND	

results in more severe cystitis, and this appears to be largely due to urease activity and encrustation of the catheter (25).

Kidney invasion and histopathology

Infection with *P. mirabilis* tends to result in unique kidney pathology. For instance, *P. mirabilis* is the only species that causes a high incidence of kidney stone formation in a rat model of pyelonephritis (52), and it causes more kidney stones and greater kidney damage than other urease-positive organisms such as *P. stuartii* in murine models of ascending UTI and CAUTI (25, 41). Specifically, kidney colonization by *P. mirabilis* in the ascending model of UTI is most often associated with moderate pyelonephritis, including neutrophilic interstitial nephritis within the peripelvic renal cortex and occasional damage to the surrounding renal parenchyma (25, 47). The severity of pyelonephritis is more strongly influenced by the additive effect of Pta and hemolysin than urease (25, 47). The same is true in the murine model of CAUTI, with *P. mirabilis* infection similarly resulting in moderate pyelonephritis, largely independent of urease activity (25).

In addition to directly damaging kidney tissue and inducing inflammation, *P. mirabilis* proliferates within the tubular epithelium of the kidneys in both mice and rats, resulting in necrosis and nephrosis (25, 52). In contrast to pyelonephritis, the severity of nephrosis correlates with urease activity in the murine models of ascending UTI and CAUTI, indicating a role for the urease enzyme and alkaline pH in renal tubule damage (25). These foci of inflammation can also develop into inflammatory

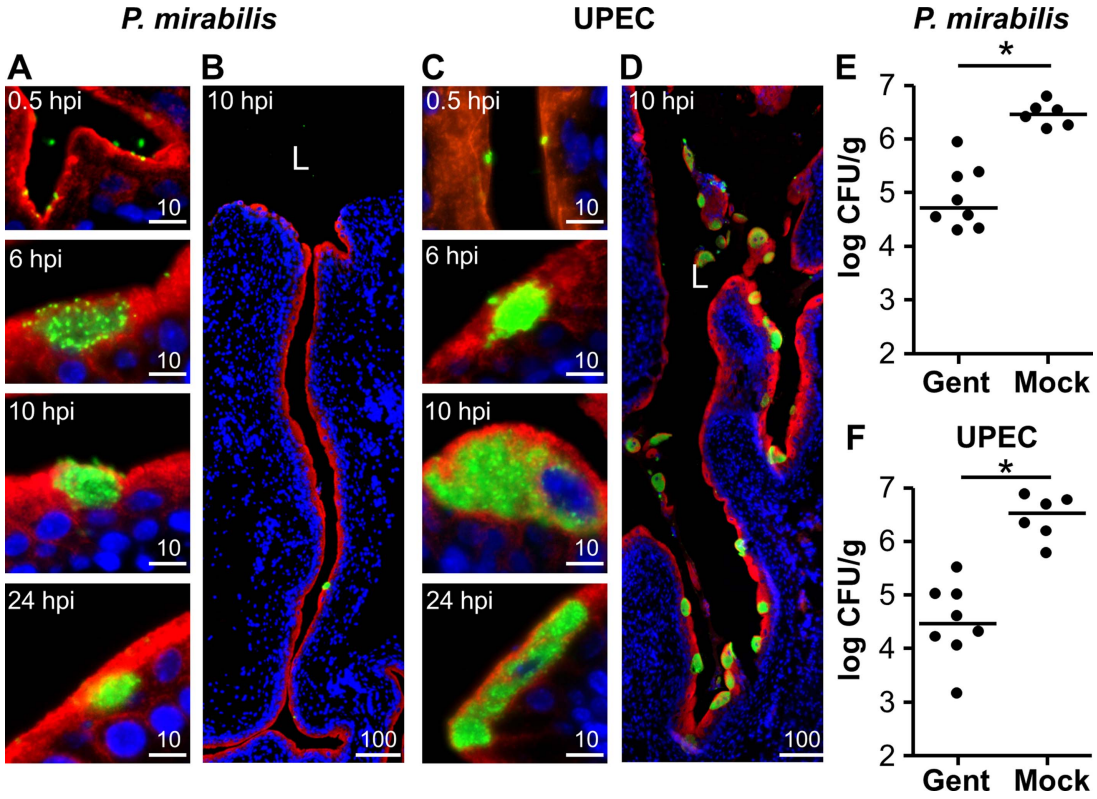

Figure 6 ***P. mirabilis*** **invades the urothelium, but infrequently forms intracellular bacterial communities (IBCs).** (A–D) Representative images of *P. mirabilis* (A and B) and uropathogenic *E. coli* (UPEC) (C and D) attachment and invasion. Bacteria (green), UPIIIa (red), and DNA (blue) show localization of the bacteria relative to the apical surface of the urothelium. Scale bars, 10 μm. (B and D) A regional view of the bladder section containing the 10 hpi IBC shown in A and C, respectively. Scale bars, 100 μm. L, bladder lumen. (E and F) Quantification of *P. mirabilis* (E) and UPEC (F) bladder invasion at 0.5 hpi following either *ex vivo* gentamicin treatment (Gent) or mock treatment (Mock) ($n = 6–8$). *$P < 0.05$. Figure adapted, with permission, from reference 43.

lesions, another characteristic feature of *P. mirabilis* pyelonephritis (25, 47, 52).

Internalization of *P. mirabilis* by human renal proximal tubular epithelial cells (HRPTECs) has also been directly demonstrated *in vitro* using a hemolysin mutant to avoid confounding by the cytotoxic effects of the toxin. Interestingly, internalization requires protein synthesis by *P. mirabilis*, but does not require active phagocytosis or protein synthesis by the HRPTECs (48, 50). Thus, invasion of host cells by *P. mirabilis*, at least *in vitro*, is predominantly mediated by bacterial factors. Hemolysin is also thought to be the primary virulence factor responsible for direct lysis of HRPTECs (48, 53).

Innate Immune Responses to *P. mirabilis* UTI

Although innate immune responses to UTI are an active area of investigation, most of these studies have focused on uropathogenic *E. coli* (UPEC) (54–56). Because there are several key differences between *P. mirabilis* UTI and UPEC UTI, including urolithiasis, bacterial metabolism during UTI, and intracellular versus luminal niches in the bladder, we will focus sharply here on studies that specifically examine *P. mirabilis*. Likewise, adaptive immune responses to vaccines are described elsewhere in this review (*see* **Vaccines** section).

P. mirabilis induces a proinflammatory response during UTI; mice infected with *P. mirabilis* have elevated levels of CXCL1 at 72 h postinfection (hpi) and interleukin-10 (IL-10) at 6 and 96 hpi in their urine (25). Notably, the cytokine response is further elevated during coinfection with *P. stuartii*, with increased levels of CCL2, CCL5, CXCL1, IL-6, IL-10, IL-17A, tumor necrosis factor alpha (TNF-α), beta interferon (IFNβ), and IFNγ at 48 hpi. In contrast, *P. stuartii* monoinfection did not lead to increased levels of any of the measured cytokines (25). Some of the elevated cytokines, such as IL-10, are anti-inflammatory (57), suggesting there are switches between

pro- and anti-inflammatory responses as the infection progresses. This is consistent with changes in innate immune responses observed for other uropathogens, including UPEC and group B streptococcus (54, 56, 58). TNF-α and IL-6 are also elevated in bladder homogenates from mice at 48 hpi (59).

Neutrophils are one of the first innate responses to UTI, and are recruited by host uroepithelial cell signaling in response to conserved bacterial structures (pathogen-associated molecular patterns, or PAMPs) (60). CXCL1, mentioned above, is a potent neutrophil chemoattractant, and leukocytes are frequently detectable in urine during *P. mirabilis* UTI. Appropriately, there have been several studies investigating the interaction of *P. mirabilis* with these leukocytes. By 10 to 24 hpi in the mouse model of UTI, *P. mirabilis* forms large clusters in the bladder lumen that draw a massive infiltration of neutrophils (Fig. 7) (43). Neutrophil extracellular traps (NETs) are webs of decondensed chromatin and antimicrobial proteins that are released in response to infection (61), and neutrophils in regions adjacent to the *P. mirabilis* bacterial clusters have been observed with extruded DNA that colocalized with extracellular H2A, suggesting development of NETs during *P. mirabilis* UTI (43). Supporting the mouse model data, proteomic signatures indicative of

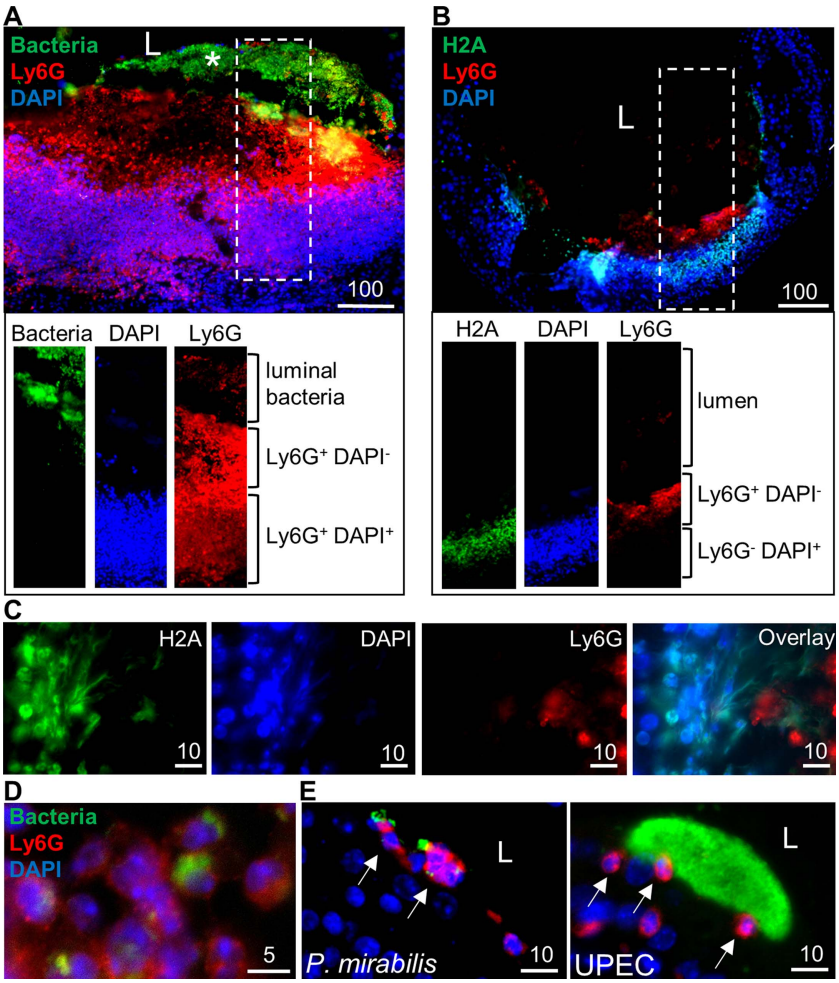

Figure 7 *P. mirabilis* induces neutrophil recruitment and NET formation. (A and B) Visualization of neutrophil recruitment at extracellular clusters at 24 hpi. Individual channels for the region enclosed in the dashed rectangle are shown below at the same magnification. Scale bars, 100 μm. (C) Identification of NET formation in regions of neutrophil recruitment at 24 hpi. Individual channels representing nuclear stains (H2A and DAPI) and membrane stains (Ly6G) show the overlap of DAPI and H2A distant from Ly6G staining. Scale bars, 10 μm. (D) Neutrophil phagocytosis of *P. mirabilis* at 24 hpi. Arrows indicate neutrophils that have phagocytosed bacteria. (E) Individual neutrophil recruitment in sections of murine bladders infected with *P. mirabilis* without clusters at 24 hpi and UPEC-infected sections at 10 hpi. Bacteria (green), Ly6G (red), and DNA (blue) show neutrophils adjacent to bacteria. Arrows indicate intact neutrophils. Figure adapted, with permission, from reference 43.

"NETosis" have been detected in urine samples from patients with *P. mirabilis* UTI (62, 63). Although neutrophil-mediated phagocytosis and NETosis can be effective bacterial clearance mechanisms, this line of attack may be less effective against *P. mirabilis* encased within clusters or urinary stones (12, 43). Neutrophils also respond to bacteremic *P. mirabilis* UTIs, and an increase in band neutrophils (>10% white blood cell count) is associated with an increased risk of *P. mirabilis* bacteremia (odds ratio 4.18) (64).

Inflammasomes are protein complexes that form in response to a variety of stimuli and act to induce inflammation (65). One particular type, the NLRP3 inflammasome, has been specifically linked to *P. mirabilis* in the intestine, where *P. mirabilis* induces a potent IL-1β response (66). In this setting, NLRP3 activation is dependent on HpmA hemolysin-induced K^+ efflux (66). NLRP3 inflammasomes are also activated by crystalline material, and thus urease activity during UTI may further boost a potent inflammatory response (43, 65).

Tamm-Horsfall protein (THP, also called uromodulin) is the most abundant protein in normal human urine (67). Mice deficient in THP are susceptible to UTI (68), and *P. mirabilis* likewise causes more severe infection in THP-deficient mice (69). THP is heavily glycosylated and has been proposed to be a competitive ligand for UCA/NAF fimbriae (*see* **Fimbriae and Adhesins** section) (69).

Flagellin is another conserved structure that is recognized by the innate immune response, specifically toll-like receptor 5 (TLR5) (70), and flagellar motility is a fundamental feature of *P. mirabilis* (*see* **Flagella** section). In the intestine, Lypd8 protein prevents flagellated bacteria, including *P. mirabilis*, from invading colonic epithelium and causing inflammation (71). Installation of purified *P. mirabilis* flagellin into the bladder elicits leukocyte infiltration, histological changes in bladder tissue, and elevated *Cxcl1*, *Cxcl10*, and *Il6* mRNA (72). Interestingly, pretreatment with flagellin did not aid clearance of *P. mirabilis* in a subsequent challenge, and instead led to increased bacterial recovery from the kidneys (72).

Immune evasion

P. mirabilis has several tools for evading the innate immune response. These bacteria readily invade cultured cells (*see* **Internalization, Cytotoxicity, and Histopathology**). However, although invasion has been observed during experimental UTI, *P. mirabilis* is typically found in the bladder lumen (43). It is possible that invasion plays a larger role during pyelonephritis. Urinary stones may also provide shelter from attack by leukocytes or antimicrobial peptides (3, 12, 19, 73). *P. mirabilis* is noted for its general resistance to killing by antimicrobial peptides, particularly polymyxins (74). Two components of this resistance are Zap protease, which degrades antimicrobial peptides (see **Toxins** section), and lipopolysaccharide (LPS) modifications to alter surface charge (75). Notably, different types of *P. mirabilis* LPS O-antigen elicit distinct proinflammatory cytokine IL-8 responses from cultured urothelial and renal cells (76). Furthermore, *P. mirabilis* produces a lysozyme inhibitor named PliC (77). Finally, at least two major antigenic proteins on the bacterial surface, MR/P fimbriae and flagella, are subject to phase variation. Thus, bacteria producing altered flagellins or phase-off MR/P fimbriae may evade both innate and adaptive immune responses.

P. mirabilis as a possible trigger of autoimmunity

Rheumatoid arthritis (RA) is a chronic autoimmune disorder that primarily attacks the joints. There is an intriguing correlation between *P. mirabilis* and RA, suggesting that, in some populations, *P. mirabilis* UTI may be a triggering event for autoantibody development (78). Specifically, amino acid sequences IRRET in UreC (a component of urease) and ESRRAL in HpmB (an accessory protein that allows secretion of HpmA hemolysin) may lead to collagen autoantibodies due to cross-reactivity in individuals with particular HLA-DR4 subtypes. A correlation between *P. mirabilis* and RA has been observed in multiple patient studies (78); however, the urease/hemolysin hypothesis has not yet been directly tested. Importantly, other microbes have also been linked to RA, and it is possible that there are multiple infectious triggers for RA in vulnerable populations (79).

P. mirabilis is also associated with inflammatory bowel disease, which likewise has autoimmune origins. In a TRUC mouse ulcerative colitis model, *P. mirabilis* and *Klebsiella pneumoniae* correlated with colitis (80). Similar to the Lypd8 mice mentioned above, *P. mirabilis* bacteria were observed in the colonic mucus adjacent to epithelial cells in colitic mice, but not in wild-type mice (71, 80). While wild-type mice were negative for *P. mirabilis*, wild-type pups fostered on TRUC dams developed colitis and were positive for *P. mirabilis* and *K. pneumoniae*; furthermore, administration of TRUC-

derived *P. mirabilis* and *K. pneumoniae* strains to specific pathogen-free wild-type mice elicited colitis (80).

APPROACHES TO STUDYING VIRULENCE

Animal Models

The first murine model of UTI was described in 1967 (81), and, while several different experimental methods have been explored for *P. mirabilis* infection studies, the most widely used model for investigating *P. mirabilis* pathogenicity is based on a method developed in the 1980s, referred to as the Hagberg protocol for ascending, unobstructed UTI (82). This protocol was initially developed to study *E. coli* virulence, particularly bacterial attachment to host bladder cells. Female CBA mice were favored as the model organism in this protocol because of several observations: (i) bacteria were better able to attach to uroepithelial cells from mice than rats; (ii) CBA mice exhibited greater susceptibility to colonization and experimental UTI than BALB/c, C57BL/6, or C3H/HeN mice; and (iii) the anatomy of male mice was not permissive for transurethral inoculation directly into the bladder. However, many mouse strains are susceptible to bladder colonization by *P. mirabilis* and ascension to the kidneys. For example, CF-1 mice have been utilized for noninvasive biophotonic imaging studies to monitor bacterial progression from the bladder to the kidneys and response to antibiotic treatment (83) (Fig. 8).

Two overviews of the procedures for induction of urinary tract infection in mice have been published in the *Journal of Visualized Experiments* (JoVE) (84, 85). In brief, 6- to 9-week-old mice are anesthetized and the periurethral and perianal areas are sterilized, in general, with 10% povidone iodine. A 25-mm segment of gas-sterilized polypropylene tubing (0.28 mm inner diameter, 0.61 mm outer diameter) is threaded over a sterile 30-gauge hypodermic needle in such a way that approximately 15 mm of tubing extends beyond the tip of the needle. For transurethral inoculation, approximately 10 mm of the protruding polypropylene tubing is inserted through the urethra, beneath the pelvic bone, so that the bacterial inoculum is instilled directly into the bladder. This is generally performed using a mechanical syringe pump to slowly infuse a 0.05-ml inoculum over a 30-second interval to reduce the likelihood of reflux into the kidneys, so that the bacteria must actively ascend the ureters to colonize the kidneys and establish an upper urinary tract infection.

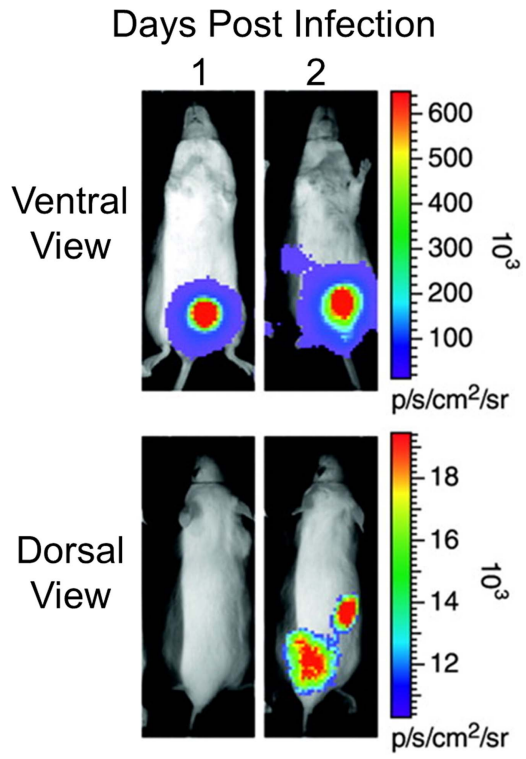

Figure 8 Real-time monitoring of *P. mirabilis* UTI using biophotonic imaging. Mice were inoculated with a *P. mirabilis* strain, Xen 44, engineered to constitutively produce luciferase. A representative animal is shown. Bacteria were initially observed in the bladder (ventral view), with kidney progression visible by day 2 (dorsal view). Figure adapted, with permission, from reference 83.

Initial studies of *P. mirabilis* pathogenesis using the murine model of ascending UTI were conducted using an inoculum of 2×10^{10} CFU/ml (1×10^{9} CFU/mouse) and time points of 2, 7, or 14 days postinoculation (39, 40, 86). For *P. mirabilis* HI4320, inoculation with this high dose resulted in significant mortality in mice at later time points (25% after 7 days, and 35% after 14 days), as well as severe pyelonephritis, renal damage, and urolithiasis (39). Inoculation with a lower dose (2×10^{8} CFU/ml, or 1×10^{7} CFU/mouse) was therefore determined to be ideal for studying the contribution of *P. mirabilis* virulence factors to pathogenicity. The contribution of specific genes to fitness and disease progression are generally assessed by one of two ways: (i) independent challenge, in which one group of mice is inoculated with the wild-type strain and the other is inoculated with the mutant of interest to see if the mutant exhibits significant differences in bacterial burden, or (ii) cochallenge with a 1:1 mixture of mutant to wild-type, where the mutant must compete against the wild-type parent in the same mouse. In a cochallenge, wild-type and mutant bacteria

are distinguished using a marker, such as antibiotic resistance, and a competitive index is calculated for the mutant by dividing the ratio of mutant/wild-type recovered from the mouse to the ratio of mutant/wild-type in the inoculum (Fig. 9).

With respect to catheter-associated UTI, the presence of a catheter segment within the bladder provides bacteria with a new substrate for attachment and colonization and also elicits numerous changes within the bladder environment, including induction of a potent proinflammatory response (25, 83, 87, 88). Thus, as *P. mirabilis* most commonly causes complicated or catheter-associated UTI, several adaptations to the standard ascending model have been utilized to introduce and maintain a foreign body in the bladders of mice. One such method uses 6-mm segments of polyethylene tubing that have been coiled and sterilized with ethanol, precolonized by *P. mirabilis* for biofilm formation, and stretched back to an uncoiled position for transurethral insertion into the bladder, where they will spontaneously recoil to prevent loss of the catheter during normal urination (83). Another method uses a 4-mm segment of silicone catheter tubing, sterilized by autoclaving, and introduced into the bladder at the time of transurethral inoculation (25). Both methods require reducing the bacterial density of the inoculum approximately 100-fold over the ascending UTI model to reduce mortality within 7 days of inoculation, and both models result in a greater incidence of cystitis and pyelonephritis than the ascending model. Furthermore, use of the silicone catheter segment was shown to induce a potent proinflammatory response during mock infection (25, 87), thereby mimicking the host response to catheterization that is observed in humans. Different catheter segment lengths may be required for different mouse strains and ages. However, for CBA/J mice and inoculation with *P. mirabilis* HI4320, rapid encrustation of the catheter promotes retention of the catheter segment in the vast majority of mice (25).

The predominant murine models of UTI and CAUTI rely solely on female mice because of the technical challenges of transurethral inoculation that are posed by the anatomy of male mice. A model of ultrasound-guided percutaneous catheter implantation into the bladder was therefore developed to permit studies of CAUTI in both female and male mice (89). Comparison of percutaneous catheter implantation and transurethral catheter placement revealed that both methods resulted in a similar incidence of catheter encrustation during infection with

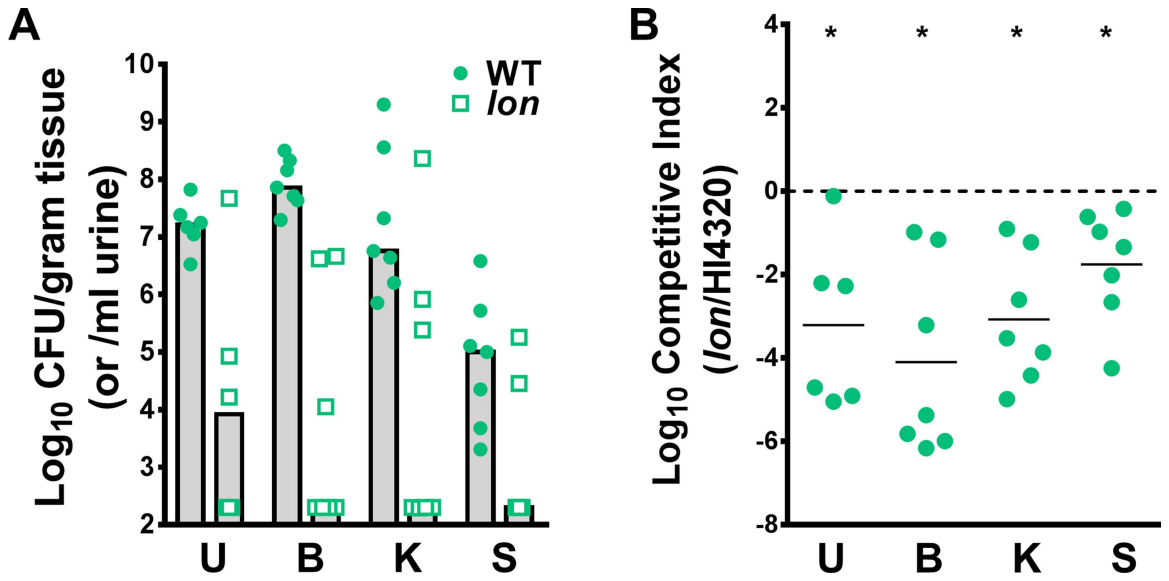

Figure 9 Example of a competitive index (CI) calculated from a cochallenge CAUTI experiment. Mice were challenged with a 1:1 ratio of wild-type *P. mirabilis* HI4320 and a *lon* mutant; a 4mm segment of catheter tubing was retained in the bladder for the duration of the study. *P. mirabilis* was recovered at 4 days postinoculation (dpi). Wild-type and mutant bacteria were distinguished by plating on solid media with or without antibiotic selection. (A) Cochallenge data. Solid circles represent wild-type CFU, and open squares are mutant CFU recovered from each mouse. Bars show median CFU. The limit of detection in this assay is 200 CFU/g tissue. (B) *In vivo* CIs calculated from cochallenge data. Each dot represents the CI from an individual animal in the urine (U), bladder (B), kidneys (K), or spleen (S). Bars indicate the median CI. Significant differences in colonization (*P<0.05) were determined with the Wilcoxon signed-rank test. A CI <1 indicates a fitness defect. Figure adapted, with permission, from reference 124.

P. mirabilis. Thus, while this model may better approximate suprapubic catheterization than urethral catheterization, it will facilitate investigation of CAUTI and testing of catheter coatings in male mice in addition to female mice.

Comparative Genomics

P. mirabilis lives in diverse environments, and has long been noted for strain variability in swarming behavior and LPS O-antigen structure (90–92). Given these observations, it might seem that this species would possess great diversity in its genomic content, much like the mosaic pangenome of *E. coli* (93, 94). However, several lines of evidence point toward a remarkable conservation of the *P. mirabilis* chromosome.

A proteomic comparison of the *P. mirabilis* HI4320 reference strain with three other genomes, AOUC-001, CYPM1, and BB2000, shows that the overwhelming majority of predicted proteins are at least 99% identical across all four strains (Fig. 10A). Furthermore, alignment of the first two fully annotated *P. mirabilis* genomes, HI4320 and BB2000, shows a high degree of synteny with only a few gaps due to insertions or deletions (Fig. 10B). The major differences that are visible are due to the insertion of bacteriophage, a conjugative transposon, and the mobile genetic element ICE*Pm1*, described later.

Virulence factors, such as urease, HpmA hemolysin, and MR/P fimbriae, are detected in the vast majority of strains, regardless of isolation source (95, 96). For example, *hpmA* was found by Southern blot in 63/63 isolates tested, and correlated with hemolytic activity (97); likewise, a survey of 211 isolates using a combination of PCR and dot blot found that all encoded *hpmA* (98). Zap protease is also widespread, including all *P. mirabilis* tested from a diverse O-serogroup collection (99). Similarly, ZapA-associated protease activity was detected in the urine of 16/17 *P. mirabilis*-infected patients (100).

Mannose-resistant hemagglutination is another defining characteristic of *P. mirabilis*, because both activity and the causative *mrp* fimbrial genes are nearly ubiquitous in this species (95, 96, 101). In addition, *P. mirabilis* encodes an abundance of fimbrial operons (*see* **Fimbriae and Adhesins** section) relative to other bacterial species, and the majority of these are conserved across diverse isolates (101) (Fig. 11). The presence of a given fimbrial operon does not correlate with the isolate source. Of the 17 fimbrial operons encoded by *P. mirabilis* HI4320, only one, *fim3*, is detected in fewer than half of *P. mirabilis* isolates. A second operon, *uca*, is notable because it is present in the majority of isolates, but is located on a mobile element and may be found in different regions of the chromosome (101).

Despite the overall conservation of the *P. mirabilis* chromosome, there is variability within the species. A few loci in particular are hypervariable and merit further mention (Fig. 10A).

ICE*Pm1*

Comparative genomic hybridization of *P. stuartii* and *Morganella morganii* with a *P. mirabilis* HI4320 microarray revealed an integrative and conjugative element (ICE) common to all three species (102) (*see* **Integrative and Conjugative Element ICE*Pm1*** section). Further analysis of this 94-kb element, called ICE*Pm1*, revealed genes encoding two previously identified virulence factors: *Proteus* toxic agglutinin (Pta) and Nrp siderophore (103–105). Carried within ICE*Pm1* is the *Yersinia* spp. high-pathogenicity island (HPI), which includes the *nrp* operon. Consistent with a virulence role, ICE*Pm1* is found more often in urinary isolates than colonizing isolates (100% versus 65%) (102). Furthermore, ICE*Pm1* has been observed to transmit between clinical isolates in a laboratory setting (106). Examination of sequenced genomes reveals that ICE*Pm1*, when present, is not always inserted at the same genetic locus.

P. mirabilis strains may encode other conjugative elements, but they do not appear to be as prevalent as ICE*Pm1*. For example, HI4320 encodes another conjugative transposon, named as either ICE*Pmi*USA1 or ICE*Pmi* HI4320, that is a member of the SXT/R391 family of ICEs (107–109). No genes in ICE*Pmi*USA1 have thus far been identified as virulence associated. However, other ICEs in the SXT/R391 family carry multiple antibiotic resistance genes, and some of these ICEs are found in *P. mirabilis* (110–112).

T6SS

Because the type VI secretion system (T6SS) of *P. mirabilis* is involved in strain self-recognition and competition between strains (*see* **Secretion Systems** section), it is not surprising that there is a high degree of variability in these genes. Specifically, the genes encoding the T6SS secretion apparatus are highly conserved, but the secreted effectors vary in sequence, type, and number. For example, *P. mirabilis* HI4320 and BB2000 encode T6SS

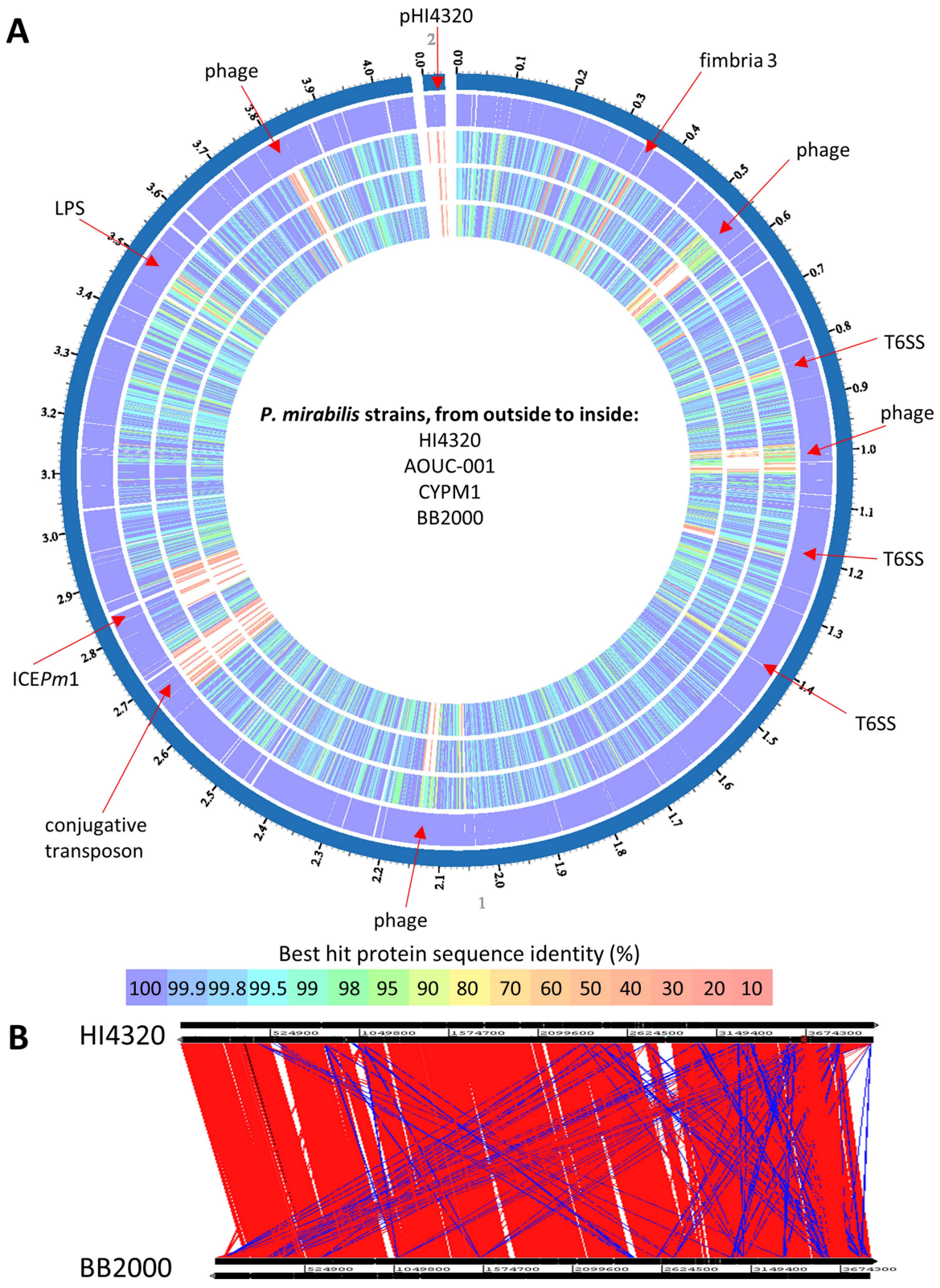

Figure 10 Conservation of *P. mirabilis* sequences. (A) Comparison of proteomes of three *P. mirabilis* strains against the HI4320 type strain using the PATRIC Proteome Comparison service (120). The majority of predicted proteins are ≥99% identical across all four genomes (blue and purple). Notable highly variable proteins (≤70% identical; orange and red) are indicated with arrows. (B) Genome alignment showing synteny (red) between *P. mirabilis* HI4320 and BB2000. The largest gaps are ICE*Pm*1, a conjugative transposon, and phage. Most blue lines indicate highly repetitive transposase genes. Plot generated using the Artemis Comparison Tool (346).

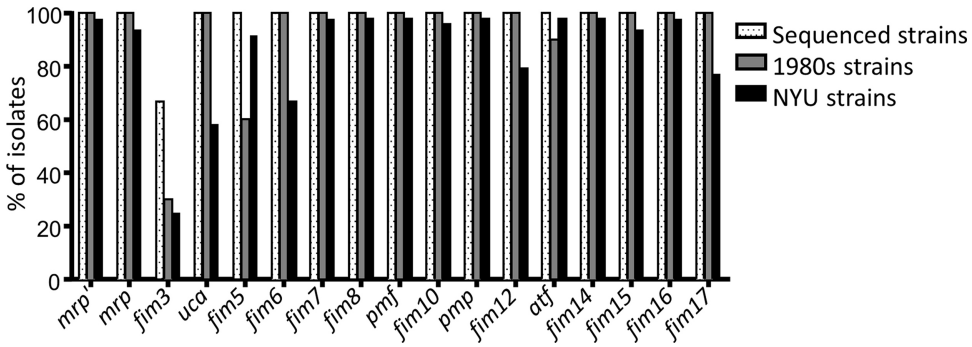

Figure 11 Conservation of fimbriae encoded by *P. mirabilis*. The percentage of isolates with each fimbria is shown. For the six sequenced strains, fimbriae were identified using BLAST using the HI4320 fimbrial major structural subunit gene as the query. For the 1980s (n = 10) and hospital isolates (n = 48), fimbrial genes were detected by PCR. Reproduced from reference 101, with permission.

effector operons adjacent to, and in the reverse orientation from, the T6SS secretion apparatus genes (113, 114). In both cases, the effector operons begin with *hcp* and *vgrG* homologs that are required for T6SS function (115). After that, however, the operons diverge in both sequence and number of genes; for example, BB2000's *idr* operon comprises five genes, while HI4320's *pef* operon has nine (113, 114) (Fig. 12). Furthermore, HI4320 encodes at least two more operons identified as likely T6SS effectors than BB2000 is predicted to encode (107, 116). Examination of other *P. mirabilis* sequenced genomes indicates that this variability continues throughout the species (Fig. 10A).

O-Antigen

Like other Gram-negative bacteria, *P. mirabilis* strains have diverse O-polysaccharides as part of their LPS; 76 O-serogroups have been described thus far for *Proteus* spp. (117). In fact, the O- and H-antigen designations for LPS and flagellar typing were originally named by Weil and Felix's observation that swarming *P. mirabilis* had a breath-like appearance (German *Hauch*, breath) while nonswarming colonies did not (*ohne Hauch*, without breath) (90). In a survey of *P. mirabilis* strains with different O-serotypes, virulence factors were widespread (urease, Zap protease, swarming), but strains differed in the levels of these activities. Specifically, strains with negatively charged O-polysaccharides displayed higher urease, protease, and swarming activities compared with positive or neutral O-polysaccharides (99). LPS is abundant on the cell surface of Gram-negative bacteria, and its properties can affect bacterial interaction with their environment. Thus, some aspects of strain variability may be determined by LPS biochemistry.

Flagellin

Flagella (*see* **Flagella and Motility** section) are targets of the innate immune system and also energetically expensive to produce (118). Correspondingly, although most flagellar genes are conserved in *P. mirabilis*, the gene encoding the whip itself is highly variable, as in other bacterial species. *P. mirabilis* also encodes a second, silent flagellar gene, *flaB*, that can recombine with *flaA* and yield hybrid FlaAB flagella (119). The properties of FlaAB hybrids have been extensively reviewed elsewhere (19).

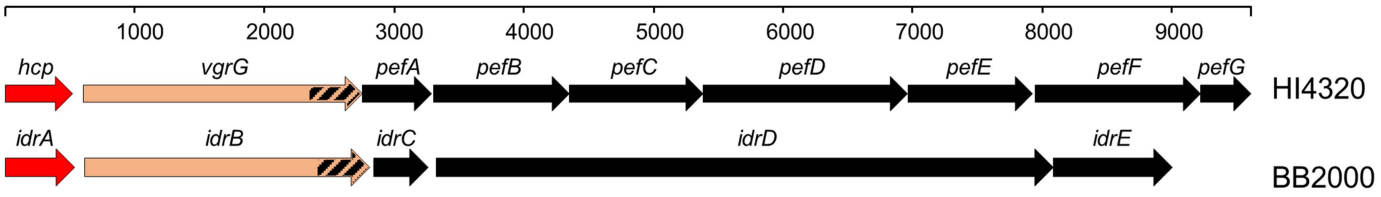

Figure 12 T6SS effector operons are highly variable. The T6SS effector operon immediately adjacent to the conserved T6SS secretion apparatus operon is depicted for *P. mirabilis* HI4320 (top) and BB2000 (bottom). The HI4320 locus, called *pef* for primary effector operon, comprises PMI0750-0758, and the BB2000 locus, called *idr* for identity recognition, comprises BB2000_0822-0826. The proteins encoded by the first gene (red) and the first 596 amino acids of the second gene (orange) are 99% identical, but the remaining ~130 amino acids of the encoded proteins share no homology. The rest of the operons are not homologous (black). A portion of IdrD shares identity with PMI0761, which is not part of the *pef* operon. The scale at the top is in nucleotides.

Phage

Like other bacteria, *P. mirabilis* genomes are peppered with integrated phage. HI4320 encodes three apparently complete and three degenerate prophages (107). CRISPR-Cas systems are encoded in approximately one-third of sequenced *P. mirabilis* genomes as determined by the Bacterial Bioinformatics Resource Center PATRIC (120); notably, CRISPR is not present in two strains commonly used for experimentation: HI4320 and BB2000 (107, 116).

Differential expression of phage genes has been observed in *P. mirabilis* during swarming (121, 122); specifically, one phage is inserted adjacent to the *rcs* operon, which encodes a regulator of flagella and swarming. Furthermore, phage have been used to transduce swarming ability into nonswarming strains (123). Thus, it is likely that phage account for some of the observed differences in swarming behavior between strains.

Plasmids

Plasmids are not a defining feature for *P. mirabilis*. The original *P. mirabilis* sequenced genome, HI4320, included a 36-kb plasmid that was designated pHI4320 (107), and a signature-tagged mutagenesis study as well as a transposon insertion-site sequencing study indicated that mutations in pHI4320 led to decreased fitness in mice (103, 124). However, several of the targeted genes were involved in plasmid stability, and pHI4320 does not encode any obvious virulence genes (107). In the National Center for Biotechnology Information (NCBI) database, a minority of *P. mirabilis* strains have been reported to carry distinct plasmids, at least some of which encode antibiotic resistance genes (125).

Transcriptomics

P. mirabilis undergoes dramatic shifts in its appearance and surroundings, and it follows that many of these responses result from changes in transcription. Global analysis of gene expression (transcriptomics) has been conducted for *P. mirabilis* under multiple conditions, initially using microarrays and, more recently, RNA-seq.

Microarrays

The four following studies (104, 121, 126, 127) were conducted using a microarray with 70-mer oligonucleotide probes designed to hybridize with each of the 3,719 predicted open reading frames from an early draft version of the *P. mirabilis* HI4320 genome (107).

Swarming microarray

Perhaps the most dramatic change *P. mirabilis* undergoes is the cyclic switch from elongated, hypermotile swarmer cells to short, nonmotile consolidated cells during culture on solid surfaces (19). This transformation was the target of the first *P. mirabilis* transcriptomic study, (i) where swarm and consolidate transcripts were shown to be more similar to each other than to RNA derived from broth culture, and (ii) while many genes are induced during consolidation, very few are upregulated during active swarming (121). The data were consistent with earlier reports of increased expression of certain virulence genes during swarming (128, 129), and swarmer cells being less metabolically active than consolidates (130). Curiously, although *P. mirabilis* is largely nonmotile during consolidation, flagellar transcripts were among the most highly transcribed messages in both swarm and consolidate (121). Based on the accumulated transcription and metabolic data, the consolidation phase has been proposed to be a time of preparation for the next round of swarming, by increasing nutrient uptake systems, central metabolism, and respiration. Because *P. mirabilis* swarming is very robust and occurs under conditions not permissive for other species of swarming bacteria, the preparation that occurs during consolidation phase may contribute to how *P. mirabilis* is able to swarm under a wider range of conditions than other species, including on solid surfaces such as hard agar and catheters.

Iron limitation microarray

Iron is sequestered by the host to combat bacterial infection, and pathogens activate iron acquisition systems during UTI (*see* **Metal Acquisition** section). *P. mirabilis* was previously thought to lack common iron-scavenging systems in earlier studies. However, microarray analysis conducted on iron-restricted *P. mirabilis* revealed 21 iron-regulated systems, including two new acquisition systems that are detailed later in this review (104).

Ascending UTI microarray

A critical point for studying how *P. mirabilis* causes disease requires knowledge regarding the physiological state of this pathogen during UTI. To answer this question, urine was collected from experimentally infected mice at 1, 3, and 7 days postinoculation (dpi) for RNA extraction and microarray hybridization (126). Iron acquisition, urease, and peptide transporters were induced during UTI, consistent with an iron-restricted, urea- and peptide-rich urine environment. The genes encoding MR/P fimbriae (*see* **Fimbriae and Adhesins**

section), which were previously shown to contribute to infection, were the most highly upregulated of the transcriptome compared with broth culture (Fig. 13). However, some known virulence factors were either poorly expressed or downregulated during UTI, including genes encoding *P. mirabilis* fimbriae (PMF), Zap metalloprotease, hemolysin, and *Proteus* toxic agglutinin (Pta). This suggests that voided urine provides an important, but incomplete, snapshot of bacterial gene expression during UTI.

Interestingly, central metabolic pathways that were required during infection differed in several ways compared with a previous study of uropathogenic *E. coli* (131). Nitrogen assimilation gene expression suggested that *P. mirabilis* has greater access to nitrogen compared with *E. coli*, but follow-up experiments indicated this was not simply due to ammonia derived from urease activity (126). In contrast with *E. coli*, *P. mirabilis* induced glucose uptake and glycolysis genes, suggesting that *P. mirabilis* is able to access nutrient sources not available to

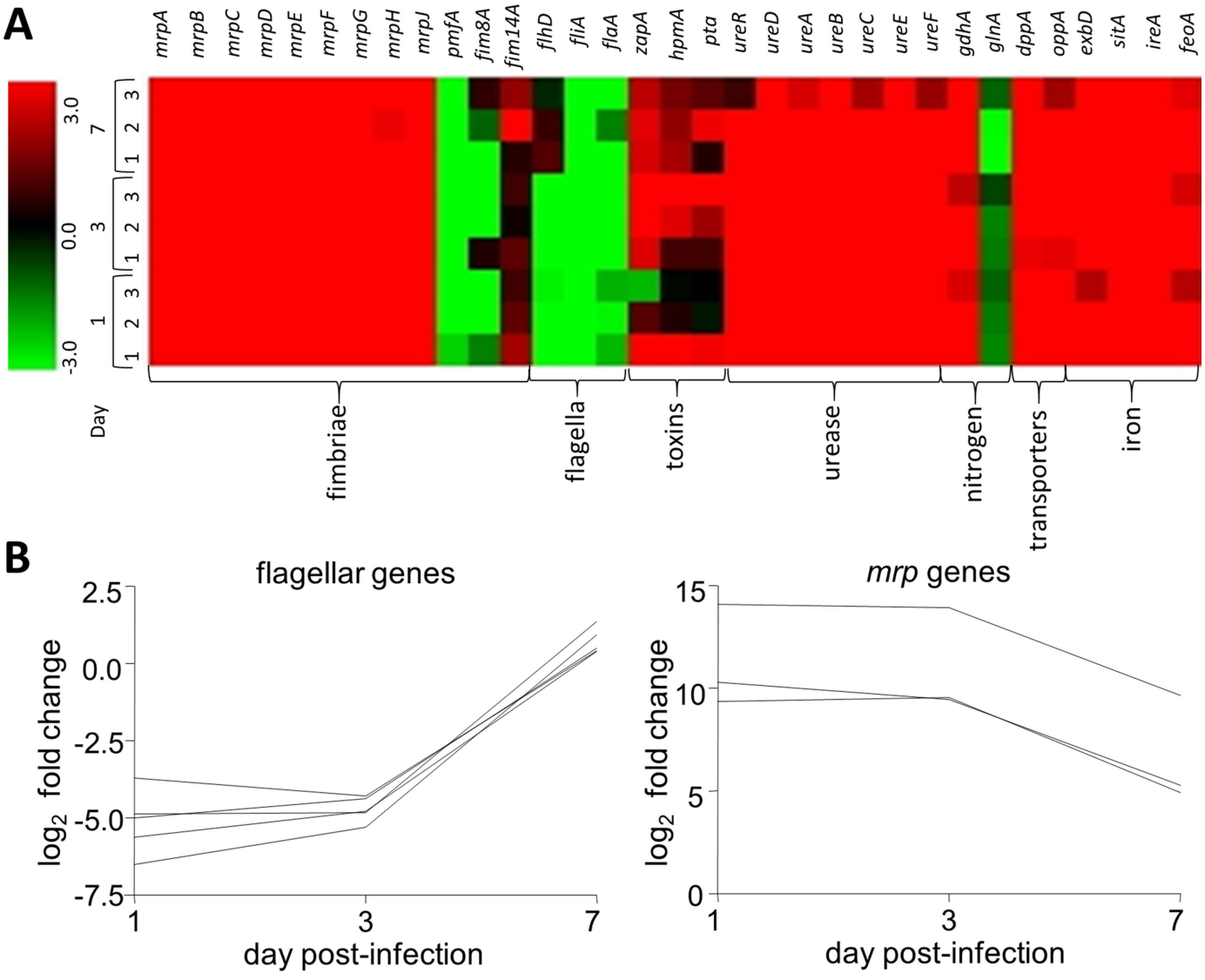

Figure 13 *P. mirabilis* gene expression during experimental UTI. (A) Heat map of expression data for specific virulence-associated genes, depicting the ratio of expression in LB broth versus *in vivo*. The legend at the left indicates the color associated with $\log_2$ fold change: red, upregulated *in vivo*; green, downregulated *in vivo*; black, not differentially regulated. (B) Adherence and motility genes are inversely regulated during UTI. Each line represents fold change of a specific flagellar (left panel) or fimbrial (right panel) gene *in vivo* relative to mid-logarithmic phase culture *in vitro*. Genes in the *mrp* operon are highly induced early during infection, but expression falls by 7 days postinfection. Flagellar genes are initially repressed, but expression increases late in infection. Figure adapted, with permission, from reference 126.

E. coli (perhaps because of the activity of toxins on bladder epithelium). Gene expression at 1, 3, and 7 days postinoculation was also compared. Flagellar genes were initially repressed, but this repression was relieved by day 7. In contrast, *mrp* genes were highly transcribed throughout the infection, but their degree of induction was lower at day 7; this topic is further detailed in the fimbrial section (*see* **Fimbriae and Adhesins** section).

The transcriptional regulator MrpJ is encoded by the *mrp* fimbrial operon (*see* **Fimbriae and Adhesins** section). Originally proposed as a switch between adherent and motile states (132), MrpJ was found to contribute to other phenotypes as well (133). Microarray experiments comparing an *mrpJ in vivo* mimic, where *mrpJ* is expressed *in trans* at levels comparable to those detected in mice during experimental UTI, with an empty vector control showed that MrpJ's regulatory network extends considerably beyond repression of flagella to include, among others, regulation of additional fimbriae and the type VI secretion system (127). MrpJ and MrpJ paralogs are discussed later in this review (*see* **Transcriptional regulation by MrpJ** section).

RNA-seq

The next three studies (122, 134, 135) compared gene expression for targeted mutants with their isogenic parent strain by using RNA-seq. In addition to the aforementioned microarray study, broth-cultured and swarmer cells have also been compared by RNA-seq using the BB2000 laboratory strain (122). Even though the methods for collecting and analyzing swarmer cells were different in these two studies (121, 122), similar results were obtained for the broth-swarmer comparison regarding the genes encoding flagella, lipoproteins, iron transport, and hemolysin, among others. FliL is a flagellar protein that, when mutated, leads to elongated swarmer-like cells under nonswarming conditions (pseudoswarming) (136). Comparison of a *fliL* mutant cultured in broth to induce pseudoswarmer cells with the wild-type broth RNA-seq data set revealed an increase in propanediol utilization in the *fliL* mutant. This suggests a possible new role for these genes in swarmer cell differentiation (122).

The Rcs phosphorelay is a repressor of swarming and an activator of biofilm formation (134, 135, 137–139). RNA-seq was used to compare a broth-cultured *rcsB* mutant with its isogenic parent strain PM7002 (134, 135). In this condition, the *rcsB* mutant undergoes inappropriate elongation that is similar to the *fliL* phenotype. These studies showed that RcsB controls pathways important for swarming, including cell division (*minCDE*) and motility (flagella and flagellar regulators). Furthermore, RcsB activates biofilm-associated genes, including genes encoding MR/P, PMF, and UCA fimbriae (*see* **Biofilms** section). Interestingly, RcsB also represses virulence genes that have previously been shown to be activated during swarming (*zapABD*, *hpmBA*) and type VI secretion genes (*tss*, *ids*, and *idr/pef* operons).

Mutagenesis

The first targeted mutation to be made in *P. mirabilis* was a *ureC* urease mutant (40) (Fig. 14). This mutant was constructed using a single crossover, Campbell-type insertion via an R6K *ori-pir* suicide vector introduced by conjugation (140), an approach that is still used by multiple groups studying *P. mirabilis*. This initial paper noted several difficulties with methods for mutant construction in *P. mirabilis*, because conjugative-incompatible plasmids, phage transduction, and spontaneous curing of multicopy plasmids all resulted in failure to yield chromosomal mutations (40). Later on, *sacB* counterselection was used to facilitate identification of double-crossover events (141). The ability to directly construct and test mutants in the mouse UTI model was a boon for dissecting *P. mirabilis* virulence, and allelic exchange via mating with suicide plasmids continues to be used for mutant construction. Even so, mutant construction remained labor intensive and prone to failure, particularly in some clinical isolates.

Subsequently, sequencing of the HI4320 genome revealed that this strain naturally carries a plasmid that is closely related to R6K and encodes a π protein (107), possibly contributing to the difficulty in constructing mutants in this background using typical suicide vectors. Thus, another method was developed for constructing mutations, using a group II intron mutated to specifically target a gene of interest (142, 143). Advantages over the prior allelic exchange method are the relatively short time required, higher rate of success, and lack of passaging or counterselection that would normally be required to resolve double-crossover events. The drawbacks are that the choice of insertion sites is limited, mutations have polar effects on downstream genes, and the method is insertion based (that is, it is not simple to delete sequences). The latter problem can be managed by use of *cre*-lox recombination to remove the antibiotic resistance cassette carried within the intron, resulting in an un-

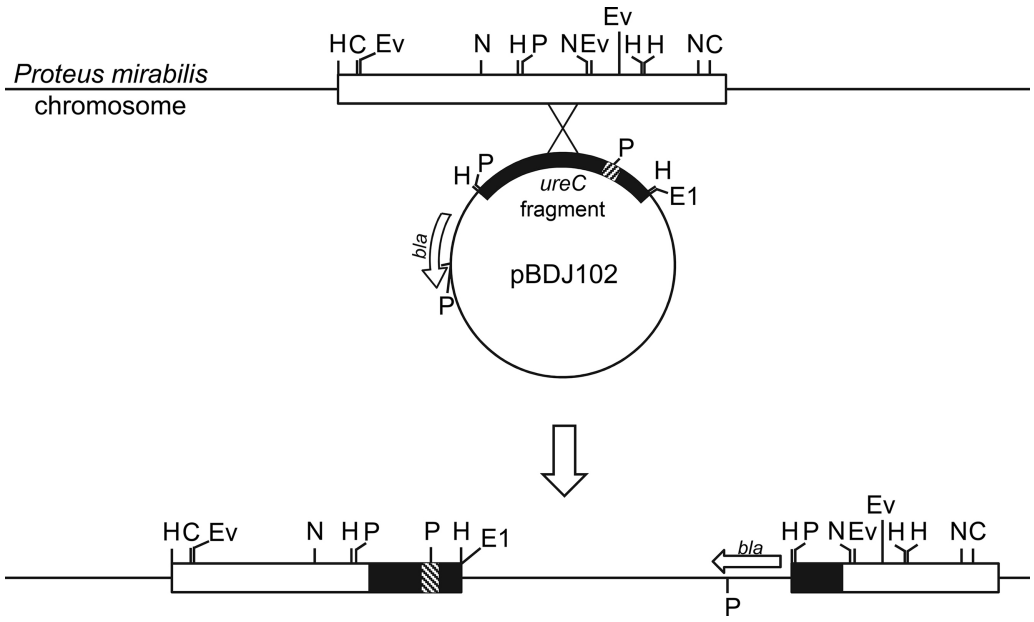

Figure 14 Integration of the urease suicide plasmid into the chromosome of *P. mirabilis* HI4320 by homologous recombination. *E. coli* SM10 λ *pir* (Kan^r), carrying transfer genes integrated into its chromosome, was used to mobilize pBSJ102 (Ap^r) into *P. mirabilis* HI4320. Integration of pBDJ102 into the chromosome was selected on medium containing tetracycline and ampicillin. Transconjugants (Ap^r Tet^r) were urease negative. Bla, β-lactamase; C, ClaI; Ei, EcoRI; Ev, EcoRV; H, HindIII; N, NruI; P, PvuI. The 1.5-kb HindIII fragment of *ureC* (solid), a 277-bp deletion (striped), and chromosomal urease gene sequences (open) are shown. Adapted from reference 40, with permission.

marked mutant (121). Additional introns can be inserted, with the potential to remove intervening sequences via an additional round of *cre*-lox recombination.

Genes that have been specifically mutated and tested in a mouse model of UTI, either independently or by direct cochallenge against a parental strain, are shown in Table 4. It is important to note that the studies presented in Table 4 include a range of *P. mirabilis* strains, mouse strains, infectious doses, and experiment lengths, but exclude mutants generated by transposon insertion and targeted mutants that were only tested for virulence in an *in vitro* assay, such as cell culture.

Genome-Wide Mutagenesis

Transposon mutagenesis in *P. mirabilis* was first described in a publication from 1991 using a Tn*5* derivative (144, 145). The mini-Tn*5* transposon was carried on a suicide plasmid with the π protein-dependent origin of replication from R6K, *oriT* for conjugal transfer from donor strain to recipient strain, and the IS*50*$_R$ transposase gene *tnp*. This approach has since been used to generate libraries for isolation of mutants defective for a given phenotype, such as swarming motility (114, 138, 146–150), sensitivity to antimicrobial peptides (75, 151), and biofilm formation (152).

In 1995, this approach was revolutionized through the development of STM (153), in which each transposon mutant has a specific DNA sequence within the transposon that acts as a barcode. STM led to the first genome-wide pathogenesis studies by permitting identification of unique mutants within a mixed population and allowing for assessment of mutants lost during the selective process of the infection, and therefore containing transposon insertions in genes that contribute to colonization and pathogenicity. This approach was successfully utilized three times with *P. mirabilis* strain HI4320 in a murine model of ascending UTI, identifying a combined total of 54 genes that represented important fitness factors for colonization (summarized in Table 5) (103, 154, 155).

In the first *P. mirabilis* STM study, mice were inoculated with 96 tagged mutants as the input sample, and bacteria recovered from the bladders of 5 mice 2 days post-inoculation were used as the output samples (155). Only two mutants were reproducibly underrepresented in the output samples from all five mice: B2 (determined to be an insertion in a secreted protease, now identified as PMI3441, a U32-family peptidase), and B5 (determined to be an insertion in the *rpoN* operon, now identified as PMI3645, an RNase adaptor protein RapZ). The fitness defect of each mutant was assessed by direct cochallenge

Table 4 Targeted mutations that have been tested in mice

Gene	Locus[a]	Description	Virulence gene[b]	Reference
ureC	PMI3685	Urease α-subunit	Y	12, 39, 40, 43
hpmA	PMI2057	Hemolysin	N	44, 47, 192
mrpA	PMI0263	Major mannose-resistant/*Proteus*-like fimbrial protein	Y	43, 214, 226, 229, 232
pmfA	PMI1877	PMF major fimbrial subunit	Y	213, 214, 241
flaD	PMI1621	Flagellar hook-associated protein 2	Y	44
flaAB	PMI1619-20	Flagellin 1 and flagellin 2	N	302
mrpG	PMI0269	MR/P fimbrial subunit	Y	141
zapA[c]	PMI0279	Metalloprotease	Y	129
mrpH	PMI0270	MR/P fimbrial adhesin	Y	221
atfA	PMI2728	ATF major fimbrial subunit	N	244
mrpJ	PMI0271	Fimbrial operon regulator	Y	127, 132
mrpI	PMI0262	Fimbrial recombinase	Y[d]	223
luxS	PMI0379	*S*-Ribosylhomocysteine lyase	N	352
ureR	PMI3681	Urease operon transcriptional activator	Y	172
spa47	PMI2692	Type III secretion system ATPase	N	143
	PMI0047	Secreted 5′-nucleotidase	N	183
rafY	PMI0288	Putative glycoporin	N	183
	PMI0842	TonB-dependent receptor	Y	183
fadL	PMI1810	Long-chain fatty acid transport protein	N	183
	PMI2596	TonB-dependent receptor	Y	183
pta	PMI2341	*Proteus* toxic agglutinin	Y	47
znuC	PMI1151	High-affinity zinc uptake system ATP-binding protein	Y	319
zur	PMI2748	Zinc uptake regulation protein	Y	319
dppA	PMI2847	Dipeptide ABC transporter, substrate-binding protein	Y	121
oppB	PMI1474	Oligopeptide ABC transporter, permease protein	N	121
cysJ	PMI2250	Sulfite reductase [NADPH] flavoprotein alpha-component	Y	121
lrhA	PMI0629	LysR-family transcriptional regulator	N	121
hexA	PMI1764	LysR-family transcriptional regulator	Y	121
pbtA	PMI0232	Siderophore biosynthesis protein	N	104
nrpR	PMI2599	Siderophore synthase	Y	104
aipA	PMI2122	Adhesion and invasion autotransporter	Y	46
taaP	PMI2575	trimeric autoagglutinin autotransporter of *Proteus*	Y	46
gdhA	PMI3008	NADP-specific glutamate dehydrogenase	Y	126
glnA	PMI2882	L-Glutamine synthetase	Y	124
ucaA	PMI0536	UCA major fimbrial subunit	Y	234
hfq[e]	PMI3365	Hfq (host factor-I protein)	Y	267
speA	PMI2094	Biosynthetic arginine decarboxylase	Y	353
speBF	PMI2093; PMI0307	Agmatinase; ornithine decarboxylase, inducible	Y	353
pfkA	PMI3203	6-Phosphofructokinase	Y	331
pgi	PMI2754	Glucose-6-phosphate isomerase	Y	331
tpiA	PMI3205	Triosephosphate isomerase	Y	331

(continued)

Table 4 Targeted mutations that have been tested in mice *(continued)*

Gene	Locus[a]	Description	Virulence gene[b]	Reference
pykA	PMI1155	Pyruvate kinase II	Y	331
gnd	PMI0655	6-Phosphogluconate dehydrogenase, decarboxylating	Y	331
talB	PMI0006	Transaldolase B	Y	331
edd	PMI2760	6-Phosphogluconate dehydratase	Y	331
sdhB	PMI0568	Succinate dehydrogenase iron-sulfur protein	Y	331
frdA	PMI3588	Fumarate reductase flavoprotein subunit	Y	331
fumC	PMI1296	Fumarate hydratase, class II	Y	331
pckA	PMI3015	Phosphoenolpyruvate carboxykinase [ATP]	N	331
argG	PMI3239	Argininosuccinate synthase	N	331
serA	PMI2031	D-3-Phosphoglycerate dehydrogenase	Y	331
rpoE	PMI1894	RNA polymerase sigma-E factor	Y	354
rseA	PMI1893	Anti-sigma E protein	N	354
	PMI1518	High-affinity nickel efflux protein	Y	124
pldA	PMI3344	Phospholipase A	N	124
ilvD	PMI3302	Dihydroxy-acid dehydratase (branched chain amino acid biosynthesis protein)	Y[f]	124
lon	PMI0117	ATP-dependent proteinase, serine peptidase	Y	124
argR	PMI3399	Transcriptional regulator, repressor of the arginine biosynthetic pathway	Y	124

[a]Based on *P. mirabilis* HI4320 annotated genome.
[b]Significant in one or more sites tested (urine, bladder, kidneys, spleen).
[c]Also found to contribute to virulence in a rat prostatitis model (199).
[d]MR/P locked-on *mrpI* mutants outcompete locked-off *mrpI* or wild-type (*see* **Fimbriae and Adhesins** section).
[e]Also found to contribute to virulence in a rat skin wound model (267).
[f]Contributed to fitness during polymicrobial infection with *Providencia stuartii*, but not during single-species infection (124).

with wild-type *P. mirabilis* HI4320, and only the PMI3645 mutant remained significantly outcompeted.

The second *P. mirabilis* STM study used 45 pools of mutants as the input samples (2,088 mutants total), and bacteria recovered from the bladders or kidneys of 5 mice per pool 4 days postinoculation were used as the output samples (103). Five hundred two mutants were identified as attenuated in the primary screen. A secondary screen was conducted with these 502 mutants divided into 19 pools, and only 114 of the mutants were reproducibly attenuated. Eighty-four of the 114 mutants were retested by direct cochallenge against wild-type *P. mirabilis* HI4320 for a longer experimental challenge of 7 days, and 37/84 (44%) of the mutants exhibited reproducible fitness defects. Nucleotide sequences were obtained from 30 of the mutants, 27 of which map to open reading frames in the current annotation of *P. mirabilis* HI4320. This approach identified several categories of mutants representing both known and novel fitness factors for UTI, including motility, iron acquisition, plasmid-encoded factors, transcriptional regulation, phosphate transport, urease activity, capsule synthesis, and metabolic pathways, the majority of which would have been difficult to identify as fitness factors by other methods.

The third *P. mirabilis* STM study screened 40 pools of mutants as the input samples (1,880 mutants total), and bacteria recovered from the bladders or kidneys of 5 mice per pool 4 days postinoculation were used as the output samples (154). Five hundred seventy mutants were identified as attenuated in the primary screen, 217 of which had a reproducible defect in the secondary screen. Ninety-three of the most attenuated mutants that did not exhibit competitive defects *in vitro* were retested by direct cochallenge against wild-type *P. mirabilis*, and 37 (40%) had reproducible fitness defects. Nucleotide sequences were obtained from 29 of the mutants, 28 of which map to open reading frames in the current annotation of *P. mirabilis* HI4320. This approach again identified fitness factors pertaining to cellular processes, transport, transcriptional regulation, motility, cell surface

Table 5 Virulence genes identified by STM and Tn-Seq

PMI number	Gene name	Isolate	STM of ascending UTI			CAUTI	Polymicrobial CAUTI
Reference			155	103	154	124	124
PMI0012	*nhaR*	4B6			U, K, O		
PMI0020	*carA*	D4-8		U, B, K			B, K
PMI0030	*exbD*	7A1			U, B, K, O		B
PMI0283	*zapE2*	9C6			K		
PMI0565	*sdhC*	10E3			U, B, K, O		
PMI0589	*aroG*	G1-38		U, B, K			
PMI0711	*serC*	G4-12		U, O			B, K
PMI0842		D6-33		U, B, K			K
PMI1000		8H4			U, O		K
PMI1045	*arnA*	G5-30		U, B, K		B, K	
PMI1184		16F1			K		
PMI1193		40A6			U, B, K, O		
PMI1421	*ppsA*	17A4			B, K, O		B, K
PMI1448		6F6			U, O		
PMI1546	*guaB*	5F1			U, B, K, O	B, K	
PMI1598	*yidA*	12E4			U		
PMI1607	*sdaA*	15C3			U	K	K
PMI1630	*fliF*	8A6			B, K	B	B, K
PMI1651	*flgE*	21B2			K		B, K
		37D5			U, B, O		
PMI1667	*cheW*	E6-43		U, B, K			B, K
PMI1761	*nuoB*	15A6			U, B, K, O		
PMI1874		E5-36		U, B, K			K
PMI2014		32C4			B		
PMI2046	*aceE*	8B5			B, K, O		
PMI2259	*metN*	23D5			U, K, O	B, K	
PMI2332	*surA*	11C4			U, B, K, O	K	K
		32E1			B		
PMI2342	*sufI*	38E2			K, O		K
PMI2345	*parE*	C6-15		U, B, K			
PMI2378	*cbbC*	11G3			U, K, O		B, K
PMI2575		36D2			B, O		
PMI2605	*nrpG*	A1-8		U, K, O			K
PMI2760	*edd*	11D4			U, K		B, K
PMI2823	*ppiA*	6D1			U, K, O		
PMI2828	*dsbA*	F4-37		U, B, K		B, K	
PMI2893	*pstS*	H4-34		U, B, K		B, K	
PMI2894	*pstC*	G1-43		U, B, K		B, K	
PMI3001		4A3			U		
		11A4			U, K, O		

(continued)

Table 5 Virulence genes identified by STM and Tn-Seq *(continued)*

PMI number	Gene name	Isolate	STM of ascending UTI		CAUTI	Polymicrobial CAUTI
PMI3021	*mrcA*	B6-23	U, B, K		K	
PMI3053	*asnC*	E6-41	U, B, K		B, K	
PMI3190	*cpsF*	11B2		B, K, O		K
		20C4		U, B, K, O		
PMI3295	*hdfR*	D5-9	U, O		K	
		C1-18	B, O			
PMI3329	*hemY*	B2-9	U		B	
PMI3333	*cyaA*	20E1		U, B, K, O	K	
PMI3359		13D1		U, O		
PMI3390		F6-34	U, B, K			
		A3-39	U, B, K			
PMI3441		B2	P			
PMI3451	*nrdD*	D6-39	B, K, O			B, K
PMI3623	*dusBC*	F1-29	U, B, K		B, K	B,K
PMI3645	*rapZ*	B5	U, B, K			K
PMI3687	*ureF*	B6-40	U, B, K			K
PMI3692		D6-26	U, B, K			
PMI3700		D1-30	U, B, K		B, K	
PMI3705		1F6		U, K, O		B, K
PMIP09	*pilX4*	C4-41	B, K, O		K	K
		A5-34	U, K, O			
		B4-38	K			

P, primary screen; U, urine; B, bladder; K, kidney; O, attenuated overall

structures, and metabolism. However, there was no overlap in the genes or operons identified in this study and the prior two STM studies; because the three combined STM studies only achieved 70% theoretical genome coverage, this is likely due to incomplete saturation and differences between the mutants present in each pool for *in vivo* competition.

In 2009, the basic technique of STM was further improved upon and integrated with next-generation sequencing techniques to allow for massively parallel sequencing and quantitation of the relative abundance of all mutants present in a given setting. Several variations of the method were developed concurrently, including insertion sequencing (INSeq) (156), transposon-directed insertion site sequencing (TraDIS) (157), transposon insertion-site sequencing (Tn-Seq) (158, 159), and high-throughput insertion tracking by deep sequencing (HITS) (160). Because Tn-Seq has been applied to the study of *P. mirabilis* pathogenicity (124), the specifics of this method will be explained in further detail.

The first step of Tn-Seq is to generate a genome-saturating transposon mutant library, generally using a Mariner transposon. Because of the saturating nature of the library, this method can also be used to identify genes that are essential for growth *in vitro*, as insertion mutants within these genes will be lacking from the starting library. Infection studies are then conducted with the transposon library, and all bacteria in the target site of infection (for instance, the bladder) are collected for extraction of genomic DNA. The frequency of each insertion mutant is then determined, *en masse*, from the input sample (the saturated library) and the output sample (the bladder), and the fitness contribution of each gene in the genome can be assessed by the change in frequency of insertion mutants for that gene from the output sample compared with the input sample.

This approach was successfully used to generate the first genome-saturating library of transposon insertion mutants in *P. mirabilis* HI4320, and allowed for identification of 436 genes (12% of the genome) estimated to be

essential for growth in Luria broth (124). As would be expected, the essential genes largely pertained to cell cycle control and division, cell wall biogenesis, replication, and ribosomal proteins, and 64% had been identified as essential genes in other bacterial species. The transposon mutant library was then used in a murine model of CAUTI to identify fitness factors for colonization of the catheterized bladder and ascension to the kidneys 4 days postinoculation (Fig. 15). Massively parallel sequencing and statistical analysis identified 629 genes (17% of the genome) as fitness factors for CAUTI; 93 genes were specifically important for colonization of the catheterized bladder, 209 for colonization of the kidneys, and 286 that were important for colonization of both the bladder and kidneys. Of the 54 genes and operons identified as fitness factors for ascending UTI in the combined STM studies, 31 (57%) were also identified in the CAUTI model by Tn-Seq (summarized in Table 5). Eight mutants were constructed for direct cochallenge with the parental strain to confirm the fitness defects that were identified by Tn-Seq, and fitness defects were verified for 7/8 (88%). Tn-Seq therefore provided confirmation of a role for known *P. mirabilis* fitness factors during CAUTI, identification of CAUTI-specific fitness factors, and a model for exploring the different metabolic pathways and transport requirements between ascending UTI and CAUTI.

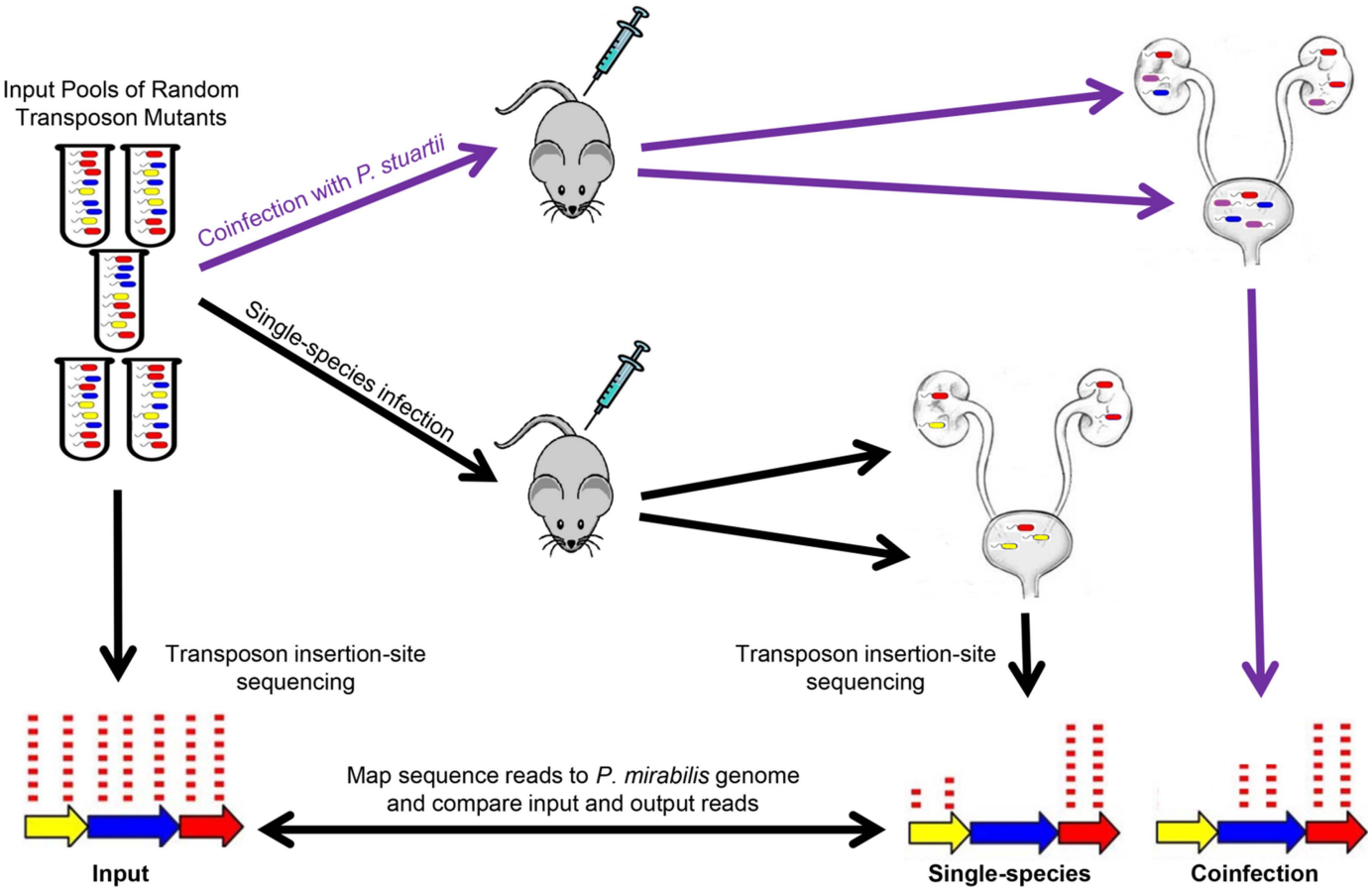

Figure 15 Conceptual model of single-species and polymicrobial CAUTI Tn-Seq. For each of five transposon mutant library pools, mice were infected as follows: (i) 5–10 CBA/J mice were transurethrally inoculated with 1×10^5 CFU of the transposon library for single-species infection, and (ii) 5–10 CBA/J mice were inoculated with 1×10^5 CFU of a 1:1 mixture of the transposon library and wild-type *P. stuartii* BE2467 (purple) for coinfection. Thus, for each input pool, the single-species infections and coinfections were conducted in parallel to utilize the same input inoculum. Input and output samples were enriched for transposon-containing sequences and subjected to next-generation Illumina sequencing of the transposon-chromosome junctions. The resulting reads were mapped to the *P. mirabilis* genome, and the abundance of reads at each insertion site from all output samples were compared with the input samples to determine a fold change for each gene. The gene in yellow represents a candidate *P. mirabilis* fitness factor for single-species CAUTI that is even more important during coinfection; the gene in blue represents a *P. mirabilis* fitness factor for single-species CAUTI that is no longer important during coinfection; the gene in red represents a factor that does not contribute to *P. mirabilis* CAUTI and was therefore recovered at a similar density from the infection output pools as the input pools. Reproduced from reference 124, with permission.

Importantly, this approach was also applied during polymicrobial infection with *P. stuartii*, in parallel with the above study, to determine how polymicrobial infection influences *P. mirabilis* fitness requirements (124) (Fig. 15). Of the 629 genes identified as *P. mirabilis* fitness factors for CAUTI, 217 (35%) were also important during polymicrobial infection. The fitness factors that were important for both infection types include fimbrial genes, components of the flagellar cascade, urease, and factors involved in inorganic ion transport and metabolism. Interestingly, an additional 1,353 candidate fitness factors were identified that appear to specifically contribute to *P. mirabilis* fitness during polymicrobial infection, including defense mechanisms (such as type III secretion and type VI secretion), signal transduction pathways, at least 10 distinct fimbrial types, iron uptake systems, respiratory nitrate reductase, the oxidative pentose phosphate pathway and the Entner-Doudoroff pathway, arginine import and biosynthesis, and branched chain amino acid (BCAA) biosynthesis. It was further determined that the requirement for BCAA biosynthesis during coinfection was due to high-affinity import of leucine by *P. stuartii*, indicating the utility of this technique for dissecting polymicrobial interactions during infection (124).

VIRULENCE FACTORS

Urease

P. mirabilis was the model organism for which the genetics of urease were first delineated. Urease is a nickel-metalloenzyme, the synthesis of which is induced by the presence of its substrate, urea (161, 162).

Structure and Activity

Apourease comprises three structural subunits, UreA, UreB, and UreC, assembled as a homotrimer of individual UreABC heterotrimers $(UreABC)_3$ (Fig. 16). To become catalytically active, the apoenzyme must acquire divalent nickel ions through a process involving four accessory proteins: UreD, UreE, UreF, and UreG. As studied by yeast two-hybrid, and immunoprecipitation with monoclonal

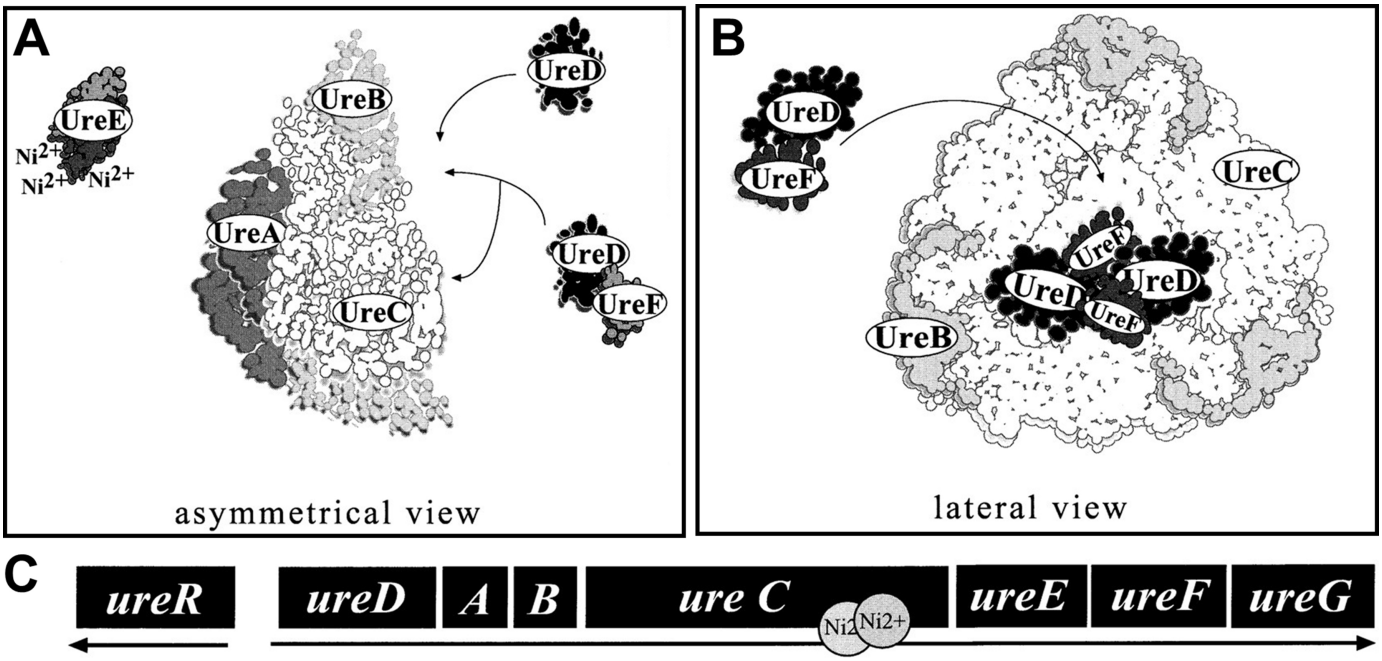

Figure 16 Model of *P. mirabilis* urease interactions with structural and accessory proteins based on yeast two-hybrid experiments. The three-dimensional structure of urease, inferred from the closely related urease of *Klebsiella aerogenes*. (A) UreD associates with UreC in the context of the apourease independently of the UreA structural protein. Although UreD and UreF interact in the absence of structural proteins, UreD is still capable of associating with the apourease without coaccessory proteins such as UreF. (B) A single molecule of UreD associated with UreABC may interact with additional UreD molecules bound to adjacent UreABC heterotrimers. These interactions could stabilize the accessory protein interactions with the apourease and hypothetically coordinate nickel uptake among the three active sites of urease. A similar hypothesis applies to UreF; homomultimeric UreF interactions *in vivo* could occur between individual UreF molecules bound through UreD to adjacent UreABC heterotrimers. (C) The 6,500-bp *P. mirabilis* urease gene cluster encodes eight proteins that comprise, regulate, and assemble the urease homoenzyme. Figure adapted, with permission, from reference 163.

antibodies to UreC and UreD, it is clear that the accessory proteins interact with the apoenzyme to deliver Ni^{2+} to the active site (163). Indeed, UreE carries a natural histidine tail that allows it to carry Ni^{2+} and also to be purified in a single step on a Ni^{2+}-nitriloacetic acid column.

In early studies using bacterial cell lysates of four *P. mirabilis* isolates, the molecular size of urease was originally estimated by molecular sieve chromatography to be 281 to 338 kDa (164), and the molecular size of the apoenzyme was later determined to be 252,600 Da (165). Including the two Ni^{2+} in each of three active sites, this brings the predicted molecular size to ~253 kDa with an isoelectric point of 5.9 for *P. mirabilis* HI4320. The affinity for substrate as estimated by K_m is relatively weak, ranging from 22 to 60 mM urea among the four isolates. However, with urea concentrations of ~400 mM urea in human urine, the enzyme would be fully saturated and working at the V_{max} within the urinary tract and therefore extremely potent.

Genetic properties and organization of the urease operon

The urease operon was originally characterized from a DNA fragment of 7.6 kb, derived from a cosmid gene bank of *P. mirabilis* genomic DNA. Six open reading frames were found within a 4,952-bp region, which were predicted to encode polypeptides of 31.0 (UreD), 11.0 (UreA), 12.2 (UreB), 61.0 (UreC), 17.9 (UreE), and 23.0 (UreF) kDa (165). Reexamination of recombinant clones for urease activity revealed that a seventh gene, *ureG*, was also required for production of catalytically active urease enzyme (166) Sequences that preceded these genes were later determined to confer urea inducibility on the operon (167), resulting in identification of UreR, a 33.4-kDa helix-turn-helix AraC family member responsible for urea induction of the operon.

Regulation by UreR

UreR is a dimer that binds to two sites within the *ureR-ureD* intergenic region at a consensus binding site of $T^{A}/_{G}{}^{T}/_{C}{}^{A}/_{T}{}^{T}/_{G}{}^{C}/_{T}T^{A}/_{T}{}^{T}/_{A}ATTG$ as predicted from DNase I protection assays (168). UreR binds to these sites in a urea-dependent manner to activate expression of the urease operon. In the absence of urea, there is no measurable binding or induction of urease expression.

Regulation by H-NS

A poly(A) tract nucleotide sequence of $A_6TA_2CA_2TGGTA_5GA_6TGA_5$ is present 16 bp upstream of the *ureR* promoter, which serves as a binding site for the gene repressor histone-like nucleoid structure protein (H-NS) (169, 170). Using a *ureR-lacZ* reporter plasmid, it was determined that H-NS represses transcription of *ureR*, and therefore represses urease expression (169, 171). H-NS and UreR compete for binding the *ureR-ureD* intergenic region, and culture conditions dictate whether the operon will be repressed or activated. H-NS binding is favored at 25°C and in the absence of urea, while UreR binding and derepression of the operon is favored at 37°C when urea is present (171).

Role in virulence

Urease is a critical virulence determinant for *P. mirabilis* urinary tract infection. Indeed, the first targeted mutation of this species involved the mutation of *ureC*, the major structural subunit of the apoenzyme (40). The ID_{50} of the *ureC* mutant is approximately 3 logs higher than the parental strain, clearly indicating the contribution of urease to disease severity. In an independent challenge with 10^9 CFU of the wild-type strain or the *ureC* mutant, the mutant was attenuated by approximately 2 logs in the bladder and kidneys 48 h postinoculation and up to 6 logs by 7 days postinoculation (39, 40). Infection with the *ureC* mutant also resulted in significantly less pathology in the bladder and kidneys of infected mice. It was later shown that a *ureR* mutant lacking urea induction of urease synthesis also resulted in attenuation by >3 logs in the bladder and kidneys (172).

The contribution of urease to pathogenicity has also been assessed in the uncomplicated murine model of UTI compared to a model of catheter-associated UTI (CAUTI), in which a catheter segment is placed in the bladder during inoculation (25). These studies determined that urease significantly contributes to cystitis in both models, but does not play as dramatic a role in pyelonephritis in the CAUTI model. However, urease activity strongly correlated with renal tubule damage and nephrosis during both UTI and CAUTI in this study.

Potentiation of urease activity during polymicrobial infection

Urine colonization in catheterized individuals is frequently polymicrobial, and *P. mirabilis* is one of the most common organisms present during polymicrobial colonization and CAUTI (4, 8, 9, 17). It is therefore noteworthy that co-culture with other uropathogens can enhance production of active urease enzyme by *P. mirabilis* (25, 41). In addition

to *P. mirabilis*, the most common CAUTI uropathogens are *Enterococcus* species, *E. coli, Pseudomonas aeruginosa*, and *K. pneumoniae*, and multiple isolates of all four species are capable of enhancing *P. mirabilis* urease activity (25). This has important implications for the pathogenesis of polymicrobial CAUTI, because enhanced urease activity resulting from coculture of *P. mirabilis* and *P. stuartii* was determined to significantly impact disease severity, being directly associated with increased urine pH, greater incidence of urolithiasis and bacteremia, and induction of a more potent and destructive inflammatory response (25, 41).

Urease inhibitors

Because of the important role of urease during *P. mirabilis* pathogenesis in the urinary tract, urease inhibitors have been explored as a potential therapeutic (173). Such inhibitors include hydroxamic acids, which bind the nickel atoms in the urease active site, and acetohydroxamic acid (AHA), a structural analog of urea. AHA is the only analog to have been tested in clinical trials and be approved by the Food and Drug Administration. However, while it showed efficacy for preventing urolithiasis (174–176), it has potentially severe side effects that limit its clinical use (177). Thus, further research is necessary to identify safe and effective urease inhibitors. It is also worth noting that, while the *ure* operon is urea inducible, structural analogs of urea such as AHA do not induce urease expression (178).

Secretion Systems

P. mirabilis secretes proteins via type I, III, IV, V, and VI systems as well as the Sec pathway and Twin Arginine Targeting (Tat) system. These pathways are predicted from the genome sequence (107), as analyzed by KEGG pathways (179) and from the individual studies described below. While examples of secreted proteins can be found for the systems noted, only a few examples of secreted proteins that have been tested for their contribution to virulence have been documented.

Proteases

In an early study, it was found that 90 to 94% of 48 *P. mirabilis* strains secreted proteolytic enzymes, detected at pH 8 by using gelatin as substrate. A correlation between the ability to swarm and protease secretion was noted. These proteases were all EDTA-sensitive metalloproteinases (180). However, the specific secretion systems involved in secretion of these proteases were not determined in this study.

Type III secretion

Nucleotide sequencing of the genome of *P. mirabilis* HI4320 (107) revealed genes appearing to encode a type III secretion system on a low GC-content pathogenicity island (143). A cluster of 24 genes clearly has the potential to encode an intact T3SS with genes for an intact needle complex and at least two effector proteins and their chaperones. The genetic organization of the T3SS is similar to that of *Shigella flexneri*, there was no evidence of mutation of the genes resulting in inactivation of the system, and RT-PCR analysis demonstrated that these genes were expressed in *P. mirabilis* HI4320. However, mutation of two genes including a putative ATPase and negative regulator of T3S had no effect on the secreted protein profile when compared to the wild-type strain (143). Furthermore, in the murine model of ascending UTI, there was no difference in CFUs between the mutant and wild-type strain in urine, bladder, or kidneys during either independent infection or cochallenge. Thus, no pathogenicity phenotype for the T3SS was identified for *P. mirabilis* HI4320 during ascending UTI. However, two components of the T3SS (PMI2688 and PMI2696) were identified as significant fitness factors during polymicrobial CAUTI by Tn-Seq (124), indicating that the T3SS may be involved in mediating host-microbe interactions during polymicrobial infection.

Type V secretion

There are three subclasses of type V secretion systems (Va, Vb, and Vc), and the nucleotide sequence of *P. mirabilis* HI4320 predicts members of all three (107, 181, 182).

Classical autotransporters (Va)

Classical autotransporters are a family of virulence proteins in Gram-negative pathogens that contain three domains: an amino-terminal leader peptide for export across the inner membrane via the Sec pathway, a surface-localizing passenger domain, and a carboxy-terminal domain for translocation across the outer membrane (181). One of the three predicted classical autotransporters encoded by *P. mirabilis* HI4320 has been studied in detail: *Proteus* toxic agglutinin (*pta*) encodes a serine protease that was previously identified as an immunogenic outer membrane protein (183) (*see* **Toxins** section). The 117-kDa protein has a 58-amino-acid-long signal peptide, a 75-kDa-long N-terminal passenger domain, and a 30-kDa C-terminal translocator (105). The autotransported protease, either cell associated or secreted, has

cytotoxic effects on cultured bladder and kidney epithelial cells. Catalytic residues Ser366, His147, and Asp533, when mutated, abolish protease activity. The protein also has autoaggregation properties not associated with the proteolytic activity. Virulence of a protease mutant, as tested in the murine model of ascending UTI, was significantly reduced.

Two-partner secretion (Vb)

P. mirabilis hemolysin, encoded by *hpmA*, is exported by the protein product of *hmpB* via the type Vb two-partner secretion pathway. This requires sequential unfolding of the HpmA protein (184), for which a partial crystal structure has been solved (185). Two polypeptides, HpmB and HpmA, synthesized in that transcriptional order, are responsible for hemolysin activity of *P. mirabilis* (*see* **Toxins** section). A Fur-binding site upstream of *hmpB* overlapping the −35 site of the promoter indicates that expression is governed by iron concentration. HpmB and HpmA have 17- and 29-amino-acid leader peptides, confirmed for purified HpmA. HpmB is necessary for secretion of HpmA. HpmB and HpmA are most similar with respect to amino acid sequence to the *Serratia marcescens* hemolysin proteins ShlB and ShlA, respectively (186).

Trimeric autotransporters (Vc)

P. mirabilis HI4320 encodes three putative trimeric autotransporter proteins (107). Two of these, AipA and TaaP, are annotated as "adhesin-like" and "agglutinating adhesin-like." Based on their homology with other trimeric autotransporters, the two autotransporters would contain four antiparallel β-sheets and form homotrimers. Recombinant AipA and TaaP bind extracellular matrix proteins, produce polypeptides of 28 kDa and 78 kDa, respectively, and form high-molecular-weight homotrimers. A 51-amino-acid invasin-like motif of AipA is necessary for function. Gly247 in AipA and Gly708 in TaaP are required for trimerization and activity. AipA and TaaP confer an advantage at 7 dpi during cochallenge in the murine model of ascending UTI.

Type VI secretion

P. mirabilis has long been observed to distinguish between disparate strains when swarming on agar surfaces, and there is now substantial evidence that this phenomenon is mediated by type VI secretion systems (T6SS). The discovery of T6SSs in *P. mirabilis* stemmed from an unusual observation about this species. The Dienes phenomenon, first described in 1946 by Louis Dienes, refers to the fascinating ability of two *P. mirabilis* swarming colonies of a single strain to merge with each other, while swarms of different strains form a line of demarcation where they meet (187) (Fig. 17). Formation of the Dienes line requires direct cell-cell contact by living bacteria, and involves killing of at least one strain at the boundary (188) (Fig. 18).

The structural components of the T6SS are Hcp and VgrG, which comprise the hollow tube and puncturing

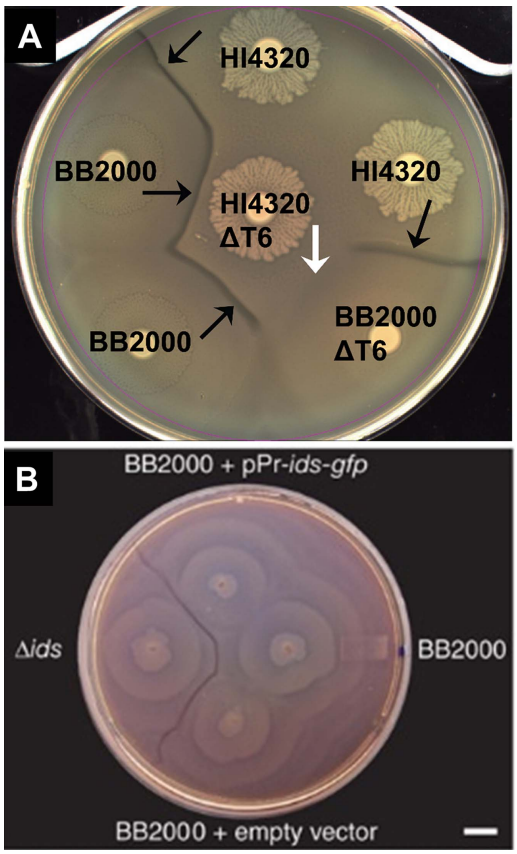

Figure 17 Contact-dependent preemptive antagonism is dependent on the T6SS. (A) A Dienes line (black arrows) forms between two different wild-type isolates, HI4320 and BB2000 (strain A and B kill each other). Loss of the T6SS (ΔT6) in either isolate by disruption of PMI0742 does not affect the discriminatory Dienes line (strain A kills strain B or strain B kills strain A). Loss of the T6SS in both isolates allows nonidentical swarms to merge, and the lack of T6SS-dependent killing appears as recognition (white arrow). (B) Swarm plate of the wild-type strain BB2000, BB2000 *idsABCDEF* deletion mutant (Δ*ids*), and BB2000 with the *idsA-gfp* vector pKG100 (labeled pPr-*ids-gfp*) or with an empty vector. A visible boundary formed between swarms of the wild type and the deletion mutant. Swarms of the wild type merged regardless of the presence of pKG100. Scale bar = 1 cm. Figure adapted, with permission, from reference 114 (A) and reference 189 (B).

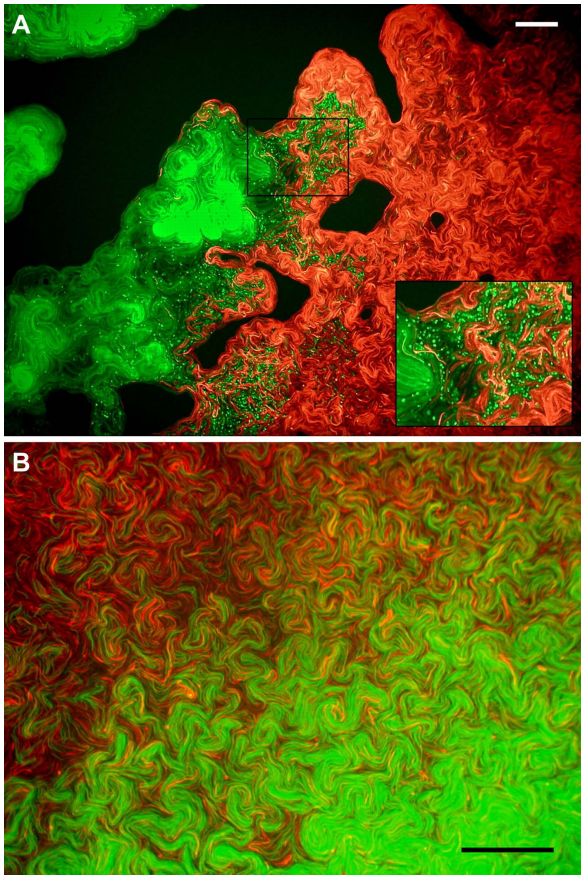

Figure 18 Incompatible Dienes types have distinctive reactions when swarming colonies meet. (A) A *P. mirabilis* strain expressing red fluorescent protein (DsRed) (2R) intersecting with a strain expressing green fluorescent protein (GFP) (3G). Strain 3G produces round cells, whereas strain 2R produces no round cells. The dark areas are agar with no growth. Magnification, ×400. (Inset) Intersection and rounded cells in more detail (magnification, ×800). (B) Intersection zone for strain 2 expressing either GFP or DsRed (2G and 2R) without boundary formation or rounded cells (magnification, ×1,000). Scale bars = 50 μm. Figure adapted, with permission, from reference 188.

tip of the apparatus, VipA and VipB (or TssBC) that form the tube-like structures or sheath of the apparatus, and ClpV to mediate ATP hydrolysis for polysheath disassembly (115). Work conducted in *P. mirabilis* strain BB2000 identified an operon that contributed to Dienes line formation, named *ids* for identification of self (150), which was found to encode Hcp and VgrG (150) and, therefore, provided the first link to T6S and Dienes line formation. Further investigations in *P. mirabilis* strains BB2000 and HI4320 determined that formation of the Dienes line represents either T6S-mediated killing of one strain by the other, or both strains killing each other using T6SSs (113, 114).

Using a transposon screen for *P. mirabilis* HI4320 mutants that failed to kill opposing strains, a 33.5-kb region of chromosome, different from the Ids locus, was identified as harboring the T6SS apparatus (PMI0749-PMI0733) and the primary effector operon (*pefABCDEFG*) (PMI0750-PMI0758) of this strain (114). This operon was found to encode a single immunity protein, PefE, which was responsible for providing immunity from killing by the Pef effectors. However, strain HI4320 was also found to encode at least four other potential T6S effector operons that could use the T6S apparatus, including *idsABCDEF* (150, 189) and three additional operons (PMI0207-PMI0212, PMI1117-PMI1121, and PMI1332-PMI1324) (107, 114) (Fig. 19). Differential use of these systems or possibly even recombination between them may therefore contribute to the wide range of strain-killing activities and Dienes types exhibited by *P. mirabilis* isolates.

A direct role for any individual *P. mirabilis* T6S operon during infection has yet to be elucidated. For instance, none of the T6S operons encoded by *P. mirabilis* HI4320 exhibited fitness defects in the murine model of CAUTI by transposon insertion-site sequencing (Tn-Seq) of monospecies infection. However, all the known *P. mirabilis* T6S operons were strikingly overrepresented as fitness factors during coinfection with *P. stuartii* (124), indicating a potential role for T6S in mediating competitive and cooperative interactions during polymicrobial infection. It remains to be determined if this system is important for mediating microbe-microbe interactions or microbe-host interactions in this infection model.

Toxins

Although the complete genome sequence of *P. mirabilis* strain HI4320 revealed numerous potential toxins, only three have been well characterized for a role in virulence. These are hemolysin, *Proteus* toxic agglutinin, and the ZapA metalloprotease.

Hemolysin

Secreted pore-forming toxins are a common feature of pathogenic bacteria. In particular, hemolysins are secreted pore-forming toxins that insert into eukaryotic cell membranes, causing efflux of sodium ions and cell damage (190). Two hemolysins have been described for members of the *Proteus* genus (191), one that is calcium dependent and similar to the α-hemolysin of *E. coli* (*hlyA*), and another that is calcium independent. The calcium-independent hemolysin is encoded by two genes

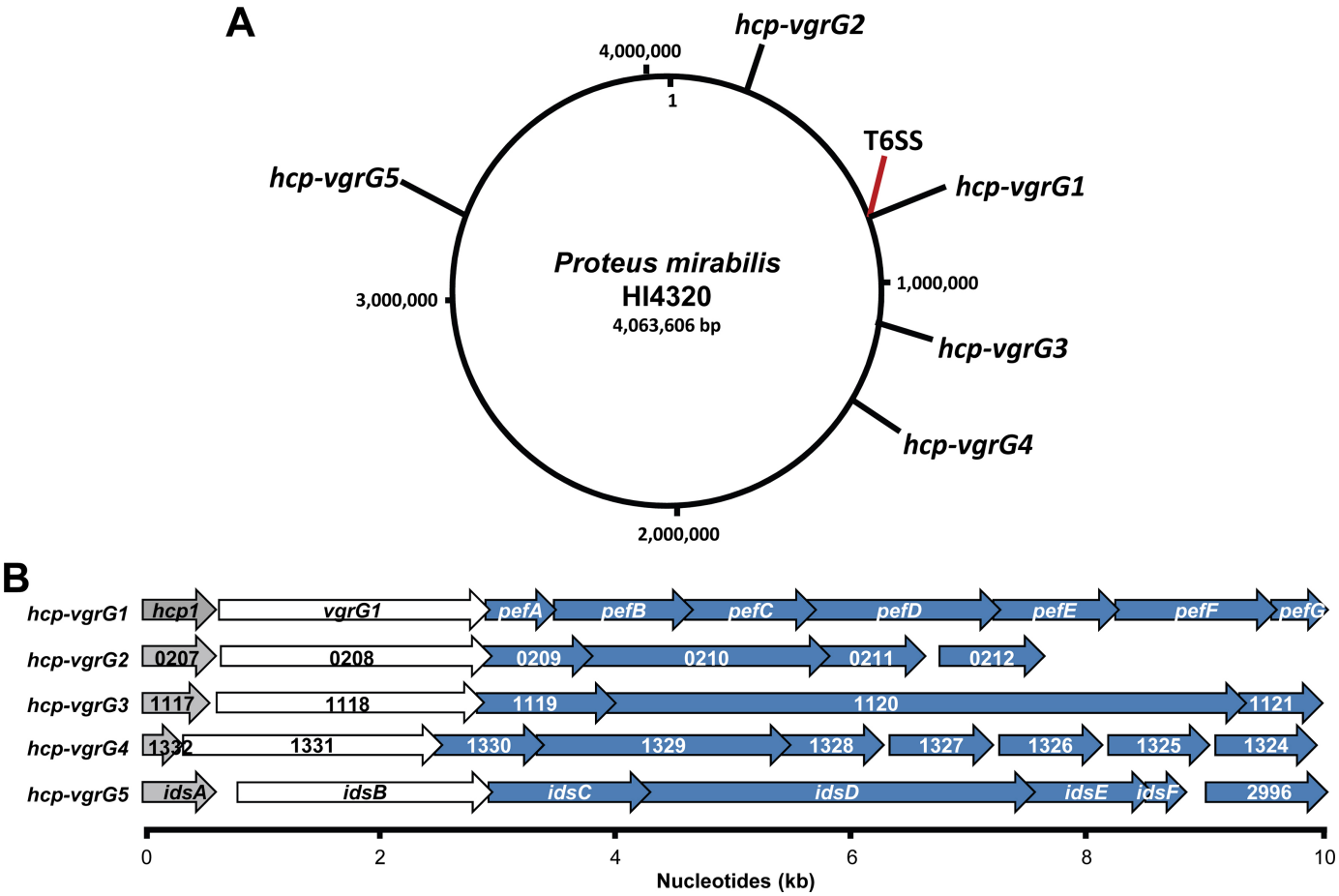

Figure 19 The *P. mirabilis* HI4320 genome contains one primary and four orphan *hcp-vgrG* effector operons that are expressed during swarming. (A) A circular representation of the *P. mirabilis* HI4320 genome depicting the location of the primary *hcp-vgrG* effector operon (*hcp-vgrG1*), divergent T6SS, and the four orphan *hcp-vgrG* effector operons (*hcp-vgrG2-5*). (B) PMI0750 to PMI0758 encode the primary *hcp-vgrG1* effector operon (*pef*) adjacent to the T6SS operon; PMI0207 to PMI0212 encode the *hcp-vgrG2* effector operon; PMI1117 to PMI1121 encode the *hcp-vgrG3* effector operon; PMI1332 to PMI1324 encode the *hcp-vgrG4* effector operon; and PMI2990 to PMI2996 are the *ids* operon (*hcp-vgrG5*). Genes with homology to *hcp* (gray), *vgrG* (white), and predicted T6SS effectors (blue) are shown. Reproduced from reference 114, with permission.

comprising a two-partner secretion system: *hpmA*, which produces a 166-kDa secreted exoprotein, and *hpmB*, which produces a 63-kDa translocase protein that is required for both the activation and secretion of HpmA through cleavage of an N-terminal peptide (186). HpmA is the predominant hemolysin in *Proteus* species and appears to be the only hemolysin encoded by *P. mirabilis*, present in 268/274 (98%) of *P. mirabilis* clinical and fecal isolates from Brazil and the United States while none of these isolates encoded *hlyA* (97, 98). Similarly, *hpmA* is present in all 7 complete *P. mirabilis* genome sequences available through NCBI as of May 2017. An N-terminal fragment of HpmA, called HpmA265, has been crystallized and its structure solved (Fig. 20) (185). This fragment lacks the C-terminal pore-forming domain, but can

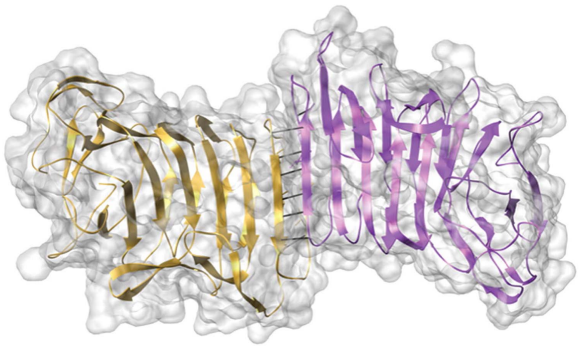

Figure 20 HpmA265 crystallographic dry dimer interface leads to a filamentous appearance. Solid lines represent hydrogen bonds shared between β23 strands of both subunits. Reproduced from reference 185, with permission.

still activate full-length HpmA in the absence of HpmB when the proteins are mixed with erythrocytes. The formation of HpmA265 dimers suggests that full-length HpmA may also function as a dimer.

HpmA mediates lysis of a broad range of cell types from numerous host species and appears to be the primary *P. mirabilis* virulence factor responsible for cytotoxicity to human renal proximal tubular epithelial cells (HRPTECs) (48, 51, 53, 192). Deletion of *hpmA* dramatically decreases cytotoxicity, and allows for internalization of *P. mirabilis* by HRPTECs *in vitro* (48, 53). Because HRPTECs form a protective barrier for the kidney parenchyma, it was hypothesized that hemolysin may be a critical virulence factor that mediates spread of *P. mirabilis* into the kidneys and development of pyelonephritis (28). However, deletion of *hpmA* does not appear to impact tissue colonization or damage during independent challenge in the murine model of ascending UTI (44, 47, 192), indicating that either hemolysin has less of an impact during experimental infection than the *in vitro* cell culture studies suggest, or the activity of other virulence factors mask its contribution *in vivo*. In agreement with this finding, *hpmBA* was not identified as a fitness factor for UTI or CAUTI in any of the genome-wide transposon mutagenesis studies (103, 124, 154, 155), likely because of a combination of complementation *in trans* by the other hemolysin-producing transposon mutants present during infection and possibly production of other cytolysins with similar functions.

Proteus toxic agglutinin

The genome of *P. mirabilis* strain HI4320 encodes six putative autotransporters (107) (*see* **Secretion Systems** section), of which only the *Proteus* toxic agglutinin (Pta) has been fully characterized. Pta was initially identified as an outer membrane surface-expressed protein recognized by the murine immune system (183), and determined to be encoded within the integrative and conjugative element ICE*Pm1* in *P. mirabilis* strain HI4320 (102) (*see* **ICE*Pm1*** section).

Pta is a 120-kDa protein that is catalytically processed to become a ~110-kDa active protein within the outer membrane (105). Expression of this protein in *E. coli* promotes autoaggregation of the bacteria, as well as lysis of bladder epithelial cells *in vitro*. Both properties of Pta require translocation to the outer membrane and cytotoxicity requires serine protease activity from the passenger domain, but protease activity is not required for autoaggregation. Pta is also classified as a subtilisin-like alkaline protease owing to the observation that expression of *pta* is induced by alkaline pH and protease activity is maximal at pH 8.5 to 9.0, conditions that would be encountered by *P. mirabilis* during urinary tract infection due to its urease activity.

Pta contributes to colonization of the bladder and kidneys in a murine cochallenge model of ascending UTI, as well as dissemination to the spleen (105). Interestingly, HpmA and Pta have an additive effect on cytotoxicity both *in vitro* and during experimental UTI, particularly with respect to cystitis and possibly interstitial nephritis (47). However, Pta appears to be the more potent toxin during experimental infection, because the disruption of *pta* has a much greater impact on infectivity than loss of *hpmA*. Similar to *hpmA, pta* is present in all seven of the complete *P. mirabilis* genome sequences in NCBI as of May 2017, and was also encoded in eight *P. mirabilis* infection and fecal isolates (47).

ZapA metalloprotease

P. mirabilis produces a metalloprotease with broad specificity, originally thought to be an IgA protease but later determined to be capable of cleaving IgA, IgG, secretory component (the heavily glycosylated protein that complexes with dimeric and polymeric IgA), antimicrobial peptides hBD1 and LL-37, complement protein C1q and C3, fibronectin, actin, collagen, laminin, casein, and gelatin (193–197). In all cases, cleavage was sensitive to the metal chelator EDTA, indicating that the enzyme is a metalloprotease. This protease was identified as a 55-kDa metalloprotease of the serralysin family, encoded by *zapA* (198).

The contribution of ZapA to pathogenicity has been explored both *in vitro* and *in vivo*. Intact IgG and IgA1 can interact with Fc receptors on neutrophils to stimulate a respiratory burst, and this process is significantly reduced when IgG has been cleaved into Fab and Fc fragments *in vitro* by the *P. mirabilis* metalloprotease (196). Similarly, cleavage of hBD1 and LL-37 by ZapA reduces their antimicrobial activity (197). Thus, ZapA may contribute to evading the innate immune response during infection. A ZapA-deficient mutant, specifically constructed by insertional inactivation of *zapA* in the chromosome of *P. mirabilis* BB2000, was used to assess virulence in the murine model of ascending UTI (129).

CBA mice were transurethrally inoculated into the bladder with 10^6 CFU *P. mirabilis* BB2000 or the *zapA* mutant. After 7 days, quantitative cultures indicated that the *zapA* mutant was dramatically attenuated (by 3 logs in the urine and 5 logs in the bladder or kidney), indicating that the protease contributed strongly to virulence of *P. mirabilis* BB2000. The same wild-type and mutant pair was tested in a rat model of prostatitis (199). Unlike the wild type, inoculation of the *zapA* mutant resulted in reduced levels of acute prostatitis as determined by lower levels of tissue damage, bacterial colonization, and inflammation (Fig. 21).

Integrative and Conjugative Element ICE*Pm*1

Pathogenicity islands (PAIs) are a specific group of genomic islands that contribute to genomic variability and virulence of bacterial pathogens. PAIs carry virulence determinants and are typically present in pathogenic strains but absent in nonpathogenic strains of the same species. These islands consist of large genomic regions ranging from 10 to 200 kb, and often have different G+C contents compared to the host. They also frequently contain mobile genetic elements, are flanked by direct repeat sequences, have mosaic-like structure, insert at the site of tRNA genes, and have likely been acquired by horizontal gene transfer (200, 201).

A subset of PAIs has been identified that can excise from the bacterial chromosome, following a recombination event at the site of direct repeats flanking the island, and actively transfer via a type IV secretion system to another bacterium. These are called *Integrative and Conjugative Elements* (ICE), and many *P. mirabilis* strains carry an ICE designated ICE*Pm*1 (102) (*see* **Comparative Genomics** section).

ICE*Pm*1 is a 94-kb region with a G+C content of 44.84%, which differs substantially from that of the *P. mirabilis* genome (38.88%) (102, 107), and contains core modules and a syntenic structure consistent with prototypical ICEs (108, 202) (Fig. 22). Direct repeats flank ICE*Pm*1, and at the left-most end the 52-bp direct repeat is located with the 5′-coding end of $tRNA_{Phe}$ gene (*attL*). The direct repeat at the right-most end (*attR*) is part of the 3′ end of a truncated $tRNA_{Phe}$ gene. In the genome of *P. mirabilis* HI4320, ICE*Pm*1 is annotated as being integrated into the phenylalanine tRNA gene *pheV*. However, ICE*Pm*1 can integrate into either *pheV* or *pheU* sequences (106).

ICE*Pm*1 contains 91 open reading frames, with the core genes constituting putative integration, replication, and conjugative modules, including an integrase, genes for a putative tyrosine-like recombinase, putative helicase that could act as a relaxase, six transposases, and five plasmid-transfer-related proteins (102). A 26-gene region encodes eight putative exported proteins and nine putative membrane proteins comprising the T4SS.

ICE*Pm*1 also encodes known "cargo" genes that contribute to virulence, interspersed between the core modules. These cargo genes include the *nrp* operon (PMI2596-

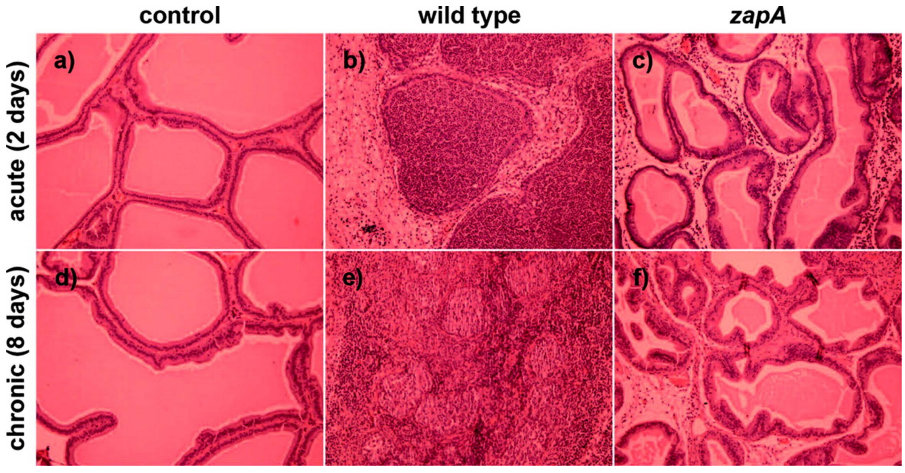

Figure 21 Tissue histology of acute and chronic *P. mirabilis* prostate infections. (a to c) Hematoxylin and eosin-stained rat prostate sections, showing the typical appearance of saline-treated controls (a) and WT (b)- and ZapA$^-$ mutant (c)-infected prostate tissue in acute infection. (d to f) Histology of chronic infection for saline controls (d), WT infection (e), and ZapA$^-$ mutant infection (f). Reproduced from reference 199 with permission.

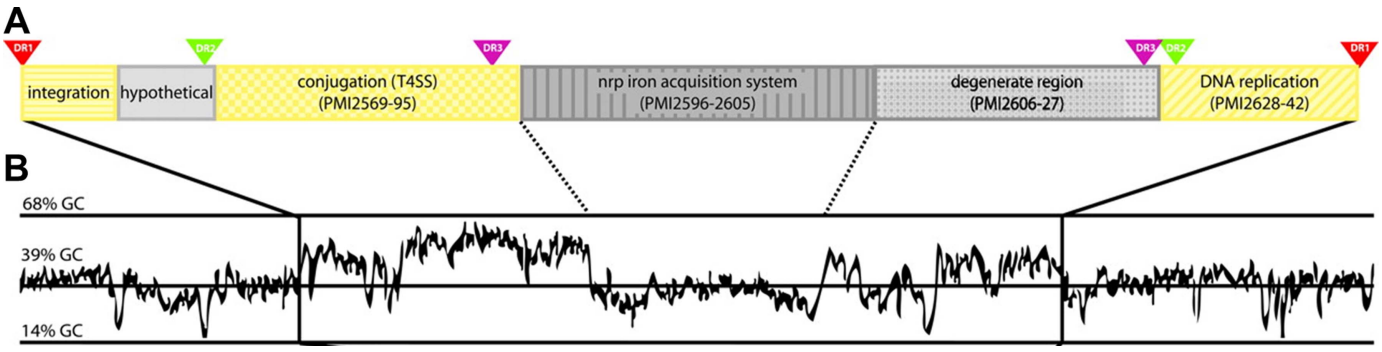

Figure 22 Characteristics of ICE*Pm*1. (A) Modular structure of ICE*Pm*1. Modules in yellow represent core modules; variable regions are depicted in gray. Direct repeats (DRs) are represented as triangles. (B) G+C content of ICE*Pm*1 and the flanking chromosome. Boundaries of ICE*Pm*1 are denoted by vertical black lines. Horizontal lines represent G+C content, with the middle line representing 39% G+C (that of the *P. mirabilis* HI4320 genome). DRs show the modularity of the island and suggest the evolutionary history of acquisition of regions of ICE*Pm*1. Reproduced from reference 102, with permission.

PMI2604), which encodes genes for the synthesis, transport, and uptake of an iron siderophore (*see* **Metal Acquisition** section), and *Proteus* toxic agglutinin (Pta), which contributes to aggregation of *P. mirabilis* and represents a potent autotransported protease toxin (46, 104, 105, 183).

Highly conserved homologs of ICE*Pm*1 were present in all 39 *P. mirabilis* urinary isolates tested and were also found in *P. stuartii* (6 of 10 isolates) and *M. morganii* (11 of 38 isolates) from cases of catheter-associated bacteriuria (102). ICE*Pm*1 was also found at a reduced frequency in colonizing isolates of *P. mirabilis* (15 of 23 isolates) that were cultured from the oropharynx, nasopharynx, wound, groin, or perianal area.

When the ICE-encoded integrase is activated, the ICE can excise from the chromosome, form a circular intermediate, and subsequently transfer to a recipient cell via a mating pore formed by the ICE-encoded T4SS (108, 203). Transfers occur at a frequency of 1.35×10^{-5} transconjugants/donor to ICE*Pm*1-deficient *P. mirabilis* (106). Insertional inactivation of a putative integrase gene (PMI2549), a specific recombinase of the tyrosine-like family, on ICE*Pm*1 decreases transfer frequencies to below the limit of detection. Mutation of the relaxase of ICE*Pm*1 also eliminates transfer (106).

Fimbriae and Adhesins

Fimbriae (pili) are hair-like protein structures that extend from the bacterial surface and usually mediate adherence to surfaces. Gram-negative bacteria produce a subset, called chaperone-usher fimbriae for their method of secretion and assembly (204, 205). *P. mirabilis* HI4320 encodes 17 chaperone-usher fimbrial operons (107). Although the function of most of these is not yet defined, transcription has been detected from all 17 operons, and most of these fimbriae are encoded by *P. mirabilis* isolated from diverse sites (Fig. 11) (101). For example, a PCR screen for the predicted major structural subunit gene for each fimbria showed that 85% of clinical isolates encode at least 14 unique fimbriae (101). Of seven clades defined for classical chaperone-usher fimbriae, three are represented in *P. mirabilis* (γ_1, γ_2, and π) (Table 6) (101, 206).

P. mirabilis may produce multiple types of fimbriae at once. For example, at least two fimbrial morphologies have been seen on a single bacterium by transmission electron microscopy (207, 208). In a mass spectrometry study, proteins from 6 of the 17 fimbriae were detected in a sheared surface protein preparation from a single broth culture (MR/P, UCA, PMF, ATF, Fim8, and Fim14) (101). This ability sets *P. mirabilis* apart from other bacteria, such as *E. coli*, that tend to produce one type of fimbria at a time (209). Likewise, *P. mirabilis* devotes a larger share of its chromosome to encoding fimbriae than most other fimbriated pathogens; for example, uropathogenic *E. coli* typically encode 9 to 12 fimbrial operons (93).

Because fimbriae are often found to contribute to virulence, there are multiple studies examining the roles of *P. mirabilis*-encoded fimbriae in UTI (Table 6) (19–20, 210). *P. mirabilis* obtained from healthy stool or diarrhea, urine, or blood can adhere to voided human uroepithelial cells regardless of the bacterial source (211), which is consistent with the conservation of fimbrial genes in this species (101). In general, mutations in

Table 6 Classes of *P. mirabilis* fimbriae and their contribution to virulence

Fimbria	Genes	Class[a]	Implicated in virulence[b,c]							Protein	MrpJ paralog	Ref
			IC	CO	STM	SS CAUTI	CO CAUTI	Exp	*In vitro*			
MR/P′	PMI0254-PMI0261	π				✓	✓				PMI0261	124
MR/P	PMI0262-PMI0271	π	✓	✓			✓	↑	✓	✓*	PMI0271	43, 95, 101, 124, 126, 141, 207, 214, 222, 223, 226, 227, 229–232, 242, 355
Fimbria 3	PMI0296-PMI0304	π					✓				PMI0296	124
UCA	PMI0532-PMI0536	γ_1	✓	✓		✓	✓	↓	✓	✓	PMI0532	101, 124, 126, 225, 233–238
Fimbria 5	PMI1060-PMI1067	π					✓	↓			PMI1060	124, 126
Fimbria 6	PMI1185-PMI1190	γ_1									None	
Fimbria 7	PMI1193-PMI1197	γ_1									None	
Fimbria 8	PMI1464-PMI1470	γ_1						↓		✓	PMI1470	101, 126
PMF	PMI1877-PMI1881	π	✓	✓		✓	✓	↓		✓*	None	101, 124, 126, 213, 214, 241, 242, 248
Fimbria 10	PMI2207-PMI2214	γ_1					✓				PMI2209, PMI2207	124
PMP	PMI2216-PMI2224	π				✓	✓			✓	PMI2224	124, 245
Fimbria 12	PMI2533-PMI2539	γ_2					✓				None	124
ATF	PMI2728-PMI2733	γ_1	⊘	⊘			✓			✓	PMI2733	101, 124, 244
Fimbria 14	PMI2997-PMI3003	ND			✓		✓	↑		✓	PMI3003	101, 124, 126, 154
Fimbria 15	PMI3086-PMI3093	π					✓	✓			None	124, 126
Fimbria 16	PMI3348-PMI3352	γ_1					✓				None	124
Fimbria 17	PMI3435-PMI3440	γ_1					✓				None	124

Table adapted from reference 19.

[a]Greek classification was determined as in references 206 and 100. The operon encoding Fimbria 14 lacks a chaperone, and thus cannot be classified in the Greek system.

[b]The mutant was tested in: IC, independent challenge experiment; CO, cochallenge experiment; STM, signature-tagged mutagenesis experiment; SS CAUTI, Tn-Seq CAUTI model with *P. mirabilis* alone; CO CAUTI, Tn-Seq CAUTI model during coinfection with *Providencia stuartii*; Exp, expressed *in vivo*; *in vitro*, virulence attributes (e.g., cell adherence, hemagglutination) detected using *in vitro* assays.

[c]✓, positive for the trait; ⊘, negative for the trait; ↑, induced *in vivo* compared with *in vitro* culture; ↓, repressed *in vivo* compared with *in vitro* culture.

*Immunogenic.

individual fimbrial genes result in bacteria that are still able to colonize the urinary tract, but are less fit in direct competition cochallenge experiments (212–214). This suggests that the 17 fimbriae have overlapping or redundant functions. Furthermore, as surface-localized, abundant, immunogenic proteins, *P. mirabilis* fimbriae have been tested as vaccine candidates with some success (*see* **Vaccines** section) (215–219).

Mannose-resistant *Proteus*-like fimbriae (MR/P)

These are the most extensively studied of the fimbriae encoded by *P. mirabilis*. MR/P fimbriae were originally

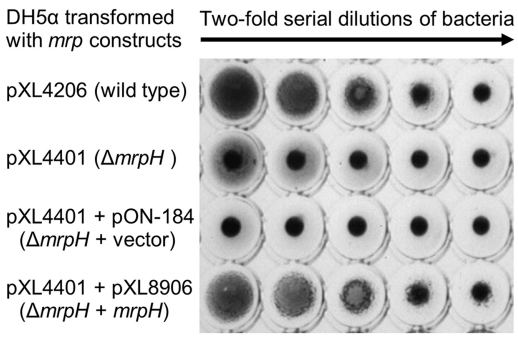

Figure 23 Mannose-resistant hemagglutination (MRHA) patterns of MR/P fimbriae expressed in *E. coli*. *E. coli* DH5α expressing the entire *mrp* operon under its native promoter (*mrpA-J*) (pXL4206), *mrp* minus *mrpH* and *mrpJ* ("Δ*mrpH*"; pXL4401), Δ*mrpH* plus empty vector (pON-184), or Δ*mrpH* plus complemented *mrpH* (pXL8906) were cultured in Luria broth at 37°C and mixed with chicken erythrocytes. MRHA only occurs when MR/P tip adhesin MrpH is present. Figure adapted, with permission, from reference 221.

named for their ability to agglutinate untreated erythrocytes in the presence of mannose, a trait that was frequently found in *P. mirabilis* isolates (207) (Fig. 23). This was in contrast to mannose-sensitive agglutination, e.g., type 1 fimbriae from *E. coli*, or mannose-resistant *Klebsiella*-like (MR/K) agglutination, which occurred in the presence of tannic acid-treated bovine erythrocytes (220). MrpA is the major structural subunit of the fimbria, and MrpH is a two-domain adhesin that is located at the tip of MR/P fimbriae. Extensive details on MR/P structure and assembly have been recently reviewed elsewhere (19).

Expression

The *mrp* gene cluster consists of two transcripts. Genes required for fimbrial structure and assembly are encoded by *mrpABCDEFGHJ* (221). The last gene, *mrpJ*, encodes a transcriptional regulator and is discussed later. The second transcript comprises a single gene, *mrpI*, which is divergently transcribed from the rest of the *mrp* genes (222). MrpI is a recombinase that flips a 252-bp invertible element containing the *mrpABCDEFGHJ* promoter (222). The transcriptional start site lies within the invertible element (127), and thus the orientation of this element dictates whether or not *mrp* fimbrial genes are transcribed. MrpI is the sole recombinase for the invertible element, and therefore mutations in *mrpI* result in bacteria that either constitutively produce MR/P fimbriae ("locked on") or are devoid of MR/P fimbriae ("locked off") (223). The orientation of the element may be easily detected using PCR-based assays (Fig. 24A), and phase variation of MR/P fimbriae has been observed at the single-cell level (Fig. 24B).

The nine genes in the *mrp* operon are the most highly induced genes by bacteria in urine collected from experimentally infected mice compared with *in vitro* broth culture (126). Correspondingly, even when mice are infected with *P. mirabilis* cultured so the population is almost completely phase off, after 7 days, the majority of the bacteria have the invertible element in the on orientation (222). MR/P fimbriae are produced at a relatively low level *in vitro*, with the highest amounts produced during 48-h static culture in broth or culture under 5% oxygenation, followed by aerated broth, and finally, growth on an agar surface (224–226). Expression of *mrp* genes is both induced and subject to positive selection in a 5% oxygen atmosphere, which is logical for a virulence factor given reduced oxygen availability in the bladder (226). That is, an *mrp* locked on mutant outcompetes locked off in broth, and, at the same time, *mrpA* expression increases during oxygen limitation (226). Transcription of the recombinase *mrpI* may also be regulated by oxygen levels (226). Furthermore, orientation of the invertible element is influenced by the bacterium's ability to assemble fimbriae. Assembly requires disulfide bond formation, and mutation of the gene encoding thiol:disulfide interchange protein DsbA leads to an increase in element-off bacteria (226).

In vitro function

In addition to hemagglutination, MR/P fimbriae mediate *in vitro* phenotypes that give clues to their function during infection. Biofilm formation (*see* **Biofilms** section), measured in plastic multiwell plates, on glass coverslips, as pellicles in culture tubes, or in static cultures in glass tubing, is dependent on MR/P fimbriae (221, 227, 228). Interestingly, phase variation contributes to biofilm development. MR/P locked on bacteria establish biofilms more rapidly than wild type, but over time the wild-type biofilm is much thicker (65 μm versus 12 μm) and has a classic structured channel appearance (227). In contrast, the locked on biofilm is short, very dense, and lacks channels. MR/P locked on bacteria autoaggregate (226, 227), which is reminiscent of the bacterial clustering that happens prior to stone formation in the bladder (43) (Fig. 25A–D). Furthermore, MR/P fimbriae allow *P. mirabilis* to adhere to some cultured cell lines, including T24 and Vero (229, 230). There are conflicting reports about MR/P-mediated binding to shed bladder epithelial cells, where purified MR/P and MR/P-positive

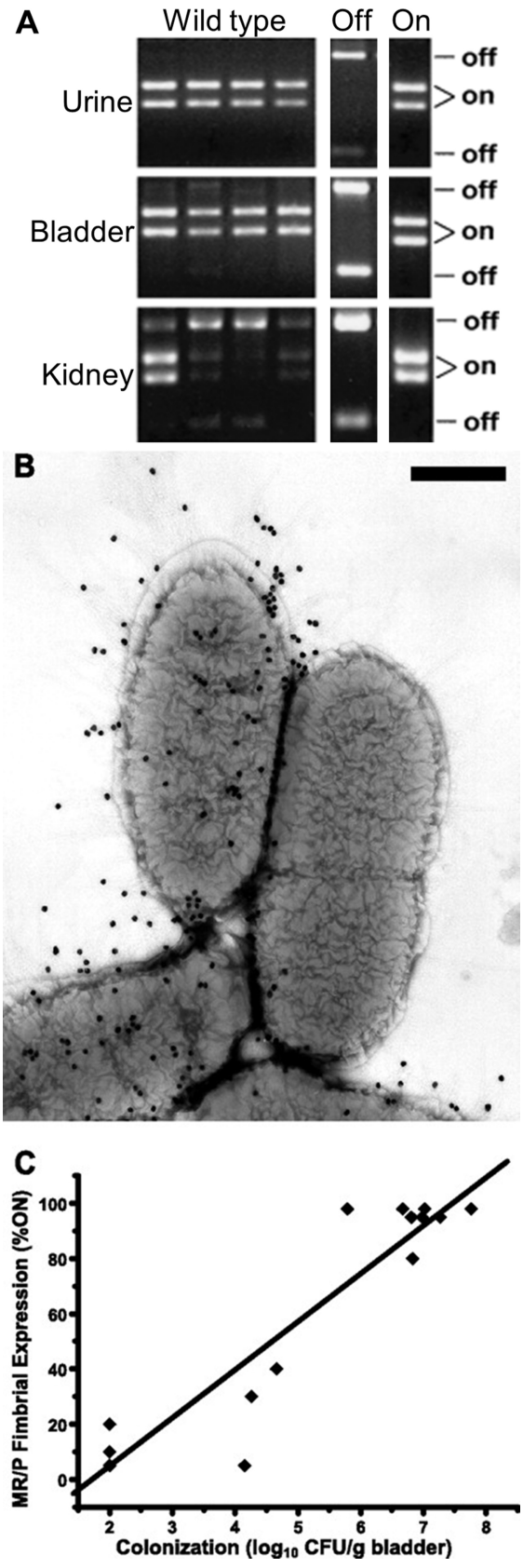

P. mirabilis bound cells (231), but there was no difference in binding between a different wild-type strain and its isogenic *mrpA* mutant (232). It is possible that these two studies were in fact not examining the same fimbria (19).

Contributions to infection

MR/P fimbriae contribute to UTI as described in multiple studies (Table 6). The magnitude of deficiency of an *mrp* mutant in mouse model independent challenges varies from study to study, from the initial *mrpA* experiment, where a 6- to 18-fold decrease was observed in urine, bladder, and kidneys, to a 4 log defect in the bladder for an *mrpG* mutant (141, 214, 232). A mutation in *mrpH*, which encodes the fimbrial adhesin, does not decrease fitness in independent challenge, although the mutant was unrecoverable following a one-week co-challenge experiment (221). Subsequent cochallenge infections with an *mrpA* or an *mrpA-D* mutant likewise resulted in the mutant being significantly outcompeted in both the bladder and kidneys (214, 229).

Newer evidence may explain the observed variability in the requirement for MR/P expression. Two studies have reported equal numbers of recovered bacteria from the bladders of mice infected with wild-type compared with an *mrpA* mutant (43) or *mrp* locked off (227). However, in both studies, the *mrp* mutant was not found in the same location as wild type, suggesting that MR/P fimbriae not only facilitate adherence to urinary tract tissue, but also dictate the localization of *P. mirabilis* within the bladder. Notably, both of these studies used a relatively early endpoint (24 hpi) (43, 227) compared with other mouse independent challenges lasting 7 days (141, 214, 221, 232). Thus, the location of *P. mirabilis* in the urinary

Figure 24 Phase variation of *P. mirabilis* MR/P fimbriae. (A) Urine, bladder and kidney samples were collected at 7 dpi from mice infected with wild-type *P. mirabilis* HI4320, an MR/P locked-off mutant or an MR/P locked-on mutant and subjected to the invertible element (IE) assay. (B) Electron micrograph showing the phase variation of MR/P fimbrial expression in a broth culture of *P. mirabilis*. MrpH, the tip adhesin of MR/P fimbriae, is immunogold labeled. Note that the top left bacterium is gold labeled, while the top right bacterium is unlabeled. Scale bar, 500 nm. (C) Correlation between MR/P fimbrial expression and bacterial colonization in the bladder. Bladders from mice challenged with *P. mirabilis* HI4320 were collected at 7 dpi, and bacteria were both quantitatively cultured and subjected to the IE assay. A positive correlation was found between MR/P fimbrial expression (percentage of IE in the ON orientation; *y* axis) and bacterial colonization in the bladder ($\log_{10}$ CFU/g tissue; *x* axis): $y = 17x - 30$, $r^2 = 0.9$, $n = 18$, $P < 0.0001$. Figure adapted, with permission, from reference 223 (A) and reference 226 (B and C).

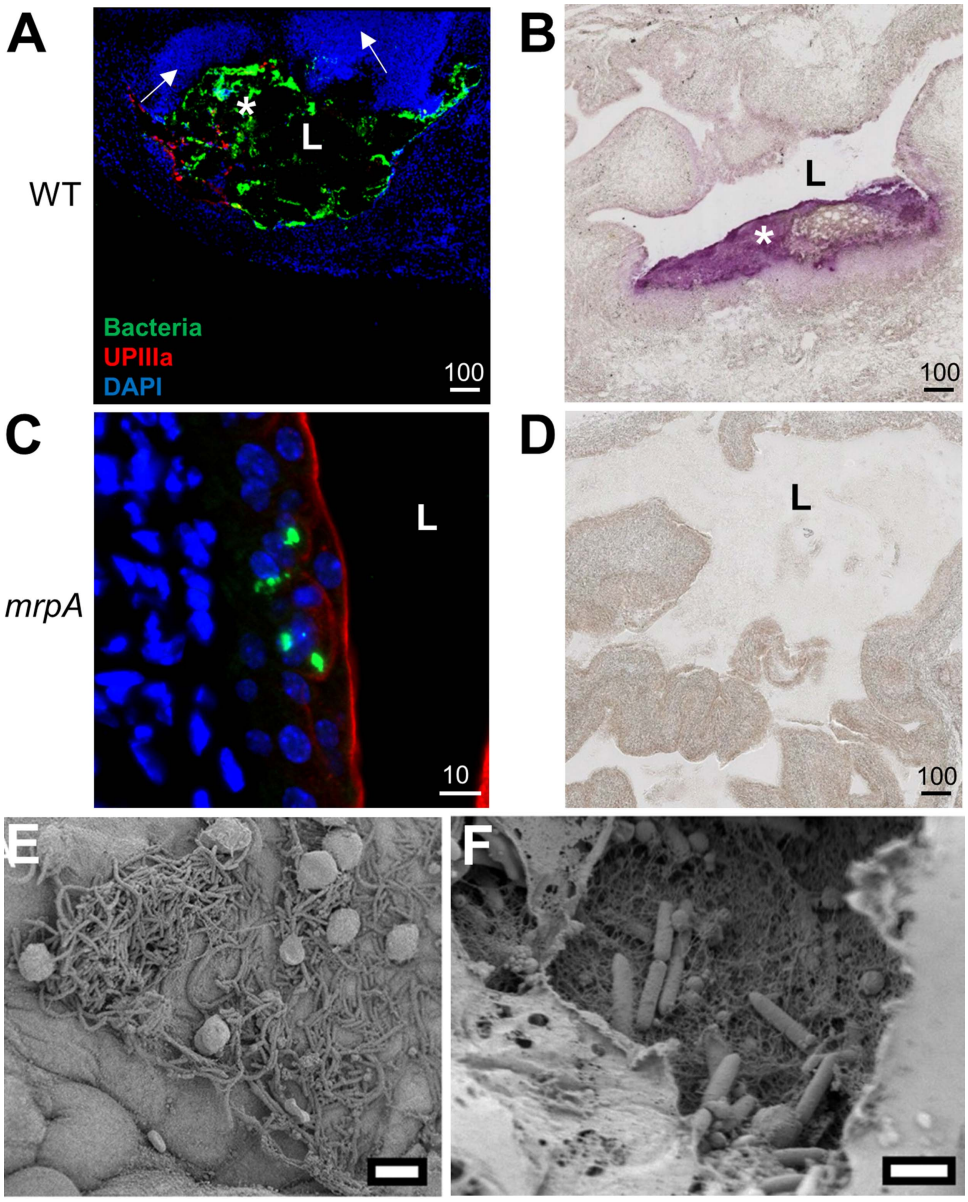

Figure 25 *P. mirabilis mrpA* mutant is defective in cluster formation. (A–D) Representative sections of (A and B) *P. mirabilis* wild-type and (C and D) *mrpA*-infected murine bladders at 24 hpi. (A and C) The wild-type-infected bladder shows a regional view of clusters, whereas the mutant-infected bladder shows a close-up of the urothelial surface. Bacteria are in green, UPIIIa in red, and DAPI in blue. (Scale bars, in micrometers, are as marked.) (B and D) Alizarin Red staining of bladder sections. Only wild-type *P. mirabilis*-infected bladders contain significant mineral deposition. L, bladder lumen; an asterisk indicates an extracellular cluster. Arrows indicate regions with increased DAPI signal. (E and F) Scanning electron micrographs of MR/P ON and MR/P OFF cells colonizing the murine bladder at 4 dpi. MR/P ON colonized the bladder uroepithelium (E), while MR/P OFF colonized the lamina propria where bladder cells had sloughed off (F). Bars = 10 μm (E), 2 μm (F). Figure adapted, with permission, from reference 43 (A–D) and reference 227 (E and F).

tract, whether extracellular, intracellular, or bound to regions where uroepithelial cells have sloughed off, may be important for its long-term survival (Fig. 25E and F).

Although prior studies suggested that MR/P fimbriae bind a receptor in renal cells and contribute to pyelonephritis (231, 232), recent data point to their importance in cystitis. First, when bacteria are isolated from the bladder or urine of infected mice, the invertible element of the *mrp* promoter is overwhelmingly (95 to 100%) in the on orientation, allowing transcription of *mrp* genes. In contrast, the invertible element orientation is highly variable in the kidneys, ranging from mostly on to 85% off (222, 223). Second, the percentage of bacteria with

the *mrp* invertible element in the on orientation directly correlates with the amount of bladder colonization (Fig. 24C) (226). Third, when a locked-on *mrpI* mutant is competed against wild-type bacteria in a 7-day mouse cochallenge experiment, locked-on bacteria outcompete wild type in the bladder but not the kidneys (223). Fourth, *P. mirabilis* locked-on *mrpI* mutants adhere to the luminal surface of the bladder when examined 24 hpi, while locked-off bacteria adhere to regions where umbrella cells have been shed, revealing the lamina propria (227). Fifth, wild-type *P. mirabilis* forms large clusters in the bladder lumen within 24 hpi, but an *mrpA* mutant does not form clusters and is primarily intracellular (43) (Fig. 25A–D). The precise function of MR/P fimbriae and their contributions to cystitis and/or pyelonephritis will be difficult to address until their binding target(s) are identified.

Uroepithelial cell adhesin

A fimbrial preparation from *P. mirabilis* cultured to stationary phase in a minimal medium at 37°C was used to isolate a long, 4-nm-thin protein that adhered to human uroepithelial cells obtained from voided urine (233). The importance of this protein, uroepithelial cell adhesin (UCA), in uroepithelial cell adhesion was subsequently confirmed when a mutation of the gene encoding the major structural subunit of UCA (*ucaA*) was tested with desquamated cells (234).

A second group working on UCA renamed the protein "nonagglutinating fimbriae" (NAF) and found the protein in shear preparations obtained from diverse *P. mirabilis* isolates (235). UCA/NAF are readily expressed under several laboratory conditions at 37°C, including Luria broth or agar; production may be enhanced by addition of serum to Luria broth or during culture on urine agar (225, 235).

Expressing cloned *uca* genes in *E. coli* conferred the ability to bind uroepithelial cells (236). However, no fimbriae were observed on the recombinant *E. coli*; only *ucaA* was sequenced, and it is not clear whether all genes in the *uca* operon were present in the expression construct (236). A UCA/NAF preparation purified from *P. mirabilis* binds to cultured cells, including EJ/28 (urinary carcinoma), HEp-2 (laryngeal carcinoma), and MDCK (canine kidney epithelium) (225, 237), although these results have not been confirmed using other methods, such as by comparing adhesion of a *uca* mutant to that of wild type.

Although UCA fimbriae are encoded by most *P. mirabilis* isolates, their sequence is more variable than other fimbriae (101). Antiserum raised against purified fimbriae further indicated that UCA is widely present but variable in size (235). It is possible that variations in UCA may explain distinct phenotypes reported by different groups, who are typically using locally obtained isolates in their experiments. Notably, the *uca* operon is part of a mobile element and flanked by phage genes; in the first two fully sequenced *P. mirabilis* genomes, HI4320 and BB2000, the *uca* operon is not in the same chromosomal locus (101).

In vitro receptor experiments

A possible receptor for UCA/NAF has been identified using fimbrial protein purified from a shear preparation using differential centrifugation (235, 238). Purified UCA/NAF bound *in vitro* to glycolipids, including asialo-GM_1, asialo-GM_2, and lactosyl ceramide (238). A follow-up study suggested that another molecule, galectin-3, was also a receptor for purified UCA/NAF on MDCK cells (237). The possible receptors have not been identified in healthy bladder tissue, although galectin-3 is a marker for bladder cancer (239). Thus, it is not apparent whether these molecules are true *in vivo* targets for UCA.

Infection studies

Given that bladder cell adherence is a defining feature of UCA, it is perhaps paradoxical that a *ucaA* mutant is significantly attenuated in the kidneys but not the bladder during either independent or cochallenge of the murine urinary tract (234). When this *ucaA* mutant was injected into the tail vein of mice, bacteria were only recoverable from 7/16 mice 7 days postinoculation, while the wild-type parent was recovered from 15/16 mice (234). Transcription of *ucaA* has been detected in urine from infected mice, although the level was 2.5-fold decreased relative to *in vitro* broth culture (126). UCA also contribute to CAUTI, where *ucaA* and *ucaB* were both detected in a Tn-Seq study (124).

P. mirabilis fimbriae

P. mirabilis fimbriae (PMF) were initially identified when a *P. mirabilis* cosmid gene bank was screened using antiserum generated against UCA (224). These fimbriae are encoded by the *pmfACDEF* operon (240). Despite initial speculation that PMF was the unidentified MR/K agglutinin (224), a *pmfA* mutant had no effect on either MR/P or MR/K-type agglutination (213). Nevertheless,

PMF contribute to UTI in mouse models, with an 83-fold decrease in recoverable CFU for a *pmfA* mutant during independent challenge in the bladder (213). The defect was more profound in cochallenge, where the mutant was significantly attenuated in both bladder and kidneys (241). In a hematogenous model, where *P. mirabilis* was introduced through the tail vein of mice, the *pmfA* mutant was unrecoverable from the kidneys of 55% of mice 7 days postinoculation, while the wild-type parent was still recovered from 94% (241). There are conflicting data on whether PMF mediate adherence to voided human uroepithelial cells (213, 241); however, a *pmfA* mutant had diminished adherence to cultured T24/83 bladder carcinoma cells (241). In summary, evidence exists for PMF to contribute to infection in the bladder, kidneys, or both, and the receptor(s) have not yet been identified. PMF also contribute to fitness during CAUTI (124).

Interestingly, although PMF are expressed during UTI and mice infected with *P. mirabilis* generate an immune response against these fimbriae, *pmf* genes are repressed in urine relative to *in vitro* culture (126, 242). This suggests that PMF may be transiently produced during infection, or that PMF-producing bacteria are not readily voided in urine. A *pmfA*/*mrpA-D* double mutant is more attenuated during a triple challenge in mice than either single mutation or wild type, but interestingly, the double mutant is still infective in independent challenge (albeit less than the wild-type parent strain) (214). This is consistent with overlapping roles for the *P. mirabilis* "pan-fimbriome" and suggests that other fimbriae also contribute to adherence in the urinary tract (Fig. 26).

Ambient temperature fimbriae

Ambient temperature fimbriae (ATF) were first identified in a preparation of sheared surface proteins derived from an *mrpA* mutant (212). The *atf* operon was originally reported to consist of three genes, *atfABC* (243) as isolated from a cosmid clone, but subsequent genome sequencing revealed three additional genes (*atfDEF*) including an *mrpJ* paralog (107). Although ATF are produced at 37°C (101, 212), they are optimally expressed following static culture at 23°C (212). In a similar vein, an *atfA* mutant is recovered at the same rate as wild type from either independent or cochallenge mouse studies (244). However, when an *mrpA* mutant was examined by immunofluorescence microscopy in infected mice, AtfA was readily detected (Fig. 27) (223, 227). This suggests that ATF may play a role in infection that is masked by other fimbriae, such as MR/P, and also there may be a fimbrial hierarchy that determines gene expression. ATF may contribute to biofilm formation under some conditions (228).

P. mirabilis P-like fimbriae

This fimbria was first discovered in a sheared protein preparation from a canine UTI isolate of *P. mirabilis*, where *P. mirabilis* P-like (PMP) fimbriae were found along with UCA (245). PMP fimbriae have also been implicated in both single-species and polymicrobial CAUTI, where *pmpG* was identified by Tn-Seq (124), and a *pmpA* mutant was found to be attenuated in a diabetic mouse UTI model (246). The *pmp* operon was also reported to be directly regulated by cyclic AMP receptor protein (Crp) (246).

Fimbria 14

Fimbria 14, so named because it is encoded by the fourteenth of the 17 chaperone-usher fimbrial operons in HI4320, seems like it should be nonfunctional because the *fim14* operon completely lacks a chaperone and has a frameshift mutation in usher gene *fim14C* (107). However, putative minor fimbrial subunit *fim14B* was detected in an STM screen for genes that contribute to UTI (154), and putative major structural subunit Fim14A was identified in a preparation of sheared surface proteins (101). The last gene in the operon, *fim14D*, is induced during UTI (126), and genes from the *fim14* operon were found to contribute to polymicrobial CAUTI (124). Although chaperone-usher secretion apparatuses are usually specific for a single fimbrial type, it is likely that Fimbria 14 is assembled using one or more of the other 16 chaperone-usher systems encoded by *P. mirabilis*.

Other fimbriae

The remaining fimbriae encoded by *P. mirabilis* are poorly characterized (Table 6). *P. mirabilis* have been reported to employ an unknown fimbria to agglutinate tannic acid-treated erythrocytes, a pattern that is called mannose-resistant *Klebsiella*-like (MR/K) (95, 207, 208, 247). This ability is variable for *P. mirabilis*, with some studies suggesting that MR/K agglutination by *P. mirabilis* is widespread (207, 208), but others suggesting that MR/K is more often seen for *Proteus vulgaris* or *Proteus penneri* (95, 247, 248). MR/K fimbriae produced by *P. stuartii* and *P. penneri* mediate attachment to catheter surfaces, and therefore may contribute to catheter colonization by *P. mirabilis* strains that possess MR/K fim-

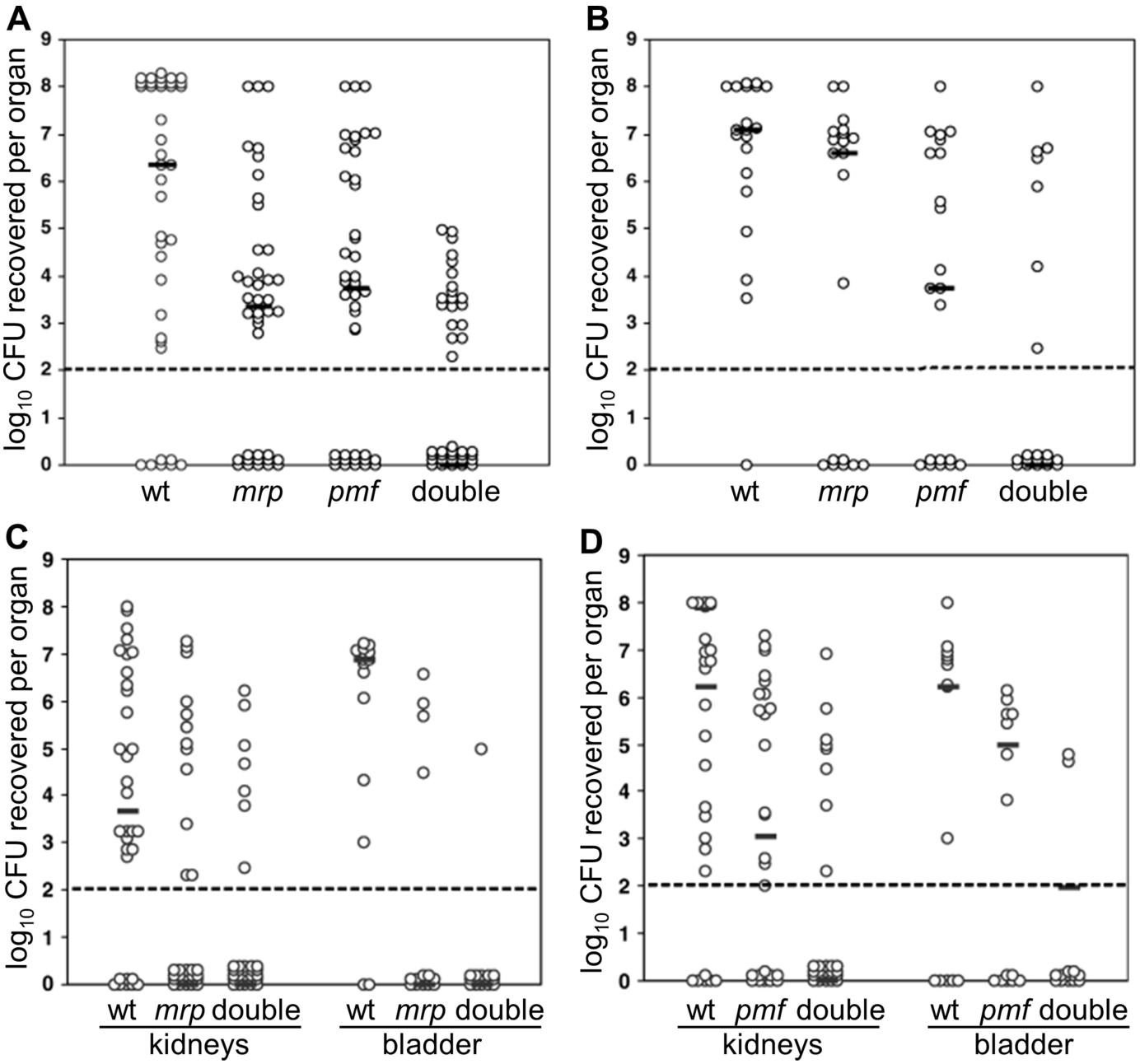

Figure 26 MR/P and PMF fimbriae have additive roles in urinary tract infection. Virulence of wild-type *P. mirabilis* Pr2921 (wt), single fimbrial mutants *(mrpA-D* or *pmfA*), and double *mrpA-D pmfA* mutant was assessed in an ascending UTI model in mice at 7 dpi. (A and B) Independent challenge. The double mutant is significantly less fit compared with either single mutant. (A) CFU recovered per kidney. (B) CFU recovered per bladder. (C and D) Mice were challenged with a 1:1:1 mixture of three strains (trichallenge). (C) Trichallenge with wt, *mrpA-D*, and *mrpA-D pmfA* double mutant. (D) Trichallenge with wt, *pmfA*, and *mrpA-D pmfA* double mutant. Each dot represents the $\log_{10}$ CFU recovered from each organ. The median (horizontal bar) is indicated for each group. The range of detection in this assay is 10^2 to 10^9 CFU per organ. Figure adapted, with permission, from reference 214.

briae (247, 249). They have also been shown to mediate adherence to Bowman's capsules in kidney glomeruli (231). Some of the 17 fimbriae are more variable in sequence than others. For example, one operon, *fim3*, is present in fewer than half the isolates in a diverse collection (101). Likewise, UCA is widespread in *P. mirabilis*, but its size and sequence are variable, so UCA binding properties might not be constant from strain to strain (101, 235). Thus, MR/K agglutination could be mediated by one or more of these fimbriae.

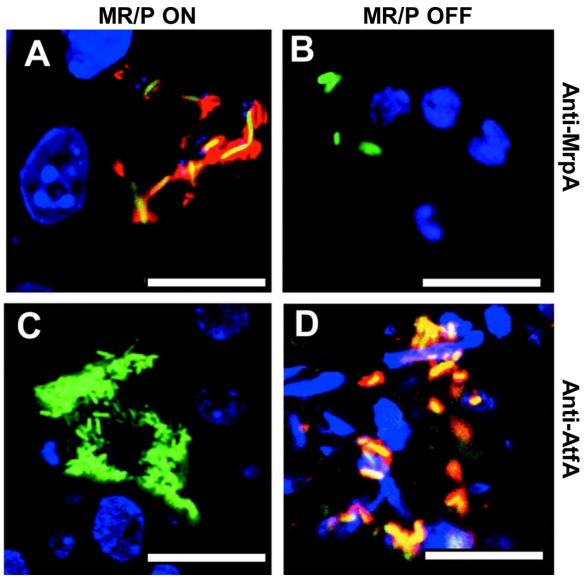

Figure 27 MR/P and ATF expression during ascending UTI. (A and B) Phase-locked mutants express MR/P fimbriae (MR/P ON) (A) or do not express MR/P fimbriae (MR/P OFF) (B) during experimental UTI at 2 dpi. Green, GFP-expressing *P. mirabilis*; blue, DAPI-stained bladder cell nuclei; red, rabbit anti-MrpA reacted with goat anti-rabbit IgG conjugated to Alexa Fluor 568; yellow, colocalization of bacteria and MR/P. (C and D) MR/P ON does not express ATF (C), but MR/P OFF does (D). Green, GFP-expressing *P. mirabilis*; blue, DAPI-stained bladder cell nuclei, red, rabbit anti-ATF serum reacted with goat anti-rabbit IgG conjugated to Alexa Fluor 568; yellow, colocalization of bacteria and ATF. Bars = 10 µm. Reproduced from reference 227, with permission.

Transcriptomic and high-throughput sequencing methods are beginning to shed light on the complex collection of the 17 fimbriae. Transcripts from three additional fimbriae, *fim5*, *fim8*, and *fim15*, were detected by microarray analysis of urine from infected mice, although both *fim5* and *fim8* were decreased compared with *in vitro* culture (126). In addition, Fim8A, E, and F protein were detected by mass spectrometry from sheared surface proteins produced during *in vitro* culture (101). Southern blot analysis suggested that *P. mirabilis* strains encoded two copies of *mrp* genes (229). Subsequent genome sequencing revealed the *mrp′* operon, which is an apparent duplication of the *mrp* operon; the two operons are encoded next to each other in the chromosome (107). Tn-Seq analysis of genes that contribute to single-species CAUTI suggest a role for *mrp′* but not *mrp*, which is unexpected given the well-documented contributions of MR/P fimbriae to uncomplicated UTI (124). Most of the remaining fimbriae were also detected in polymicrobial CAUTI Tn-Seq with *P. stuartii* but not single-species CAUTI (*mrp*, *atf*, *fim3*, *fim5*, *fim12*, *fim14*, *fim15*, *fim16*, *fim17*, plus orphan fimbrial genes PMI1812, PMI1920, and PMI3023), indicating once again that the contributions of these multiple fimbriae may be subtle, and much work remains to discern their functions (124).

Nonfimbrial adhesins

P. mirabilis produces other, nonfimbrial adhesins that are described elsewhere in this review, including autotransporter proteins Pta, AipA, and TaaP (*see* **Toxins** and **Type V Secretion** sections). *P. mirabilis* also encodes two putative type IV pili (107).

Transcriptional regulation by MrpJ

MrpJ is a transcriptional regulator encoded at the end of the *mrp* fimbrial operon (132). Like other *mrp* genes, it is not expressed well *in vitro*, but is among the most highly induced genes in urine collected from infected mice (126). MrpJ was originally proposed to serve as a balance between adherent and motile states (reciprocal regulation); when MR/P fimbriae are produced (adherent state), MrpJ is also produced and switches off flagella (motility) (132). That is, expression of *mrpJ* on a plasmid represses FlaA flagellin, in turn inhibiting both swimming and swarming motility (132) (Fig. 28). Similarly, an *mrpI* locked-on mutant constitutively produces MR/P fimbriae but not flagella, while disruption of *mrpJ* in the locked-on back-

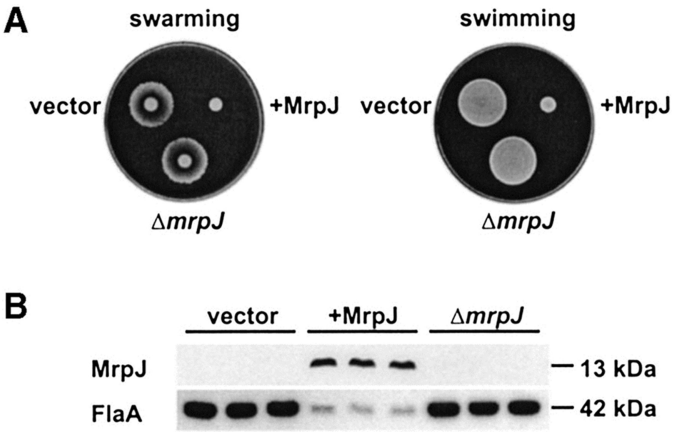

Figure 28 Elevated expression of MrpJ in *P. mirabilis* inhibits motility due to reduced flagella production. The three strains assayed here are *P. mirabilis* HI4320 transformed with pLX3607 (vector), pLX3805 (+MrpJ), and pLX5401 (Δ*mrpJ*). (A) The three strains were assayed for swarming on 1.5% Luria agar and for swimming in 0.35% Luria agar. (B) Three overnight Luria broth cultures of each of the three strains were adjusted to the same optical density, and equal volumes processed for SDS-PAGE and subsequent Western blot analyses with antiserum against MrpJ or *P. mirabilis* flagella (FlaA). Reproduced from reference 132, with permission.

ground results in a bacterium that produces both fimbriae and flagella (132).

MrpJ is predicted to be a 110-amino-acid protein consisting of a helix-turn-helix (HTH) DNA-binding domain and a unique C-terminal tail (132, 133). It is a member of the xenobiotic response element (XRE) superfamily of transcriptional regulators. Consistent with other HTH proteins, mutation of residues predicted to form DNA contacts interferes with MrpJ's ability to repress swimming motility (133). However, deletion of the C-terminal domain has almost no effect on motility repression, suggesting that this region is disposable for reciprocal regulation (133). Consistent with its role as a repressor of motility, MrpJ directly binds the promoter of the master flagellar regulatory genes *flhDC* (127, 133).

In addition to influencing motility, MrpJ also appears to be involved in autoregulation of the *mrp* operon. Expression of *mrpJ* on a plasmid results in elevated *mrpA* expression (127), and an *mrpJ* mutant produces less MrpA protein (132). The *mrpJ* mutant also has the *mrp* invertible element overwhelmingly in the off orientation, even under *mrp*-inducing conditions (226).

Deletion of *mrpJ* has little effect *in vitro*, which may be due to either low expression of *mrp* genes in most laboratory conditions or masking of MrpJ function by redundancy (*see* **MrpJ paralogs** section) (132). However, an *mrpJ* mutant is significantly outcompeted during mouse independent and cochallenge experiments (127, 132), indicating a strong contribution to fitness and pathogenesis within the urinary tract. The exact role of MrpJ during infection is complicated considering that it regulates other virulence factors, such as production of MR/P fimbriae and flagella; MrpJ could be acting by altering either of these proteins, or eliminating coordination of motility and adherence, or by acting on other gene targets.

Transcriptomic analysis confirms that MrpJ has other virulence-associated targets, in addition to MR/P fimbriae and flagella (127). Because *mrp* genes are transcribed at a low level *in vitro*, an *in vivo* mimic has been used to study MrpJ targets, where *mrpJ* is expressed *in trans* at levels comparable to those detected in mice during experimental UTI (127). In a comparison of the *in vivo* mimic with a vector control, 217 genes were differentially regulated. Classes of MrpJ target genes include flagella, MR/P and other fimbriae, type VI secretion, metabolism, LPS modifications, virulence factors such as Zap and Pta, and transporters (127). Because many MrpJ-regulated genes have known or predicted roles in disease, MrpJ has been proposed as a master regulator of virulence.

Chromatin immunoprecipitation followed by PCR (ChIP-PCR) indicated that MrpJ binds within the invertible element of the *mrp* operon, in agreement with detection of an MrpJ-responsive element 156 to 256 bp upstream of the transcriptional start site of the *mrp* promoter (127). This is unusual, given that bacterial regulators typically bind in the vicinity of the −35 (activator) or +0 (repressor) promoter sequences so they can interact or interfere with RNA polymerase, respectively (250). However, a distant site of action for MrpJ, relative to other transcriptional regulators, is consistent with the *flhDC* promoter binding data mentioned above (127, 133).

MrpJ paralogs

Genomic sequencing of *P. mirabilis* revealed that this species encodes 14 additional *mrpJ*-type genes (107, 133). All but four are part of fimbrial operons, and they are always located at the beginning or the end of the operon (Table 6). Expression of all but two *in trans* causes repression of motility (133). Apparently, the paralogs do not all repress motility by the same mechanism, because overexpression of individual paralogs leads to flagellin levels ranging from wild-type to near-complete repression (133) (Fig. 29A). Different paralogs also induce distinctive swarming phenotypes and uniquely aberrant differentiation into swarmer cells (133) (Fig. 29B). This suggests that although most MrpJ paralogs repress motility, they likely have other, nonoverlapping functions. However, at least one paralog, UcaJ, has been shown to bind the same fragment of the *flhDC* promoter as MrpJ (133).

Comparison of MrpJ and its paralogs revealed a conserved SQQQFSRYE motif within the helix-turn-helix (HTH) DNA-binding domain, plus a highly variable C-terminal tail and short, highly variable N-terminal sequence (133). Notably, MrpJ paralogs are not restricted to *P. mirabilis* because they have been detected in fimbrial operons from related genera (251–253). Because fimbriae allow bacteria to adhere or form biofilms in specific environments, and thus respond to niche-specific signals, MrpJ paralogs have been proposed to orchestrate genetic programs that are beneficial to those environments (127, 254).

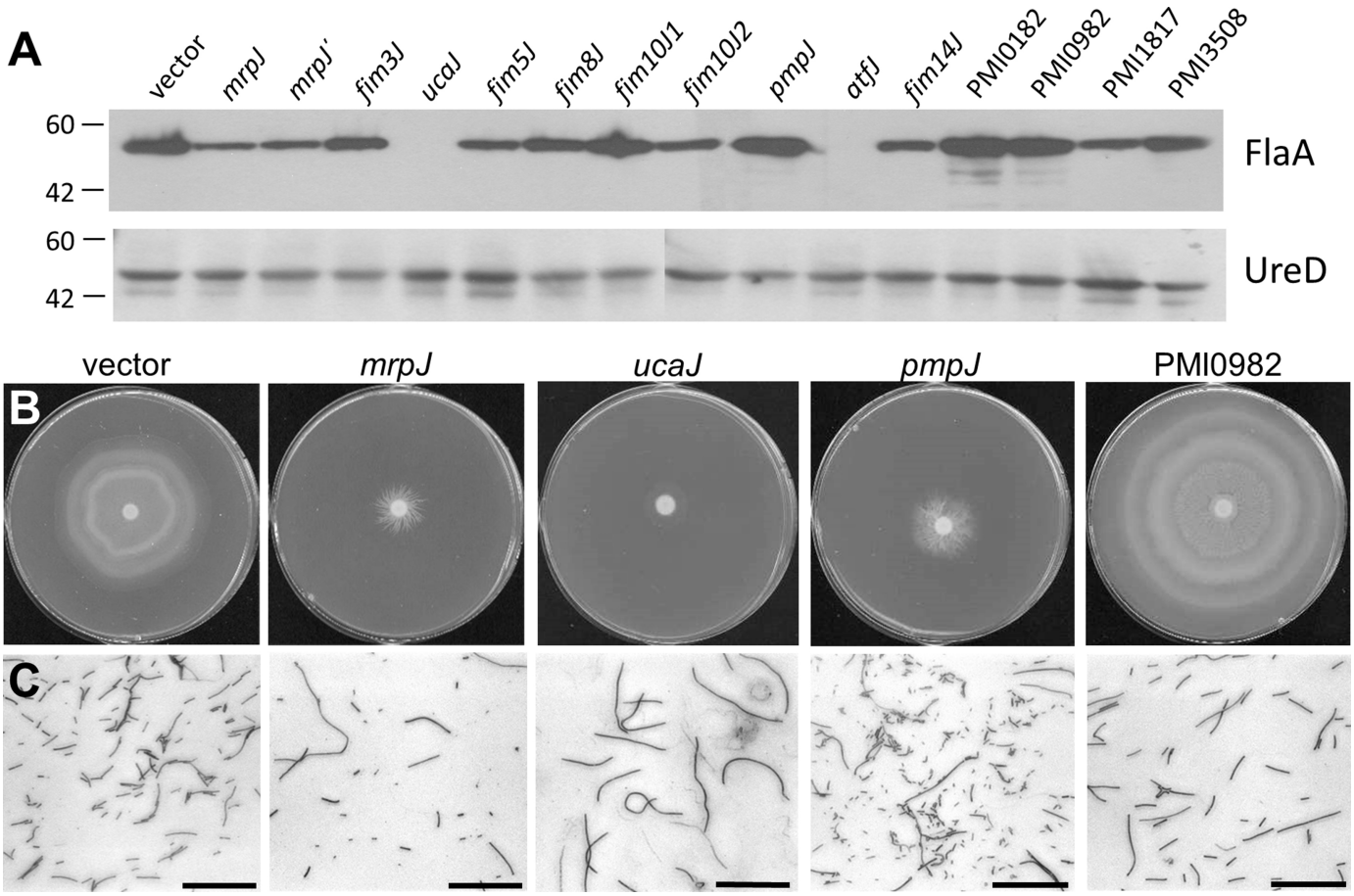

Figure 29 MrpJ paralogs exert unique control over flagella and swarming. (A) Western blot of flagellin expression in *P. mirabilis* HI4320 *mrpJ* or *mrpJ* paralog overexpression strains. Whole cell lysates of uninduced strains were denatured, electrophoresed on 10% SDS-PAGE, and blotted with anti-FlaA antibody, which recognizes the major subunit of the flagellum. Lysates were also blotted with anti-UreD antibody as a loading control (lower panel). Molecular weight markers are indicated on the left side in kDa. (B and C) *P. mirabilis* cultures were spotted onto the center of swarming agar. (B) Representative swarming phenotypes of strain HI4320 expressing *mrpJ* paralogs. (C) Gram stains of bacteria taken from the edge of swarm fronts. The reference bar is 50 μm. Figure adapted, with permission, from reference 133.

Like MrpJ itself, the MrpJ paralogs regulate other fimbrial operons in addition to repressing motility (254). Screening of MrpJ, UcaJ, AtfJ, and Fim8J showed that some paralogs positively autoregulate their operons. Strikingly, AtfA and Fim8A strongly induced their respective operons while having modest or no effects on other fimbrial genes (*mrpA*, *ucaA*, or *pmfA*); in contrast, UcaJ has no effect on the *uca* operon (254). Examination of the *atf* promoter by using deletion analysis indicated that AtfJ interacts with a region 486 to 655 bp upstream of the transcriptional start site (254). Thus, other MrpJ paralogs may share a common feature of binding DNA far away from transcriptional machinery binding sites. Deletion of the AtfJ C-terminal tail had little effect on motility repression, but was required for *atf* autoregulation (254). Protein modeling of the AtfJ C terminus suggests that this region is involved in protein-protein interactions, and it has been proposed that MrpJ paralogs exert their unique properties via their divergent C termini (133, 254). These potential, unidentified, binding partners may explain how MrpJ paralogs exert transcriptional control from distant DNA-binding sites.

Biofilms

Biofilms, which are adherent microbial communities, are a notorious problem on catheter surfaces, including urinary catheters. The ability of *P. mirabilis* to form biofilms on catheter surfaces is well established (5, 255). Less well understood is the potential establishment of biofilms within the urinary tract, and to what extent these biofilms contribute to disease. Because catheterization is a major risk factor for *P. mirabilis* UTI, biofilms within both catheters and urinary tissue will be considered here.

P. mirabilis readily adheres to a wide variety of surfaces, including clinically relevant materials such as silicone, latex, glass, and polystyrene. In the presence of urine, struvite and apatite minerals are deposited among the developing *P. mirabilis*-colonized surface, leading to a crystalline biofilm. In laboratory models, crystalline biofilms form within 6 h after inoculation with *P. mirabilis* (256); similarly, mineralization has been detected in experimentally infected mice within 24 h (43), and stones are detectable by 4 days after inoculation (12). This process occurs as a result of urease activity (*see* **Urease** section), which causes locally increased pH and subsequent mineral precipitation. This trait is a major reason why *P. mirabilis* is particularly problematic in patients with indwelling urinary catheters: crystalline biofilms can completely obstruct catheters (5, 27, 257) (Fig. 30).

Random mutagenesis to find biofilm mutants indicates that, as in other bacterial species, the biofilm lifestyle for *P. mirabilis* is complex, heterogeneous, and involves the coordination of many genes (152, 258). For example, a nonsaturating transposon screen identified altered biofilm formation in 575/3850 mutants (15%) (152). When a subset of these mutants was further examined, most were also deficient in swimming and swarming motility. Notably, swimming and swarming may be involved in both establishment of biofilms, as a means of rapidly colonizing a surface, and dispersal into new environments. *P. mirabilis* swarms on catheters, and differentiated swarmer cells have been reported on *P. mirabilis* biofilms (259, 260); thus, swarming may help distribute bacteria from the catheter to the urinary tract. However, motility may also interfere with establishing adherent communities (261), and it is likely that balance is required for fully developed biofilm formation and swarming behavior.

P. mirabilis encodes an arsenal of adhesive proteins, several of which have been shown to contribute to biofilm formation (Table 7). In particular, MR/P fimbriae have been linked to biofilm formation using multiple methods, including crystal violet-stained multiwell plates (228, 262), confocal microscopy on glass coverslips (227), glass tubing (228), bacterial clustering within the bladder lumen (43), and aggregative adherence to cultured cells (262). MR/P fimbriae allow complex biofilm architecture to develop, but only if the bacteria are allowed to modulate their fimbrial production (*see* **Fimbriae and Adhesins** section). If MR/P expression is genetically shut off, biofilm formation is greatly diminished. However, bacteria engineered to constitutively produce MR/P fimbriae produce relatively thin (12 μm compared with 65 μm for wild-type), albeit very dense, biofilms (227).

Crystalline biofilm formation is thought to increase risk of bladder stones, because one study found that 62% of patients with encrusted catheters also had bladder stones (263). Notably, *P. mirabilis* is recovered from most (65 to 79%) patients with obstructed catheters (5, 263). Infection stones and crystalline biofilms are both dense, complex bacterial communities, and at least two *P. mirabilis*

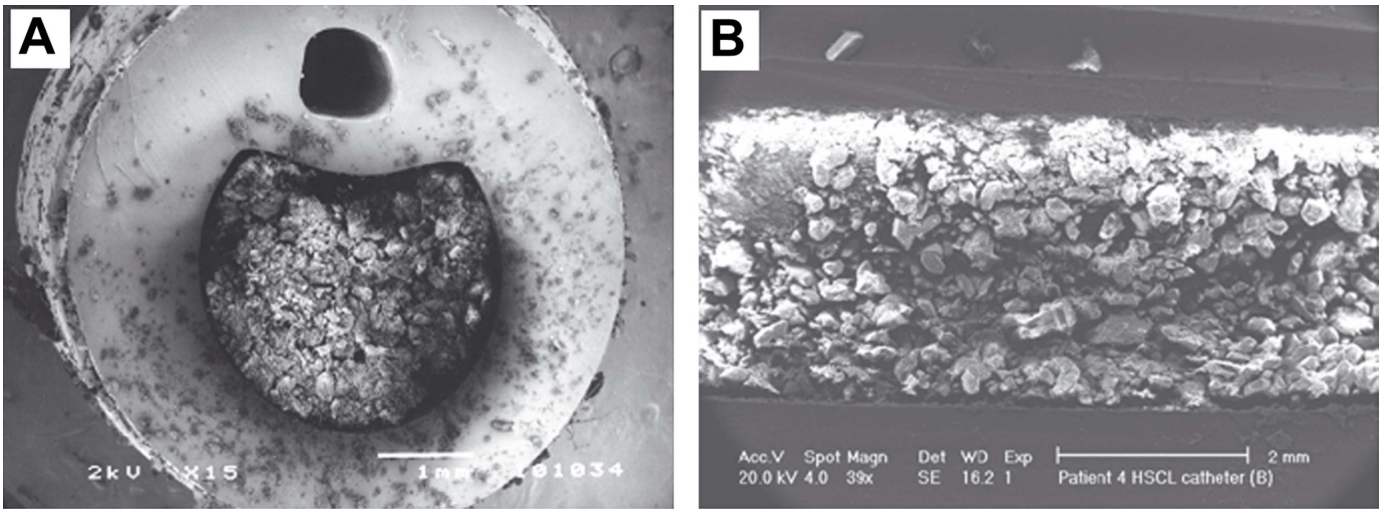

Figure 30 Scanning electron micrographs of crystalline biofilms encrusting catheters. (A) shows a cross section of an all-silicone catheter removed from a patient after 8 weeks; (B) shows a longitudinal section of a blocked silver/hydrogel-coated latex catheter removed from a patient after 11 days. In both these cases, extensive crystalline material can be seen occluding the catheter lumen. Figure adapted, with permission, from reference 347 (A) and reference 277 (B).

Table 7 Factors involved in biofilm formation

Biofilm factor	Proposed role	Reference
Urease	Nickel metalloenzyme, local increase in pH causes mineral deposition which facilitates crystalline biofilms	5, 30, 356
MR/P fimbriae	Adherence and auto-aggregation; mutants are defective in biofilm formation	43, 152, 227, 228, 262
Fimbria 10 (PMI2210)	Adherence; mutant has increased biofilm (perhaps due to fimbrial cross-talk)	152
UCA, PMF, and ATF fimbriae	Mutations have varying effects on biofilms (CFU, matrix) depending on culture conditions	228
RcsBCD (RsbA) phosphorelay	Phosphorelay system that enhances extracellular polysaccharide production; may control biofilm formation via regulation of fimbriae	135, 152, 266
Pst transporter	High-affinity phosphate transporter, mutants are defective in biofilm formation	286
Capsule or extracellular polysaccharides	Facilitates mineral aggregation into crystalline biofilms and bacterial colonization	271–273
LPS	*P. mirabilis* with different LPS charges vary in biofilm formation; *pmrI* LPS modification mutant and *waaE* inner-core LPS biosynthetic protein mutant are biofilm-defective	268–270
RsmA	RNA-binding protein; expression of *P. mirabilis rsmA* in *Escherichia coli* suppresses biofilm	357
Ppk	Polyphosphate kinase; may act by regulating MR/P fimbriae	358
Hfq	RNA chaperone; may act by regulating MR/P fimbriae or motility	267
GlnE	Glutamate-ammonia ligase adenylyltransferase; mutant has increased biofilm	152
Lrp	Leucine-responsive regulator	152
NirB	Nitrate reductase; biofilm-deficient in crystal violet assay and takes longer to block catheters	152
Bcr	Multidrug efflux pump; mutant has increased biofilm but takes longer to block catheters	152
GltS	Sodium/glutamate symport carrier protein	152
PMI1551	Putative lipoprotein	152
PMI1608	Unknown; biofilm-deficient in crystal violet assay but blocks catheters more rapidly	152
PMI2861	Putative membrane protein	152
PMI3402	MuA-like DNA-binding protein; mutant has increased biofilm in crystal violet assay and blocks catheters more rapidly	152

proteins contribute to both processes: urease and MR/P fimbriae. During experimental UTI in mice, *P. mirabilis* assembles into large clusters in the bladder lumen, where mineralization starts to occur within 24 h. Mutation of either urease or MR/P genes results in loss of both clustering and mineralization (43). *P. mirabilis* bacteria become embedded within stones, and likewise, may be embedded in extracellular matrix produced during biofilm growth (12, 264). In both cases, the bacteria may be protected from immune responses (43, 265).

Other processes also contribute to *P. mirabilis* biofilm formation (Table 7). Logically, regulators of the above biofilm factors, such as the RcsBCD phosphorelay (RcsD is also known as RsbA) (135, 152, 266) and RNA chaperone Hfq (267), control biofilm formation. Surface hydrophobicity, mediated by LPS (268–270) and capsular polysaccharides (271–273), influences both initial surface colonization and biofilm maturation.

Prevention of catheter blockage

Currently, the typical approaches to avoid urinary catheter biofilms are to (i) limit the duration of catheterization and (ii) replace blocked/encrusted catheters. Multiple groups are developing new approaches to prevent biofilm establishment, including alternative catheter materials, antimicrobial coatings or instillation of antibiofilm chemicals, mechanical or electrical biofilm dispersal, bacteriophage, and control of urinary pH (265, 274–276). Because *P. mirabilis* is the major agent of crystalline biofilm formation and catheter blockage during CAUTI, many of these efforts focus on this species. Thus far, no catheter type has been immune to *P. mirabilis* biofilm (257), although some materials and coatings delay blockage. In some cases, *P. mirabilis* colonizes antimicrobial surfaces after crystalline material has coated the catheter (277). Filling the retention balloon of urinary catheters with 10 g/liter triclosan is able to inhibit *P. mirabilis* biofilm in an *in vitro* model (278, 279), although exposure

of *P. mirabilis* to triclosan may rapidly select for triclosan resistance (280). Ultimately, a combination of these strategies may be necessary to successfully combat *P. mirabilis* crystalline biofilm formation in a clinical setting.

Methods for studying *P. mirabilis* biofilms

An important caveat for biofilm studies, in general, is that biofilms can be generated by using many techniques, and the chosen method has a strong influence on the outcome of the study (281). For example, *P. mirabilis* mutants with altered biofilm in a high-throughput crystal violet screen had no correlation with time to blockage in a catheter/artificial bladder model (152). Thus, there is a need to use a combination of simple and/or high-throughput *in vitro* methods, and more complex *in vitro* models and *in vivo* methods to study the contributions of *P. mirabilis* biofilms to infection.

A common, simple method for surveying biofilm formation involves culturing bacteria in multiwell plates, and visualizing biofilm by staining with crystal violet. The major advantage is that this assay allows for simultaneous screening of many samples; it is also easily quantifiable by dissolving the crystal violet and measuring the dye with a spectrophotometer. For this reason, the assay has been used to screen *P. mirabilis* clinical isolates and transposon mutants, as well as screen targeted mutants (152, 228, 262, 268–270, 282, 283). Other variations on this assay include the addition of short catheter segments to multiwall plates and culture in static, closed tubes (272, 284). It is, however, important to note that these methods have their limitations. While urinary catheter biofilms are subject to the flow of urine, bacteria in multiwell plates are in a closed system where nutrients are depleted. Furthermore, if urine (artificial or real) is used as the medium, *P. mirabilis* urease activity will cause a rapid increase in alkalinity to approximately pH 9. This lethal effect in static systems can be seen in a comparison of *P. mirabilis* biofilms cultured in the presence or absence of urea (285). Therefore, while the crystal violet method is useful, results may be less likely to lead to translational applications.

Continuous-flow systems, where fresh medium is supplied at a constant rate, allow study of *P. mirabilis* biofilm development in catheters (30, 260, 286). The flow can be adjusted to match physiological urine rates in humans, and a flow cell can be inserted to facilitate microscopy. Urease activity still leads to crystalline biofilm formation if urine is used as the medium, but the pH increase is not as extreme as in the multiwell plate biofilm assay and may be maintained within a physiological range. A modification of continuous flow is an artificial bladder (287). Flow is maintained into a glass chamber that serves as a bladder analog, which is maintained at 37°C via a water jacket. A catheter is inserted into the base of the bladder chamber, which may be further connected to tubing and a drainage bag. The advantage of this bladder model is that it captures several aspects of the urinary tract: continuous introduction of urine from above, insertion of a catheter from below (including inflation of the retention balloon), and retention of a residual volume of urine similar to what occurs in a catheterized patient. However, this model requires specialized equipment and is limited in how many samples can be analyzed at one time.

P. mirabilis adheres to cultured cells in an aggregative pattern that has been likened to biofilms (262). This method may be used to assess aspects of biofilm development that are host influenced, or require a biotic substrate for the developing biofilm. A drawback is that *P. mirabilis* produces toxins, such as hemolysin, which lead to cell death within a few hours and pose a challenge for studying longer-term biofilm development.

Animal models are also used to study biofilm development. Stones and clusters form in the mouse ascending UTI model (12, 40, 43), and *P. mirabilis* biofilms may be studied *in vivo* using the CAUTI mouse model (*see* **Animal Models** section) (25, 124). These models are essential for investigating the interaction of *P. mirabilis* biofilms with urinary tissues, the innate immune response, and the catheter-bladder interface.

Culture medium also greatly affects biofilm development. Using continuous flow coupled with confocal scanning laser microscopy, *P. mirabilis* biofilms were found to produce towers of biomass separated by channels in a rich medium (LB). However, in artificial urine (288), biofilms were flat, lacked channels, and had swarmer cells protruding from the surface (260). Crystalline biofilms will only develop if urine or artificial urine is used. Catheters in patients will be coated with cellular material and other material not present in artificial urine, and these coatings may further facilitate biofilm formation (255, 257).

Polymicrobial catheter-associated biofilms

P. mirabilis is frequently part of a mixed-species infection (4, 5, 9, 289), and catheter biofilms are a useful model for

studying polymicrobial UTI. Catheters taken directly from patients may be studied to explore polymicrobial biofilms (289–291), or continuous-flow systems (289, 292, 293) or static cultures (294) may be inoculated in the laboratory. Urease activity can give *P. mirabilis* a competitive advantage in catheter biofilms over *P. aeruginosa* (292); similarly, in the presence of artificial urine, *P. mirabilis* inhibits *K. pneumoniae* biofilm formation (294). The CAUTI mouse model, in which a catheter segment is pushed into and retained in the bladder during the course of the experiment, is also shedding light on *P. mirabilis* as part of a mixed-species infection (25, 124) (*see* **Urease** and **Genome-Wide Mutagenesis** sections). Other aspects of mixed-species bacteriuria and infection have been recently reviewed elsewhere (3, 20).

Flagella and Motility

P. mirabilis was named for the Greek god Proteus due to its distinctive dimorphic nature, which is directly related to its motility: in the vegetative state, these bacteria exist as short motile rods (1 to 2 μm in length) with 6 to 10 peritrichous flagella, but, under permissive conditions, they differentiate into swarm cells by elongating 20- to 50-fold (20 to 80 μm in length) and expressing hundreds to thousands of flagella (295, 296) (Fig. 31). The vegetative swimmer cells exhibit normal chemotactic behavior in liquid medium, being attracted by nutrients and repelled by toxic substances or unfavorable conditions (296), while swarm cells allow for migration across solid surfaces, forming a characteristic bull's eye pattern through sequential rounds of the differentiation process (90). Swarm cell differentiation and the mechanics and regulation of swimming and swarming motility in *P. mirabilis* have been extensively reviewed elsewhere (3, 18, 19, 297). We will therefore sharply focus on the direct contribution of flagella and motility to pathogenesis.

Flagella

In contrast to other motile bacteria, all the flagellar components and chemotaxis proteins of *P. mirabilis* are encoded within a single locus in the chromosome that spans approximately 54 kb (107). Within this region, *P. mirabilis* encodes two flagellin genes, *flaA* and *flaB* (298). FlaA appears to be the predominant flagellin produced by *P. mirabilis*, but recombination can occur between *flaA* and *flaB*, resulting in occasional hybrids (119, 299, 300). Because the flagella produced by *P. mirabilis* are recognized by the host immune response and can elicit a proinflammatory response, antigenic variation and *flaAB* hybrids may play a role in immune evasion during infection (72, 183).

Flagella are not an absolute requirement for establishment of UTI, because naturally occurring nonmotile strains and flagellar mutants of *P. mirabilis* are still capable of colonizing the urinary tract in experimental models (301, 302). However, there is clear evidence for the contribution of flagella to pathogenesis. The importance of flagella to host cell invasion and ascending UTI was directly assessed by disrupting the gene encoding the flagellar filament (*flaD*) in a *P. mirabilis* mutant lacking hemolysin activity to avoid confounding by expression of the toxin. Production of the flagellar filament was found to facilitate invasion of human renal proximal tubular epithelial cells *in vitro*, in part, by allowing the bacterial cells to come into close proximity to the host cells (44). Flagella may also promote internalization through other mechanisms, because the *flaD* mutant still exhibited reduced internalization compared to the parental strain when the bacteria were centrifuged onto the cell monolayer. This mutant also exhibited reduced bladder and kidney colonization in the murine model of ascending UTI, while loss of hemolysin alone did not significantly impact pathogenesis.

A role for chemotaxis and components of the flagellar apparatus in ascending UTI was also directly indicated by signature-tagged mutagenesis (STM) studies because a positive regulator of chemotaxis (*cheW*), the flagellar M-ring (*fliF*) and flagellar hook protein (*flgE*) were all identified as fitness factors for ascending UTI (103, 154). Transposon insertion in any of these genes resulted in a defect in kidney colonization, while *fliF* and *cheW* also affected bladder colonization. Transposon insertion-site sequencing (Tn-Seq) similarly indicated a role for chemotaxis and flagella during catheter-associated CAUTI (124). Specifically, a regulator of chemotaxis (*cheR*), the flagellar master regulator (*flhDC*), and a gene involved in regulation of *flhDC* (*umoA*) were identified as fitness factors for kidney colonization, while another gene involved in regulation of *flhDC* (*umoB*) and the flagellar basal-body rod protein (*flgC*) were fitness factors for colonization of the kidneys and the catheterized bladder, and the flagellar M-ring (*fliF*) and ATP synthase (*fliI*) were fitness factors for bladder colonization (124). Thus, the flagellar M-ring has been identified as having a significant contribution to fitness through two separate mutagenesis screens in two distinct models of infection. It is also noteworthy that flagellar genes are temporally regulated during ascending

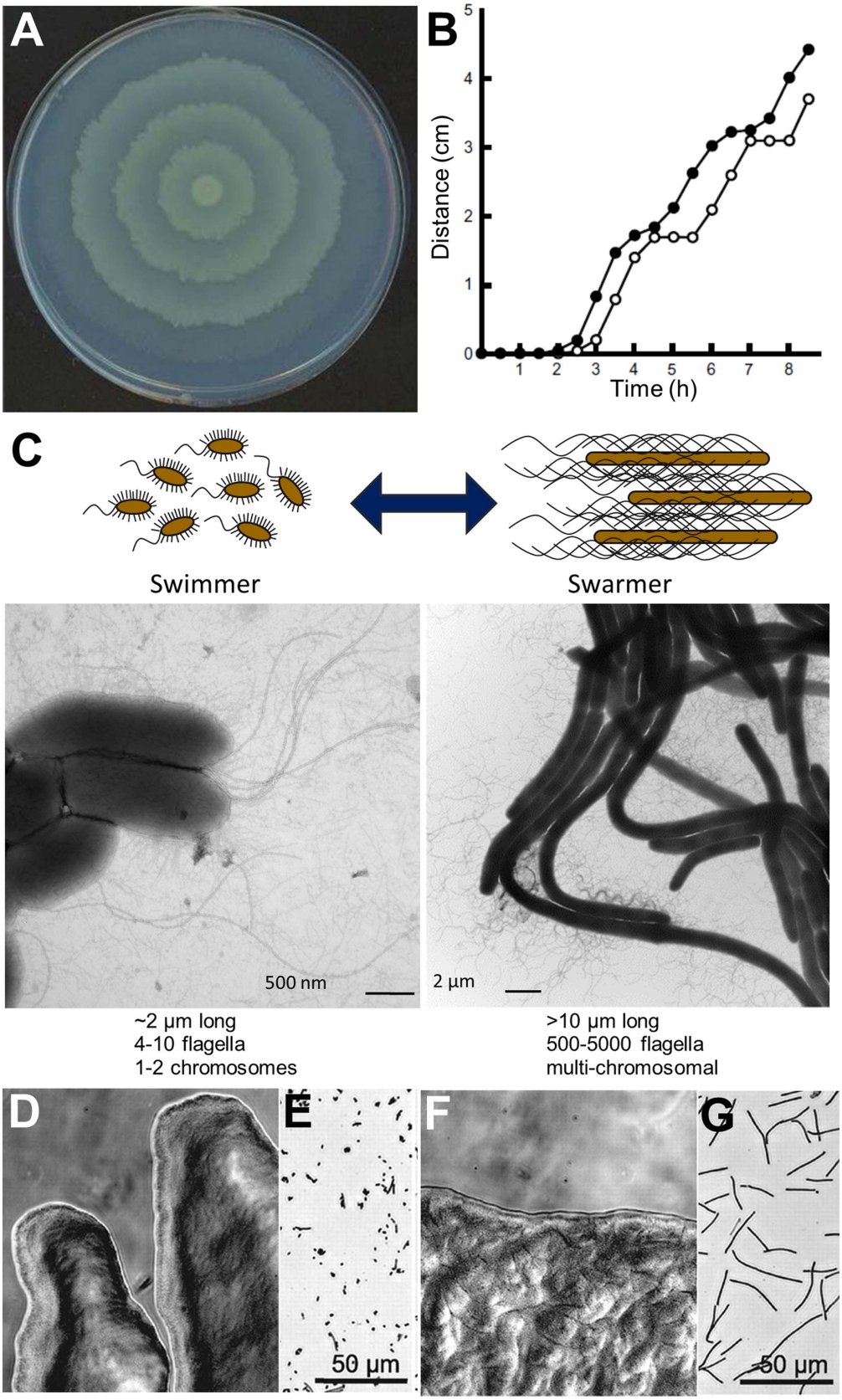
A
B
Distance (cm)
Time (h)
C
Swimmer
Swarmer
500 nm
2 µm
~2 µm long
4-10 flagella
1-2 chromosomes
>10 µm long
500-5000 flagella
multi-chromosomal
D
E
F
G
50 µm
50 µm

UTI, being poorly expressed *in vivo* relative to growth in rich medium at early time points postinoculation but increasing in expression by 7 dpi, further indicating a role for flagella in pathogenicity (126).

Motility

Despite numerous studies, the exact contribution of flagella-mediated motility to *P. mirabilis* pathogenicity remains inconclusive. *P. mirabilis* has been observed to differentiate into swarm cells on catheter surfaces, which is thought to allow for migration and entry into the catheterized urinary tract (7, 259, 287, 303) (Fig. 32). Because nonswarming mutants are only capable of migrating across hydrogel-coated catheters, swarming is likely an important aspect of initial bladder colonization in catheterized individuals. Five cues that can induce swarming in *P. mirabilis* are present in human urine (arginine, glutamine, histidine, malate, and ornithine), and may contribute to swarm cell differentiation and migration across urine-bathed catheters as they promote swarming on urine agar plates (304–306) (Fig. 33).

Once within the urinary tract, *in vitro* experiments indicate that swimming motility may facilitate contact with uroepithelial cells, thereby promoting internalization and cytotoxicity (44). Swarm cells in particular have been postulated to contribute to host cell invasion, because these differentiated cells may be capable of invading urothelial cells faster and to a greater extent than vegetative cells (45). Numerous virulence factors are coordinately expressed during swarming, including Zap protease and hemolysin, which may cause swarm cells to be more cytotoxic to the host urothelium (45, 128) (Fig. 34).

Swimming motility is also thought to contribute to dissemination within the urinary tract, in particular, ascension from the bladder to the kidneys and spread between kidneys. For instance, immunization to stimulate production of antibodies that immobilize *P. mirabilis* can prevent spread to the contralateral kidney following direct inoculation into the right renal medulla (307). Swarm cells have also been implicated for contributing to kidney colonization and development of pyelonephritis, in particular, during long-term infection, as swarm cells have been visualized within the kidney parenchyma (45, 304). However, elongated swarm cells were rarely observed during 4-day infection studies in the (uncatheterized) murine model of ascending UTI (305). Thus, while flagella clearly contribute to *P. mirabilis* pathogenesis, the importance of swimming motility and swarm cell differentiation to disease progression and severity remain to be fully elucidated.

Metal Acquisition

Bacterial pathogens compete with the host for micronutrients. One method the host uses to combat pathogens is sequestration of these nutrients so that the bacteria become starved for these ions. Bacteria that have evolved to colonize humans, therefore, have strategies to scavenge these elements, including iron and zinc (306, 308).

Iron

The most highly studied of the nutrient competition systems is iron, and much like the rest of the human body, the urinary tract is iron restricted (309). Similar to other pathogens, *P. mirabilis* encodes iron-scavenging and -uptake systems that are induced during infection (104, 107, 126).

Bacteria typically produce iron-scavenging molecules called siderophores, which bind iron with higher affinity than host iron sequestration systems (306). Early evidence suggested that *P. mirabilis* lacked siderophores because it fares poorly relative to other bacteria in iron chelation experiments and tested negative in siderophore detection assays (310, 311). In addition, *P. mirabilis* is inhibited in its ability to establish infection in an iron-deficient rat pyelonephritis model (312). However, we now know that *P. mirabilis* has at least three ways to scavenge iron: proteobactin (Pbt), a nonribosomal peptide synthesis system (Nrp), and α-keto acids. It can also use enterobactin, a siderophore produced by other enteric bacteria, although this species is not able to synthesize enterobactin on its own (104).

Figure 31 Swarming behavior of *P. mirabilis*. (A) Swarming colony of *P. mirabilis* HI4320. (B) The swarming migration distance of wild-type strain P19 (open circles) and a super-swarming *rsbA* mutant (solid circles). The periodic shift from swarming to consolidation can be seen. (C) Cartoon and transmission electron microscopy showing differentiated swimmer (broth-cultured) and swarmer cells. (D and F) The edge of an advancing swarm colony during consolidation (D) or swarming (F). (E and G) Gram stains showing consolidate (E) and swarmer cells (G) obtained from the edge of a growing *P. mirabilis* swarm. Figure adapted, with permission, from reference 19 (A and C), reference 138 (B), and reference 121 (C–G).

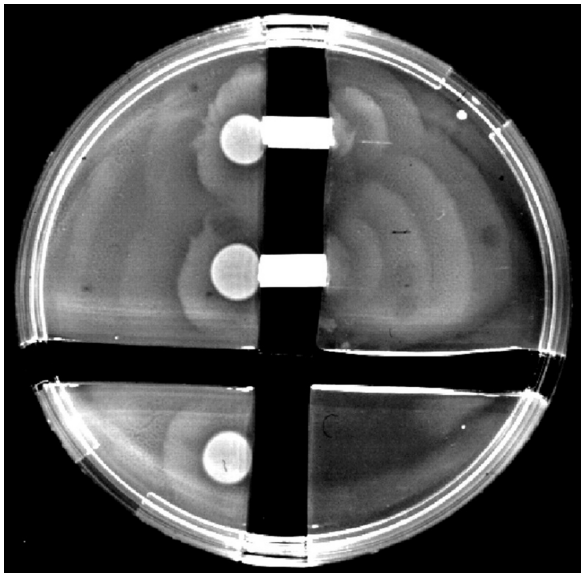

Figure 32 *P. mirabilis* swarms across 1-cm sections of hydrogel-coated latex catheter. Reproduced from reference 259, with permission.

The *nrp* system was initially identified as a possible iron-regulated swarming signaling system (313). Genome annotation, microarray analysis, and a more sensitive siderophore detection method revealed that *nrp* and a second system, proteobactin (*pbt*), are siderophore biosynthesis and transport operons (104, 107). While the *nrp* genes are homologous to yersiniabactin genes and are encoded within a high-pathogenicity island derived from *Yersinia* spp. (102), the products are not interchangeable (104). Although both siderophore systems must be mutated to produce a negative iron-scavenging result in the laboratory (chrome azurol S, or CAS assay), only the *nrp* system has a significant contribution to infection (104).

P. mirabilis produces α-keto acids from amino acids, likely via two amino acid deaminases (PMI2834 *aad* and PMI2149) (311, 314, 315). These α-keto acids act as noncanonical siderophores and can restore growth of *P. mirabilis* on iron-chelated medium when supplied externally (311, 314). Amino acid deaminase activity appears to be restricted to genera closely related to *P. mirabilis* (that is, *Proteus*, *Providencia*, and *Morganella*), because most enteric bacteria do not have Aad activity and cannot use externally provided α-keto or α-hydroxy acids to overcome iron chelation (311, 314).

P. mirabilis encodes ferric, ferrous, and heme uptake systems that have been discovered by analysis of genes and proteins differentially regulated during iron restriction, genome annotation, and transposon mutagenesis (104, 107, 316, 317). *In vivo* analyses have demonstrated that iron uptake proteins are immunogenic (183, 316) and produced in a rat intraperitoneal chamber model (318); likewise, iron-related genes are induced during UTI (126), and several of these have directly been shown to contribute to UTI (103, 154, 183, 317). Iron acquisition and storage systems are even more strongly required during polymicrobial CAUTI, suggesting that competition with other species increases pressure on *P. mirabilis* iron-scavenging capabilities (124). Details on iron-associated genes in *P. mirabilis* and their contributions to infection are listed in Table 8.

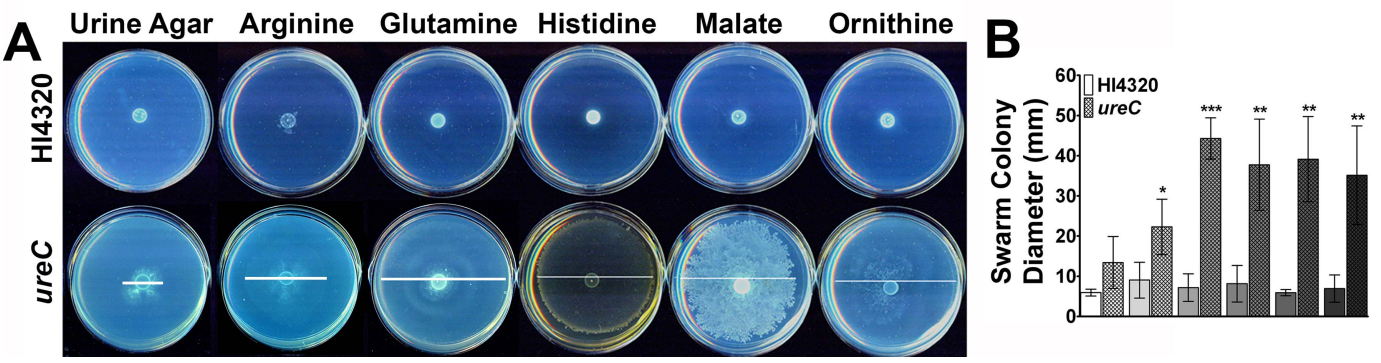

Figure 33 Swarming on urine agar in response to five cues. (A) Urine agar is not normally permissive for swarming as the high pH resulting from urease activity inhibits swarming. A *ureC* mutant is capable of modest swarming on urine agar, and supplementation with any of five swarming cues to a final concentration of 20 mM dramatically enhances swarming. (B) Quantitation of swarm colony diameter on urine agar for *P. mirabilis* HI4320 and a *ureC* mutant. White lines indicate swarm diameter. Error bars represent means and standard deviations for four independent experiments with four replicates each. Statistical significance was determined by comparing the swarm diameter under each condition to the diameter on plain medium for each strain. $*P < 0.05$; $**P < 0.01$; $***P < 0.001$. Figure adapted, with permission, from reference 348.

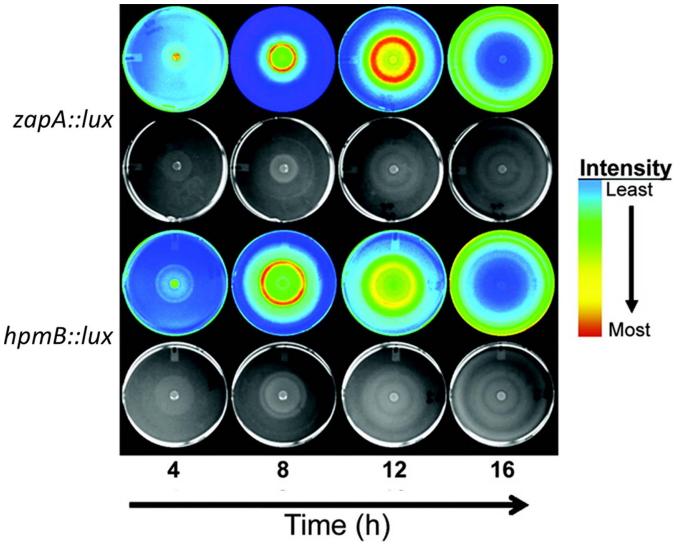

Figure 34 Expression of the virulence genes *zapA* and *hpmB* is coordinately regulated with swarming. The upstream promoter regions of *zapA* and *hpmB*, respectively, were fused to a promoterless *luxCDABE* cassette harbored on a low-copy-number plasmid and transformed into wild-type *P. mirabilis*. Each of the resulting strains was inoculated as a 5-µl spot in the center of an L agar plate and incubated at 37°C. Gene expression was measured as luminescence (Lux), which is displayed in false color corresponding to relative Lux intensity, where blue is the lowest and red is the most intense. An image of the colony growth photographed in natural light is shown below its corresponding Lux image. Expression of *zapA* (first two rows) and *hpmB* (third and fourth row) is shown at 4, 8, 12, and 16 h. Figure adapted, with permission, from reference 136.

Zinc

The high-affinity zinc importer genes *znuACB* are induced during UTI compared with laboratory culture (126), and ZnuB is recognized by the humoral immune response (183). Furthermore, a *znuC* mutant is outcompeted in mouse cochallenge experiments (319), and *znuACB* contributes to fitness in a CAUTI model (124). However, these systems are not an absolute requirement for infection, because the *znuC* mutant remains able to colonize during independent infection (319), and the requirement for *znuACB* in single-species CAUTI disappears during polymicrobial CAUTI (124). Zinc export may also contribute to infection, because exporter *ppaA* contributes to single-species CAUTI (124).

At least two virulence factors are linked to zinc: flagella and ZapA. ZapA is a member of the serralysin metalloprotease family of zinc metalloproteases, which have a conserved zinc-binding motif (197, 320). While this clearly suggests a zinc requirement for ZapA, it has not been directly tested. Work in *E. coli* showed that zinc is bound by the flagellar master regulator FlhC (321), so it is not surprising that a *znuC* mutant exhibits defects in flagella-mediated motility (both swimming and swarming) (319). Swarming is also inhibited in the presence of the transitional metal chelator TPEN, further supporting a role for zinc in motility (319). Interestingly, a zinc exporter *ppaA* mutant also exhibits aberrant swarming (322).

Nickel

Nickel is an essential component of catalytically active urease, in addition to other bacterial enzymes. However, there are few studies where *P. mirabilis* nickel homeostasis has been examined. Likewise, nickel sequestration by the host as a pathogen defense strategy has been proposed, but not yet conclusively demonstrated (323). Yet, there are some indications that nickel balance contributes to *P. mirabilis* fitness in the urinary tract. Genes from two predicted nickel import systems are induced in experimentally infected mice compared with laboratory culture: *nikAB* and *yntABCD* (126). Curiously, in a CAUTI model, these import systems were not found to be essential, but nickel export (PMI1518) was (124). Thus, nickel homeostasis appears to be important during infection, but the balance between enzymatic requirements and metal toxicity may be affected by the presence of a catheter and/or competing nutritional requirements of other bacteria.

Phosphate

Phosphorus, another essential element for life, is most often incorporated as inorganic phosphate. Phosphate sensing and uptake has been linked to virulence in many bacterial species (324), and *P. mirabilis* is no exception. Several studies have pointed to the importance of the *pstSCAB* phosphate uptake system to *P. mirabilis* virulence. Transposon mutations in *pstS* and *pstA* were both identified in a signature-tagged mutagenesis study (103), and complemented in the mouse model (325). All four genes in this operon were also required in a CAUTI model (124). One way the *pst* system contributes to virulence may be via regulation of biofilm formation (286). Interestingly, phosphate mutants outcompete wild-type bacteria during culture in human urine (325) and also during polymicrobial UTI (124), suggesting that the energy cost of operating this system may actually confer a fitness defect if the bacteria are growing under conditions in which phosphate sensing and uptake are not required.

Table 8 Iron-related genes in *P. mirabilis*

Gene designation(s)	Proposed function	PMI number(s)	Upregulated in iron limitation	Upregulated *in vivo*	Implicated *in vivo*	Antigenic *in vivo*	CAUTI		Citations
							Single	Poly	
Heme uptake									
	TonB-dependent receptor	PMI0409	✓			✓		✓	104, 183, 124
	Hemin uptake protein	PMI1424	✓	✓					104, 126
hmuR1R2STUV	Hemin uptake system	PMI1425-1430	✓	✓	✓	✓		✓	183, 104, 126, 317, 316, 124
Ferrous iron uptake									
sitDCBA	Iron ABC transporter	PMI1024-1027	✓	✓				✓	104, 126, 124
feoAB	Ferrous iron transport	PMI2920-2921		✓			✓		126, 124
Ferric citrate transport									
	Exported protease	PMI3704	✓					✓	104, 124
	Iron-related ABC transporter	PMI3705	✓		✓			✓	104, 154, 124
	Iron receptor	PMI3706-3707	✓					✓	104, 124
	Extracytoplasmic function family σ factor	PMI3708	✓					✓	104, 124
	TonB-like protein	PMI3709	✓				✓		104, 124
Siderophore production									
	TonB-dependent receptor	PMI2596	✓	✓	✓	✓		✓	183, 104, 318, 124
nrpXYRSUTABG	nrp siderophore	PMI2597-2605	✓	✓	✓			✓	104, 126, 103, 124
pbtIABCDEFGH	Proteobactin	PMI0231-0239	✓	✓				✓	154, 124

Other TonB-dependent receptors									
irgA	TonB-dependent enterobactin receptor	PMI0842	✓	✓	✓	✓		✓	183, 104, 126, 318, 124
ireA	Ferric siderophore receptor	PMI1945	✓	✓		✓	✓	✓	183, 104, 126, 318, 124
	TonB-dependent receptor	PMI0363	✓	✓				✓	104, 126, 124
	TonB-dependent receptor	PMI1548-1551	✓	✓				✓	104, 126, 124
hasR	TonB-dependent receptor	PMI3120-3121			✓			✓	103, 124
ABC-transport system									
	Iron-related ABC transporter	PMI0331	✓	✓				✓	104, 126, 124
	Iron-related ABC transporter	PMI2957-2960	✓	✓	✓		✓		104, 126, 103, 124
	Iron-related ABC transporter	PMI0229-0230	✓					✓	104, 124
Iron metabolism									
	Iron utilization protein	PMI1437	✓	✓				✓	104, 126, 124
Iron sulfur cluster formation/uptake									
	Iron sulfur cluster	PMI1411-1416	✓	✓			✓	✓	104, 126, 124
	Iron sulfur cluster	PMI3253	✓	✓				✓	104, 126, 124
	Iron sulfur cluster	PMI0176-0172	✓	✓				✓	104, 126, 124

Iron-related genes from *P. mirabilis* were identified by homology to other iron-related genes (104, 107). Genes identified as iron-related by homology but not identified using one of the four conditions shown were excluded. A checkmark indicates that one or more of the genes in the row were identified using the condition specified. Adapted from reference 19.

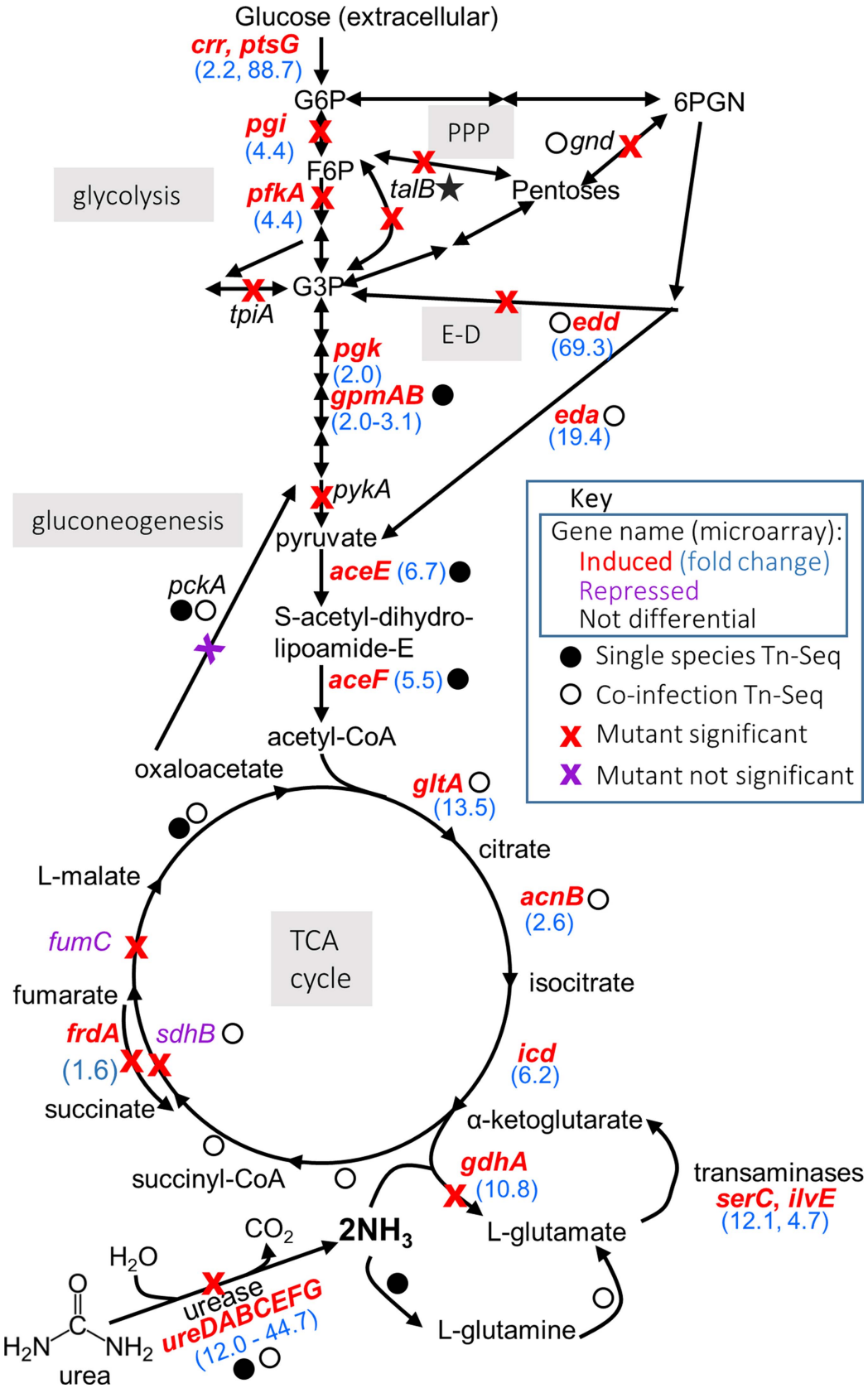
Glucose (extracellular)
crr, ptsG
(2.2, 88.7)
G6P
6PGN
pgi
(4.4)
PPP
gnd
F6P
talB
Pentoses
glycolysis
pfkA
(4.4)
G3P
tpiA
E-D
edd
(69.3)
pgk
(2.0)
gpmAB
(2.0-3.1)
eda
(19.4)
pykA
gluconeogenesis
pyruvate
pckA
aceE (6.7)
S-acetyl-dihydro-
lipoamide-E
aceF (5.5)
acetyl-CoA
oxaloacetate
gltA
(13.5)
citrate
L-malate
acnB
(2.6)
fumC
TCA
cycle
isocitrate
fumarate
frdA
(1.6)
sdhB
icd
(6.2)
succinate
α-ketoglutarate
succinyl-CoA
gdhA
(10.8)
transaminases
serC, ilvE
(12.1, 4.7)
CO2
2NH3
L-glutamate
H2O
urease
ureDABCEFG
(12.0 - 44.7)
L-glutamine
H2N
NH2
urea
Key
Gene name (microarray):
Induced (fold change)
Repressed
Not differential
Single species Tn-Seq
Co-infection Tn-Seq
Mutant significant
Mutant not significant

Metabolism in Urine

Unlike most *E. coli* strains, *P. mirabilis* isolates generally possess two important metabolic features that make them ideally suited to growth in human urine: the ability to utilize citrate as a sole carbon source, and the ability to hydrolyze urea to produce an abundant nitrogen source. Urea is the most abundant organic metabolite in human urine, at concentrations of ~400 mM (326–328). Filtration of citrate occurs in the kidney glomeruli, with approximately 10 to 35% of filtered citrate excreted in urine, making it the most abundant organic anion in human urine (329, 330). Thus, the combined use of citrate as a carbon source and ammonia as a nitrogen source provides *P. mirabilis* with a significant metabolic advantage over other uropathogens, and has implications for the carbon/nitrogen ratio that is sensed by *P. mirabilis* during growth in urine and the metabolic pathways favored by this organism.

Ascending UTI

Much has been learned regarding the metabolic pathways favored by *P. mirabilis* in the urinary tract through a combination of transcriptomics and genome-wide mutagenesis studies (Fig. 35). *P. mirabilis* appears to utilize glucose uptake and glycolysis during ascending UTI, as genes in these pathways are upregulated *in vivo* (126). The importance of glycolysis to *P. mirabilis* fitness was further verified in the murine model of ascending UTI by using mutants in glucose-6-phosphate isomerase (*pgi*), 6-phosphofructokinase transferase (*pfkA*), triosephosphate isomerase (*tpiA*), and pyruvate kinase (*pykA*) (331). Disruption of any single gene resulted in a dramatic fitness defect in bladder colonization, and all but *pykA* caused a fitness defect in kidney colonization.

Both the oxidative and nonoxidative branches of the pentose phosphate pathway for NADPH production have also been shown to contribute to *P. mirabilis* fitness within the urinary tract. Transaldolase (*talB*) catalyzes a reversible step in the nonoxidative branch of the pentose phosphate pathway. While this gene was not identified as differentially regulated by *in vivo* transcriptomics and has not been detected as a fitness factor by STM, it has been shown experimentally to contribute to *P. mirabilis* fitness in the bladder and kidneys during ascending UTI (331). Similarly, 6-phosphogluconate dehydrogenase (*gnd*) catalyzes a reaction in the oxidative branch of pentose phosphate pathway, and this gene has been shown to contribute to *P. mirabilis* fitness within the bladder and kidneys during ascending UTI (331). Notably, the D-glyceraldehyde 3-phosphate generated by the combined branches of the pentose phosphate pathway can feed directly into glycolysis.

P. mirabilis also appears to utilize the Entner-Doudoroff pathway during ascending UTI, because phosphogluconate dehydrogenase (*edd*) was upregulated during ascending UTI, identified as a fitness factor by STM, and disruption of this gene results in a fitness defect in bladder and kidney colonization (126, 154, 331). The other member of the Entner-Doudoroff pathway, a bifunctional 4-hydroxy-2-oxoglutarate aldolase/2-dehydro-3-deoxy-phosphogluconate aldolase encoded by *eda*, was also upregulated during ascending UTI, underscoring the importance of this metabolic pathway to *P. mirabilis* fitness (126). Products of the Entner-Doudoroff pathway are D-glyceraldehyde 3-phosphate, which can feed into glycolysis, and pyruvate, which can be directly catabolized to generate acetyl-CoA.

Regarding the aerobic tricarboxylic acid (TCA) cycle, subunit C of succinate dehydrogenase (*sdhC*) was identified as a fitness factor by STM, and subunit B (*sdhB*) was shown to directly contribute to fitness during kidney colonization (154, 331). Fumarate dehydratase (*fumC*) also contributes to *P. mirabilis* fitness in the bladder and kidneys (331). These results indicate a role for the aerobic TCA cycle during infection, which is further supported by the finding that cytochrome *bo3* oxidase (*cyoABCD*), a

Figure 35 Central metabolism during *P. mirabilis* UTI and CAUTI. Microarray analysis and targeted mutagenesis studies in an ascending UTI model both point to roles for glycolysis, oxidative pentose phosphate pathway (PPP), Entner-Doudoroff pathway (E-D), and both oxidative and branched/reductive TCA cycles during infection, while gluconeogenesis appears to be dispensable. Induction and requirement of *gdhA* suggests a low carbon-to-nitrogen ratio. Gene names in red were induced *in vivo* compared with broth culture as detected by microarray analysis; gene names in black were not differentially regulated, while names in purple were repressed. An "**X**" over a pathway indicates that a targeted mutant was assessed in cochallenge, with a red **X** indicating that the mutant was outcompeted and a purple **X** indicating no fitness defect. Interestingly, a different picture emerges from Tn-Seq in a CAUTI model, where a catheter remains in the bladder. Here, gluconeogenesis contributes to fitness instead of glycolysis, and ammonia uptake relies on *glnA* instead of *gdhA*. During coinfection with *Providencia stuartii* in the CAUTI model, gluconeogenesis remains important, and PPP, E-D, and the oxidative TCA cycle are once again contributors to fitness. Figure adapted from references 126, 331, and 124.

component of the aerobic respiratory chain, is upregulated during ascending UTI (126). However, fumarate reductase (*frdA*), which catalyzes the reduction of fumarate to succinate during anaerobic respiration, also contributes to *P. mirabilis* fitness in the bladder and kidneys, which may indicate use of a branched TCA cycle during infection (331). Other portions of the TCA cycle found to be upregulated during ascending UTI include citrate synthase (*gltA*), citrate hydro-lyase 2 (*acnB*), and isocitrate dehydrogenase (*icd*) (126).

In addition, transcriptomics and STM data indicate that *P. mirabilis* utilizes pyruvate catabolism via pyruvate dehydrogenase and dihydrolipoamide acetyltransferase (encoded by *poxB* and *aceEF*) to generate acetyl-CoA, which would feed into the TCA cycle through the action of citrate synthase (*gltA*) (126, 154). An abundance of factors pertaining to amino acid transport and metabolism are also upregulated during ascending UTI, including D-serine dehydratase (*dsdA*). D-Serine is present in a relatively high concentration in human urine (332, 333). Thus, *P. mirabilis* may utilize DsdA as an additional pathway for generating pyruvate and ammonia.

The transcriptome of *P. mirabilis* in the murine urinary tract also revealed a preferential role for glutamate dehydrogenase (*gdhA)* over glutamine synthetase (*glnA*) for nitrogen assimilation during ascending infection, which was recapitulated *in vitro* only when citrate was supplied as the sole carbon source (126). It was further determined that *gdhA* provides *P. mirabilis* with a competitive advantage for bladder and kidney colonization (126). Glutamate dehydrogenase is generally favored by bacteria for nitrogen assimilation when energy and carbon are limited, but there is an excess of ammonia and phosphate (334). Thus, the combined pattern of differential gene regulation coupled with mutagenesis studies indicates that *P. mirabilis* primarily utilizes pathways that feed into glycolysis, pyruvate catabolism, and citrate metabolism to fuel the TCA cycle through to production of α-ketoglutarate, which intersects with the production of L-glutamate by glutamate dehydrogenase using the excess ammonia produced by urease (126, 154).

Catheter-associated UTI

The recent use of a genome-saturating transposon library and transposon insertion-site sequencing (Tn-Seq) has provided insight into the metabolic pathways favored by *P. mirabilis* in the catheterized urinary tract compared to during ascending UTI (124). A list of fitness factors in common between CAUTI and other UTI studies is found in Table 9. However, this study indicated that the proinflammatory environment induced by the presence of a urinary catheter dramatically impacts *P. mirabilis* metabolism. For instance, while glycolysis, the pentose phosphate pathway, and the Entner-Doudoroff pathway contributed to *P. mirabilis* fitness in ascending UTI, the only gene pertaining to these pathways that was a fitness factor in the CAUTI model was pyruvate kinase (*pykF*), which catalyzes the transfer of a phosphate group from phosphoenolpyruvate to yield ATP and pyruvate. For the TCA cycle enzymes, only subunit A of succinate dehydrogenase (*sdhA*) and malate dehydrogenase (*mdh*) represented fitness factors for CAUTI. However, cytochrome *bo*3 quinol oxidase (*cyoABCDE*) remained an important fitness factor for *P. mirabilis* in the CAUTI model, indicating a continued need for aerobic respiration.

The CAUTI Tn-Seq results predominantly support a role for energy production through the catabolism of peptides and amino acids, and again implicate a role for D-serine dehydratase (*dsdA*) (124). Pyruvate catabolism remained important for both infection models, because pyruvate dehydrogenase (*aceEF*) represented an important fitness factor during CAUTI. Several genes involved in chorismate biosynthesis were also identified as CAUTI fitness factors, including *aroF*, *aroK*, and *aroL*. Chorismate is a branch point for biosynthesis of tryptophan, phenylalanine, and tyrosine. None of the tryptophan biosynthesis genes after the step catalyzed by *ubiC* (*trpEDCBA*) were identified as fitness factors for CAUTI, but *pheA* was a candidate fitness factor for bladder colonization and *tyrB* for both bladder and kidney colonization, indicating the potential importance of phenylalanine and tyrosine during CAUTI. It is also worth noting that pyruvate can be generated from chorismate in two ways: (i) *ubiC*, a fitness factor for bladder and kidney colonization, produces pyruvate from chorismate during synthesis of the ubiquinone precursor 4-hydroxybenzoate, and (ii) pyruvate is generated from chorismate and glutamine during synthesis of 4-aminobenzoate by *pabB*, a fitness factor for bladder colonization. Thus, interplay between chorismate biosynthesis and pyruvate catabolism may be important for *P. mirabilis* fitness during CAUTI.

Most striking, however, was the shift in nitrogen assimilation requirements between ascending UTI and CAUTI. In contrast to the ascending UTI studies, glutamate dehydrogenase (*gdhA*) was not identified as a

fitness factor for CAUTI, while glutamine synthetase (*glnA*) was identified as a fitness factor and verified to significantly contribute to urine and kidney colonization in the CAUTI model (124). In *E. coli*, glutamate dehydrogenase is favored when energy is limited, and glutamine synthetase is favored when energy limitation is no longer an issue (334). Thus, the preference for glutamine synthetase in the CAUTI model may reflect an excess of carbon sources in the catheterized urinary tract.

Polymicrobial infection

P. mirabilis is one of the most common organisms present during polymicrobial urine colonization and CAUTI (4, 8, 9, 17). Considering the unique features of *P. mirabilis* metabolism in urine, it is likely that the presence of this bacterium could have a dramatic impact on the metabolic pathways favored by other uropathogens during infection, and possibly *vice versa*. For instance, in the ascending model of UTI, *P. mirabilis* and *E. coli* appear to require different but complementary central metabolism pathways because *P. mirabilis* utilizes glycolysis, while *E. coli* favors gluconeogenesis (331). *P. mirabilis* also appears to utilize the pentose-phosphate pathway, the Entner-Doudoroff pathway, and the aerobic TCA cycle during ascending UTI as mutations affecting any of these pathways resulted in a fitness defect (331). Interestingly, coinfection of *P. mirabilis* with *E. coli* shifted the metabolic requirements for both species by alleviating the pentose-phosphate pathway requirement for *P. mirabilis* but making this pathway required for *E. coli* fitness during the coinfection.

Considering that a urease-negative isolate of *E. coli* was used for these experiments, the shift in metabolic requirements could be due in part to the impact of *P. mirabilis* urease on the carbon/nitrogen ratio available to *E. coli*. However, a genome-wide exploration of *P. mirabilis* fitness factors conducted during coinfection with *P. stuartii*, a urease-positive organism, similarly identified a dramatic impact on metabolic pathways in a murine model of CAUTI (124). Similar to coinfection with *E. coli*, coinfection with *P. stuartii* shifted the requirements for the pentose-phosphate pathway and also the Entner-Doudoroff pathway. Coinfection also resulted in a greater need for the import and synthesis of arginine and branched-chain amino acids. The requirement for branched-chain amino acid biosynthesis was determined to be the result of high-affinity import by *P. stuartii*, because mutation of a gene involved in branched-chain amino acid import in *P. stuartii* alleviated the requirement for synthesis by *P. mirabilis*. Regarding energy production and respiration, coinfection appeared to alleviate the requirement for cytochrome *bo3*, but imposed a requirement for the respiratory nitrate reductase system (*narGHJI*, *narXL*, *narP*, and *narK*) and an Rnf redox-driven ion pump (*rnfABCDGE*).

VACCINES

Infections associated with urolithiasis (stone formation) can be difficult to treat. Indeed, prevention of infection by vaccination may be preferable in high-risk groups such as those who are chronically catheterized in the urinary tract. To that end, there have been a number of relevant studies in murine models that suggest that vaccination is feasible, an example of which is given in Fig. 36.

Multiple approaches have been tested that include formalin-killed whole bacteria (217) and numerous surface-exposed or secreted proteins (47, 216–218, 335–339). In an early study (217), CBA/J mice were vaccinated with formalin-killed *P. mirabilis* bacteria or purified MR/P fimbriae or MrpH, the adhesin of the fimbria. For systemic immunizations, complete Freund's adjuvant was used as adjuvant; for intranasal administration, cholera toxin was used as adjuvant. Four routes of immunization were examined: subcutaneous, intranasal, transurethral, and oral. Antibodies to the antigens were measured in serum, urine, bladder, vaginal washes, and bile. For whole-killed bacteria, vaccination by the subcutaneous route resulted in protection for 60% of mice (defined as having fewer than 100 CFU per gram of tissue 7 days postinoculation), and intranasal vaccination provided protection in 67% of mice, but vaccination by the oral or transurethral routes failed to provide protection. Protection correlated with high serum antibody titers at day 21. For the intranasal route, measurable antibody was also found in the urine and bladder, albeit at a much reduced titer. When purified MR/P fimbriae were used, 60 to 63% protection, also at 2.5- to 3-log reduction, was noted by the intranasal or transurethral route. Protection also correlated with high serum antibody titer to the purified MR/P fimbriae. The tip adhesin was also examined as an antigen. Maltose-binding protein (MBP) fusions with MrpH (residues 23 to 157) and a truncated MrpH (residues 23 to 157) representing the receptor-binding domain were also used for intranasal immunization and yielded significant protection, especially for the MrpH receptor-binding domain, which provided up to 5 logs of protection in the bladder.

Table 9 Genes identified as fitness factors for CAUTI by Tn-Seq that were also identified in the ascending UTI model by STM or transcriptomics

Pathway	PMI number	Gene	Function	UTI transcriptome	UTI STM	CAUTI Tn-Seq
Amino acid transport and metabolism	PMI0145		Hypothetical protein	Up		B
	PMI0187	*dsdA*	D-Serine ammonia-lyase	Up		B, K
	PMI0347	*lysA*	Diaminopimelate decarboxylase	Up		B, K
	PMI0682	*artP*	L-Arginine ABC transporter ATP-binding protein	Down		B
	PMI0841	*lysP*	Lysine:proton symporter, AAT family	Up		K
	PMI1607	*sdaA*	L-Serine ammonia-lyase		U	K
	PMI1827	*cysK*	Cysteine synthase	Up		K
	PMI2093	*speB*	Agmatinase	Down		K
	PMI2094	*speA*	Arginine decarboxylase	Down		B, K
	PMI2259	*metN*	D-Methionine ABC transporter, ATP-binding protein	Up	U, K	B, K
	PMI2736	*potB*	Spermidine/putrescine ABC transporter, permease protein	Up		K
	PMI2822	*pabA*	Aminodeoxychorismate synthase, glutamine amidotransferase subunit	Up		B
	PMI2882	*glnA*	L-Glutamine synthetase	Down		B, K
	PMI3052	*asnA*	Aspartate-ammonia ligase	Up		B, K
Carbohydrate transport and metabolism	PMI0453	*nagA*	*N*-Acetylglucosamine 6-phosphate deacetylase	Up		K
	PMI0454	*nagB*	Glucosamine-6-phosphate deaminase	Up		B, K
	PMI0873	*nagZ*	β-*N*-Acetylhexosaminidase	Up		B
	PMI1046		Polysaccharide deacetylase		U, B, K	B, K
	PMI1776		PTS system IIB component, L-Asc family	Up		B
	PMI1828	*hpr/ptsH*	PTS system phosphocarrier protein	Up		B, K
	PMI1829	*ptsI*	Phosphoenolpyruvate–protein phosphotransferase	Up		B, K
	PMI1830	*crr*	PTS system D-glucose-specific IIA component, Glc family	Up		B, K
	PMI1943		MFS-family transporter	Down		B, K
	PMI2134	*agaA*	*N*-Acetylgalactosamine 6-phosphate deacetylase	Up		B
	PMI2141	*agaR*	Transcriptional regulator, DeoR family	Up		B, K
	PMI2414	*deoB*	Phosphopentomutase	Up		B, K
	PMI3095		*N*-Acetylglucosamine kinase	Up		K
	PMI3716	*gpmB*	Probable phosphoglycerate mutase	Up		K
Coenzyme transport and metabolism	PMI0105	*cyoE*	Protoheme IX farnesyltransferase	Up		B, K
	PMI2022	*visC*	2-Octaprenyl-3-methyl-6-methoxy-1,4-benzoquinol hydroxylase	Up		K
	PMI2353	*ribB*	3,4-Dihydroxy-2-butanone 4-phosphate synthase	Down		K
	PMI3547	*fre*	NAD(P)H-flavin reductase	Up		B, K

(continued)

Table 9 Genes identified as fitness factors for CAUTI by Tn-Seq that were also identified in the ascending UTI model by STM or transcriptomics *(continued)*

Pathway	PMI number	Gene	Function	UTI transcriptome	UTI STM	CAUTI Tn-Seq
Energy production and conversion	PMI0107	*cyoB*	Cytochrome bo3 quinol oxidase subunit 1 apoprotein	Up		B, K
	PMI0108	*cyoA*	Cytochrome bo3 quinol oxidase subunit 2	Up		B, K
	PMI0354	*nqrC*	Na^+-translocating NADH-quinone reductase subunit C	Up		B, K
	PMI0355	*nqrD*	Na^+-translocating NADH-quinone reductase subunit D	Up		B, K
	PMI0705	*pflB*	Formate acetyltransferase	Up		K
	PMI1200	*pntA*	NAD(P) transhydrogenase subunit alpha (pyridine nucleotide transhydrogenase subunit alpha)	Up		B
	PMI1753	*nuoK*	NADH dehydrogenase subunit K	Up		B
	PMI1754	*nuoJ*	NADH dehydrogenase subunit J	Up		K
	PMI1760	*nuoC/nuoD*	NADH dehydrogenase subunit C (EC 1.6.5.3)/NADH dehydrogenase subunit D	Up		B, K
	PMI1771	*ackA*	Acetate kinase	Up		K
	PMI1772	*pta*	Phosphotransacetylase	Up		K
	PMI2045	*aceF*	Dihydrolipoyllysine-residue acetyltransferase component of pyruvate dehydrogenase complex	Up		B, K
	PMI2046	*aceE*	Pyruvate dehydrogenase E1 component	Up	B, K	B, K
	PMI2740	*qor*	Quinone oxidoreductase	Up		K
	PMI2930	*glpD/glyD*	Homodimeric glycerol 3-phosphate dehydrogenase (quinone)	Down		B, K
	PMI3108	*fdoI*	Formate dehydrogenase (quinone-dependent) cytochrome b subunit	Up		K
	PMI3300	*ilvM*	Acetolactate synthase, small subunit	Up		K

In a follow-up study, the MrpH receptor-binding domain (residues 23 to 157) was translationally fused with the cholera toxin A2 domain, which was coexpressed with the cholera toxin B subunit (a holotoxin-like chimera) (218). Mice immunized with MrpH receptor-binding domain-CT complex were colonized by significantly fewer bacteria in the bladder (median $\log_{10}$ CFU per gram of tissue, 6.43 for the naive mice versus 2.00 for the immunized mice; $P = 0.02$) and the kidneys (median $\log_{10}$ CFU per gram of tissue, 5.28 for the naive mice versus 3.43 for the immunized mice; $P = 0.046$).

As well, two additional studies demonstrated that vaccination, either intranasally or transurethrally, with fusion proteins that contain both MrpH of *P. mirabilis* and FimH, the adhesin of type 1 fimbriae of *E. coli*, conferred protection against *P. mirabilis* UTI (339, 340).

In another fimbrial vaccination study (216), the main structural subunits (MrpA, UcaA, and PmfA) of three *P. mirabilis* fimbriae (MR/P, UCA, and PMF) were administered as vaccine antigens by the subcutaneous route. Mice were challenged with *P. mirabilis* either transurethrally or intravenously. MrpA protected against UTI and hematogenous challenge. UcaA protected only against hematogenous challenge. PmfA did not protect by either route of *P. mirabilis* challenge. In studies where flagellin was included with MrpA as antigens in intranasal vaccination, neither flagellin alone nor flagellin with MrpA led to protection from *P. mirabilis* challenge in the urinary tract (338). Administration of adjuvant cholera toxin in the urinary tract enhanced humoral and cytokine response but did not influence the degree of protection against UTI provided by MrpA (336).

MrpA expressed in heterologous hosts has also been tested as a vaccine antigen. MrpA was expressed as either a cell wall-anchored or secreted protein in *Lactococcus lactis* (335). Protection assays against challenge by *P. mirabilis* were tested in the mouse model, and significant induction of specific serum IgG and IgA was found in mice immunized with *L. lactis* expressing the MrpA antigen. A significant reduction of renal bacterial colonization was observed using both constructs. MrpA was

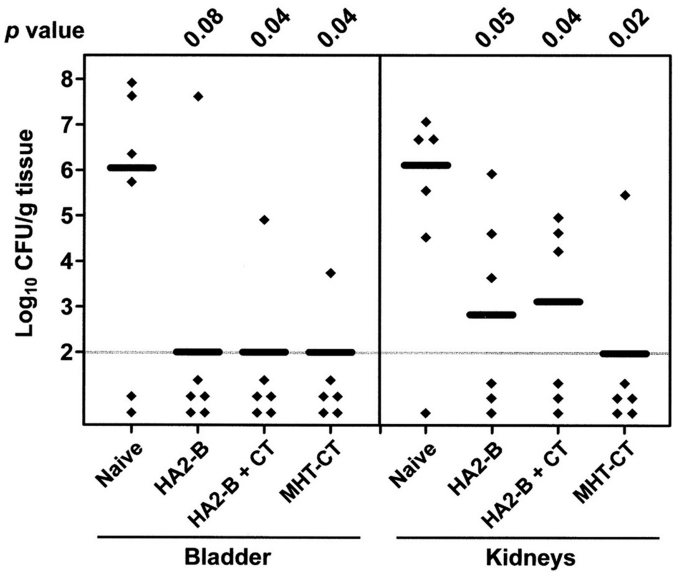

Figure 36 *P. mirabilis* colonization in bladders and kidneys of naive mice and mice nasally immunized with MrpH using cholera toxin (CT) as an adjuvant. Immunized mice were given primary immunization on day 0 and two booster immunizations on days 14 and 24. On day 34, all mice were challenged with 5×10^7 CFU *P. mirabilis*. After 7 days, bacterial burden was assessed. MHT, maltose-binding protein fusion of MrpH truncate; MHT-CT, MHT covalently coupled to CT; HA2-B, $MrpH_{23\text{-}157}$-CT chimera; HA2-B + CT, HA2-B mixed with CT. Each diamond represents the $\log_{10}$ CFU per gram of tissue from an individual mouse. Samples with undetectable colonization were given a value of 2 $\log_{10}$ CFU/g tissue (the limit of detection). Horizontal bars represent the median $\log_{10}$ CFU per gram of tissue for each column. One-tailed *P* values were determined by the Mann-Whitney test, comparing the colonization levels in bladders and kidneys of the naive mice with those of the immunized mice. Reproduced from reference 218, with permission.

also expressed as a MrpA-TetC (tetanus toxin fragment) in *S. enterica* serovar Typhimurium (337) and used for intranasal vaccination. After two immunization doses, intranasally vaccinated mice showed a significant increase in specific serum IgG against MrpA and against the LPS of the *Salmonella* strain. Significant decreases in both kidney and bladder colonization by *P. mirabilis* after transurethral challenge were noted.

A nonfimbrial secreted protein, *Proteus* toxic agglutinin, proved to be a potent protective antigen for the upper urinary tract (47). Mice intranasally vaccinated with a site-directed mutant (S366A) of *Proteus* toxic agglutinin, which inactivated the protease active site, conjugated to cholera toxin, had significantly lower bacterial counts in their kidneys ($P = 0.001$) and spleens ($P = 0.002$) than mice that received cholera toxin alone. Bladders were not protected. Serum IgG levels correlated with protection.

Last, it is interesting to note that a vaccine used in Europe, Solco-Urovac, contains heat-killed enteric bacteria including *P. mirabilis* (341, 342). The vaccine has been shown to have demonstrable, although limited, efficacy against recurrent UTI (343). Further research into *P. mirabilis* vaccines is necessary, but heat-killed bacteria and surface-exposed or secreted proteins may have efficacy as vaccine antigens, and an intranasal route may be effective for vaccination. One issue is the identification of the target population for vaccination against *P. mirabilis*. For example, the population that might benefit most from vaccination against this species is elderly catheterized patients in chronic care facilities, but they may have diminished capacity to respond immunologically to vaccination. This poses an additional hurdle for development of an effective vaccine.

SUMMARY/CONCLUSIONS

When surveying the extensive literature on *P. mirabilis* infection and considering the relatively few laboratories that have undertaken studying this pathogen, there has been remarkable progress made in identifying virulence factors and mechanisms of pathogenesis for this uropathogen. Clearly, the catheterized urinary tract is a preferred niche for *P. mirabilis*, and often the bacterium coexists with several other members of a polymicrobial community. However, monoinfection has been used for the most part to identify and characterize the virulence arsenal that includes urease, 17 different fimbriae, secreted cytolethal and cytolytic toxins and proteases, extensive networks for iron and other metal ion acquisition, flagella, and numerous secretion systems. We are just beginning to exploit relatively new tools and screens such as Tn-Seq and RNA-Seq to investigate mechanisms of pathogenesis in models of polymicrobial bacteriuria. This added layer of complexity is daunting, but ultimately manageable, and will open the door to the development of treatment strategies.

In the early days, investigators worked with simple molecular tools to identify single genes or operons involved in pathogenesis. Frankly, victories were hard fought although targets of discovery were plentiful. With the advent of facile sequencing technologies, PCR, microarrays, fruitful screens including signature-tagged mutagenesis and transposon-directed insertion site sequencing and RNA-Seq, numerous new candidate genes that contribute to colonization, establishment of infection, and damage to the host have been highlighted for *P. mirabilis*.

While often tedious, such screens are straightforward and yield a staggering number of genes that represent virulence or fitness factors. What lies ahead is the hard work of probing the biology of these new-found genes. Thus, with the groundwork presented here, we can renew our efforts to refine a view of pathogenesis that includes the interactions and temporal expression of the battery of virulence factors and metabolic cycles discussed in this review.

ACKNOWLEDGMENTS

This work was supported by Public Health Service grants from the National Institutes of Health (K99 DK105205 to C.E.A.; AI059722 and DK094777 to H.L.T.M.).

We are grateful to the many *Proteus mirabilis* researchers whose work contributed to this review.

REFERENCES

1. Adeolu M, Alnajar S, Naushad S, Gupta RS. 2016. Genome-based phylogeny and taxonomy of the '*Enterobacteriales*': proposal for Enterobacterales ord. nov. divided into the families *Enterobacteriaceae*, *Erwiniaceae* fam. nov., *Pectobacteriaceae* fam. nov., *Yersiniaceae* fam. nov., *Hafniaceae* fam. nov., *Morganellaceae* fam. nov., and *Budviciaceae* fam. nov. *Int J Syst Evol Microbiol* **66:**5575–5599.

2. Wenner JJ, Rettger LF. 1919. A systematic study of the *Proteus* group of bacteria. *J Bacteriol* **4:**331–353.

3. Armbruster CE, Mobley HLT. 2012. Merging mythology and morphology: the multifaceted lifestyle of *Proteus mirabilis*. *Nat Rev Microbiol* **10:**743–754.

4. Warren JW, Tenney JH, Hoopes JM, Muncie HL, Anthony WC. 1982. A prospective microbiologic study of bacteriuria in patients with chronic indwelling urethral catheters. *J Infect Dis* **146:**719–723.

5. Mobley HLT, Warren JW. 1987. Urease-positive bacteriuria and obstruction of long-term urinary catheters. *J Clin Microbiol* **25:**2216–2217.

6. Breitenbucher RB. 1984. Bacterial changes in the urine samples of patients with long-term indwelling catheters. *Arch Intern Med* **144:**1585–1588.

7. Jacobsen SM, Stickler DJ, Mobley HLT, Shirtliff ME. 2008. Complicated catheter-associated urinary tract infections due to *Escherichia coli* and *Proteus mirabilis*. *Clin Microbiol Rev* **21:**26–59.

8. Nicolle LE. 2005. Catheter-related urinary tract infection. *Drugs Aging* **22:**627–639.

9. Armbruster CE, Prenovost K, Mobley HLT, Mody L. 2017. How often do clinically diagnosed catheter-associated urinary tract infections in nursing home residents meet standardized criteria? *J Am Geriatr Soc* **65:**395–401. doi:10.1111/jgs.14533.

10. Hung EW, Darouiche RO, Trautner BW. 2007. Proteus bacteriuria is associated with significant morbidity in spinal cord injury. *Spinal Cord* **45:**616–620.

11. Griffith DP, Musher DM, Itin C. 1976. Urease. The primary cause of infection-induced urinary stones. *Invest Urol* **13:**346–350.

12. Li X, Zhao H, Lockatell CV, Drachenberg CB, Johnson DE, Mobley HLT. 2002. Visualization of *Proteus mirabilis* within the matrix of urease-induced bladder stones during experimental urinary tract infection. *Infect Immun* **70:**389–394.

13. Foxman B, Brown P. 2003. Epidemiology of urinary tract infections: transmission and risk factors, incidence, and costs. *Infect Dis Clin North Am* **17:**227–241.

14. Kim BN, Kim NJ, Kim MN, Kim YS, Woo JH, Ryu J. 2003. Bacteraemia due to tribe Proteeae: a review of 132 cases during a decade (1991–2000). *Scand J Infect Dis* **35:**98–103.

15. Watanakunakorn C, Perni SC. 1994. *Proteus mirabilis* bacteremia: a review of 176 cases during 1980–1992. *Scand J Infect Dis* **26:**361–367.

16. Daniels KR, Lee GC, Frei CR. 2014. Trends in catheter-associated urinary tract infections among a national cohort of hospitalized adults, 2001–2010. *Am J Infect Control* **42:**17–22.

17. Hooton TM, Bradley SF, Cardenas DD, Colgan R, Geerlings SE, Rice JC, Saint S, Schaeffer AJ, Tambayh PA, Tenke P, Nicolle LE, Infectious Diseases Society of America. 2010. Diagnosis, prevention, and treatment of catheter-associated urinary tract infection in adults: 2009 International Clinical Practice Guidelines from the Infectious Diseases Society of America. *Clin Infect Dis* **50:**625–663.

18. Morgenstein RM, Szostek B, Rather PN. 2010. Regulation of gene expression during swarmer cell differentiation in *Proteus mirabilis*. *FEMS Microbiol Rev* **34:**753–763.

19. Schaffer JN, Pearson MM. 2015. *Proteus mirabilis* and urinary tract infections. *Microbiol Spectr* **3:**3. doi:10.1128/microbiolspec.UTI-0017-2013.

20. Norsworthy AN, Pearson MM. 2017. From catheter to kidney stone: the uropathogenic lifestyle of *Proteus mirabilis*. *Trends Microbiol* **25:**304–315. doi:10.1016/j.tim.2016.11.015.

21. Garcia MM, Gulati S, Liepmann D, Stackhouse GB, Greene K, Stoller ML. 2007. Traditional Foley drainage systems–do they drain the bladder? *J Urol* **177:**203–207.

22. Willette PA, Coffield S. 2012. Current trends in the management of difficult urinary catheterizations. *West J Emerg Med* **13:**472–478.

23. Hofseth LJ, Dunn BP, Rosin MP. 1996. Micronucleus frequencies in urothelial cells of catheterized patients with chronic bladder inflammation. *Mutat Res* **352:**65–72.

24. Anderson RU. 1979. Response of bladder and urethral mucosa to catheterization. *JAMA* **242:**451–453.

25. Armbruster CE, Smith SN, Johnson AO, DeOrnellas V, Eaton KA, Yep A, Mody L, Wu W, Mobley HLT. 2017. The pathogenic potential of proteus mirabilis is enhanced by other uropathogens during polymicrobial urinary tract infection. *Infect Immun* **85:**e00808–e00816.

26. Kunin CM. 1989. Blockage of urinary catheters: role of microorganisms and constituents of the urine on formation of encrustations. *J Clin Epidemiol* **42:**835–842.

27. Stickler D, Ganderton L, King J, Nettleton J, Winters C. 1993. *Proteus mirabilis* biofilms and the encrustation of urethral catheters. *Urol Res* **21:**407–411.

28. Coker C, Poore CA, Li X, Mobley HLT. 2000. Pathogenesis of *Proteus mirabilis* urinary tract infection. *Microbes Infect* **2:**1497–1505.

29. Choong S, Wood S, Fry C, Whitfield H. 2001. Catheter associated urinary tract infection and encrustation. *Int J Antimicrob Agents* **17:**305–310.

30. Stickler DJ, Lear JC, Morris NS, Macleod SM, Downer A, Cadd DH, Feast WJ. 2006. Observations on the adherence of *Proteus mirabilis* onto polymer surfaces. *J Appl Microbiol* **100:**1028–1033.

31. Sabbuba NA, Mahenthiralingam E, Stickler DJ. 2003. Molecular epidemiology of *Proteus mirabilis* infections of the catheterized urinary tract. *J Clin Microbiol* **41:**4961–4965.

32. Kunin CM. 1997. *Urinary Tract Infections: Detection, Prevention, and Management*, 5th ed. Williams & Wilkins, Baltimore, MD.

33. Griffith DP, Osborne CA. 1987. Infection (urease) stones. *Miner Electrolyte Metab* **13:**278–285.

34. Fowler JE Jr. 1984. Bacteriology of branched renal calculi and accompanying urinary tract infection. *J Urol* **131:**213–215.

35. Lerner SP, Gleeson MJ, Griffith DP. 1989. Infection stones. *J Urol* **141:**753–758.

36. McLean RJ, Cheng KJ, Gould WD, Nickel JC, Costerton JW. 1986. Histochemical and biochemical urease localization in the periplasm and outer membrane of two *Proteus mirabilis* strains. *Can J Microbiol* **32:**772–778.

37. Prywer J, Olszynski M. 2017. Bacterially induced formation of infectious urinary stones: recent developments and future challenges. *Curr Med Chem* **24:**292–311.

38. Torzewska A, Różalski A. 2015. Various intensity of *Proteus mirabilis*-induced crystallization resulting from the changes in the mineral composition of urine. *Acta Biochim Pol* **62:**127–132.

39. Johnson DE, Russell RG, Lockatell CV, Zulty JC, Warren JW, Mobley HL. 1993. Contribution of *Proteus mirabilis* urease to persistence, urolithiasis, and acute pyelonephritis in a mouse model of ascending urinary tract infection. *Infect Immun* **61:**2748–2754.

40. Jones BD, Lockatell CV, Johnson DE, Warren JW, Mobley HL. 1990. Construction of a urease-negative mutant of *Proteus mirabilis*: analysis of virulence in a mouse model of ascending urinary tract infection. *Infect Immun* **58:**1120–1123.

41. Armbruster CE, Smith SN, Yep A, Mobley HLT. 2014. Increased incidence of urolithiasis and bacteremia during *Proteus mirabilis* and *Providencia stuartii* coinfection due to synergistic induction of urease activity. *J Infect Dis* **209:**1524–1532.

42. Huang HS, Chen J, Teng LJ, Lai MK. 1999. Use of polymerase chain reaction to detect *Proteus mirabilis* and *Ureaplasma urealyticum* in urinary calculi. *J Formos Med Assoc* **98:**844–850.

43. Schaffer JN, Norsworthy AN, Sun T-T, Pearson MM. 2016. *Proteus mirabilis* fimbriae- and urease-dependent clusters assemble in an extracellular niche to initiate bladder stone formation. *Proc Natl Acad Sci USA* **113:**4494–4499.

44. Mobley HL, Belas R, Lockatell V, Chippendale G, Trifillis AL, Johnson DE, Warren JW. 1996. Construction of a flagellum-negative mutant of *Proteus mirabilis*: effect on internalization by human renal epithelial cells and virulence in a mouse model of ascending urinary tract infection. *Infect Immun* **64:**5332–5340.

45. Allison C, Coleman N, Jones PL, Hughes C. 1992. Ability of *Proteus mirabilis* to invade human urothelial cells is coupled to motility and swarming differentiation. *Infect Immun* **60:**4740–4746.

46. Alamuri P, Löwer M, Hiss JA, Himpsl SD, Schneider G, Mobley HLT. 2010. Adhesion, invasion, and agglutination mediated by two trimeric autotransporters in the human uropathogen *Proteus mirabilis*. *Infect Immun* **78:**4882–4894.

47. Alamuri P, Eaton KA, Himpsl SD, Smith SN, Mobley HLT. 2009. Vaccination with proteus toxic agglutinin, a hemolysin-independent cytotoxin in vivo, protects against *Proteus mirabilis* urinary tract infection. *Infect Immun* **77:**632–641.

48. Chippendale GR, Warren JW, Trifillis AL, Mobley HL. 1994. Internalization of *Proteus mirabilis* by human renal epithelial cells. *Infect Immun* **62:**3115–3121.

49. Mathoera RB, Kok DJ, Verduin CM, Nijman RJM. 2002. Pathological and therapeutic significance of cellular invasion by *Proteus mirabilis* in an enterocystoplasty infection stone model. *Infect Immun* **70:**7022–7032.

50. Oelschlaeger TA, Tall BD. 1996. Uptake pathways of clinical isolates of *Proteus mirabilis* into human epithelial cell lines. *Microb Pathog* **21:**1–16.

51. Peerbooms PG, Verweij AM, MacLaren DM. 1984. Vero cell invasiveness of *Proteus mirabilis*. *Infect Immun* **43:**1068–1071.

52. Braude AI, Siemienski J. 1960. Role of bacterial urease in experimental pyelonephritis. *J Bacteriol* **80:**171–179.

53. Mobley HL, Chippendale GR, Swihart KG, Welch RA. 1991. Cytotoxicity of the HpmA hemolysin and urease of *Proteus mirabilis* and *Proteus vulgaris* against cultured human renal proximal tubular epithelial cells. *Infect Immun* **59:**2036–2042.

54. Ingersoll MA, Albert ML. 2013. From infection to immunotherapy: host immune responses to bacteria at the bladder mucosa. *Mucosal Immunol* **6:**1041–1053.

55. Ambite I, Nagy K, Godaly G, Puthia M, Wullt B, Svanborg C. 2016. Susceptibility to urinary tract infection: benefits and hazards of the antibacterial host response. *Microbiol Spectr* **4:**4. doi:10.1128/microbiolspec.UTI-0019-2014.

56. Hayes BW, Abraham SN. 2016. Innate immune responses to bladder infection. *Microbiol Spectr* **4:**4. doi:10.1128/microbiolspec.UTI-0024-2016.

57. Kolaczkowska E, Kubes P. 2013. Neutrophil recruitment and function in health and inflammation. *Nat Rev Immunol* **13:**159–175.

58. Kline KA, Schwartz DJ, Lewis WG, Hultgren SJ, Lewis AL. 2011. Immune activation and suppression by group B streptococcus in a murine model of urinary tract infection. *Infect Immun* **79:**3588–3595.

59. Peng L, Jiang Q, Pan JY, Deng C, Yu JY, Wu XM, Huang SH, Deng XY. 2016. Involvement of polyphosphate kinase in virulence and stress tolerance of uropathogenic *Proteus mirabilis*. *Med Microbiol Immunol (Berl)* **205:**97–109.

60. Weichhart T, Haidinger M, Hörl WH, Säemann MD. 2008. Current concepts of molecular defence mechanisms operative during urinary tract infection. *Eur J Clin Invest* **38**(Suppl 2)**:**29–38.

61. Papayannopoulos V, Zychlinsky A. 2009. NETs: a new strategy for using old weapons. *Trends Immunol* **30:**513–521.

62. Yu Y, Sikorski P, Bowman-Gholston C, Cacciabeve N, Nelson KE, Pieper R. 2015. Diagnosing inflammation and infection in the urinary system via proteomics. *J Transl Med* **13:**111. doi:10.1186/s12967-015-0475-3.

63. Yu Y, Kwon K, Tsitrin T, Bekele S, Sikorski P, Nelson KE, Pieper R. 2017. Characterization of early-phase neutrophil extracellular traps in urinary tract infections. *PLoS Pathog* **13:**e1006151. doi:10.1371/journal.ppat.1006151.

64. Chen CY, Chen YH, Lu PL, Lin WR, Chen TC, Lin CY. 2012. *Proteus mirabilis* urinary tract infection and bacteremia: risk factors, clinical presentation, and outcomes. *J Microbiol Immunol Infect* **45:** 228–236.

65. Guo H, Callaway JB, Ting JP. 2015. Inflammasomes: mechanism of action, role in disease, and therapeutics. *Nat Med* **21:**677–687.

66. Seo SU, Kamada N, Muñoz-Planillo R, Kim YG, Kim D, Koizumi Y, Hasegawa M, Himpsl SD, Browne HP, Lawley TD, Mobley HL, Inohara N, Núñez G. 2015. Distinct commensals induce interleukin-1β via nlrp3 inflammasome in inflammatory monocytes to promote intestinal inflammation in response to injury. *Immunity* **42:**744–755.

67. Devuyst O, Olinger E, Rampoldi L. 2017. Uromodulin: from physiology to rare and complex kidney disorders. *Nat Rev Nephrol* **13:**525–544.

68. Bates JM Jr, Raffi HM, Prasadan K, Mascarenhas R, Laszik Z, Maeda N, Hultgren SJ, Kumar S. 2004. Tamm-Horsfall protein knockout mice are more prone to urinary tract infection: rapid communication. *Kidney Int* **65:**791–797.

69. Raffi HS, Bates JM Jr, Laszik Z, Kumar S. 2009. Tamm-horsfall protein protects against urinary tract infection by *Proteus mirabilis*. *J Urol* **181:**2332–2338.

70. Steiner TS. 2007. How flagellin and toll-like receptor 5 contribute to enteric infection. *Infect Immun* **75:**545–552.

71. Okumura R, Kurakawa T, Nakano T, Kayama H, Kinoshita M, Motooka D, Gotoh K, Kimura T, Kamiyama N, Kusu T, Ueda Y, Wu H, Iijima H, Barman S, Osawa H, Matsuno H, Nishimura J, Ohba Y, Nakamura S, Iida T, Yamamoto M, Umemoto E, Sano K, Takeda K. 2016. Lypd8 promotes the segregation of flagellated microbiota and colonic epithelia. *Nature* **532:**117–121.

72. Umpiérrez A, Scavone P, Romanin D, Marqués JM, Chabalgoity JA, Rumbo M, Zunino P. 2013. Innate immune responses to *Proteus mirabilis* flagellin in the urinary tract. *Microbes Infect* **15:**688–696.

73. Mobley HLT, Belas R. 1995. Swarming and pathogenicity of *Proteus mirabilis* in the urinary tract. *Trends Microbiol* **3:**280–284.

74. Olaitan AO, Morand S, Rolain JM. 2014. Mechanisms of polymyxin resistance: acquired and intrinsic resistance in bacteria. *Front Microbiol* **5:**643. doi:10.3389/fmicb.2014.00643.

75. McCoy AJ, Liu H, Falla TJ, Gunn JS. 2001. Identification of *Proteus mirabilis* mutants with increased sensitivity to antimicrobial peptides. *Antimicrob Agents Chemother* **45:**2030–2037.

76. Chromek M, Stankowska D, Dadfar E, Kaca W, Rabbani H, Brauner A. 2005. Interleukin-8 response in cells from the human urinary tract induced by lipopolysaccharides of *Proteus mirabilis* O3 and O18. *J Urol* **173:**1381–1384.

77. Callewaert L, Vanderkelen L, Deckers D, Aertsen A, Robben J, Michiels CW. 2008. Detection of a lysozyme inhibitor in *Proteus mirabilis* by a new reverse zymogram method. *Appl Environ Microbiol* **74:**4978–4981.

78. Rashid T, Ebringer A, Wilson C. 2017. The link between *Proteus mirabilis*, environmental factors and autoantibodies in rheumatoid arthritis. *Clin Exp Rheumatol* **35:**865–871.

79. Pretorius E, Akeredolu OO, Soma P, Kell DB. 2017. Major involvement of bacterial components in rheumatoid arthritis and its accompanying oxidative stress, systemic inflammation and hypercoagulability. *Exp Biol Med (Maywood)* **242:**355–373.

80. Garrett WS, Gallini CA, Yatsunenko T, Michaud M, DuBois A, Delaney ML, Punit S, Karlsson M, Bry L, Glickman JN, Gordon JI, Onderdonk AB, Glimcher LH. 2010. *Enterobacteriaceae* act in concert with the gut microbiota to induce spontaneous and maternally transmitted colitis. *Cell Host Microbe* **8:**292–300.

81. Keane WF, Freedman LR. 1967. Experimental pyelonephritis. XIV. Pyelonephritis in normal mice produced by inoculation of *E. coli* into the bladder lumen during water diuresis. *Yale J Biol Med* **40:**231–237.

82. Hagberg L, Engberg I, Freter R, Lam J, Olling S, Svanborg Edén C. 1983. Ascending, unobstructed urinary tract infection in mice caused by pyelonephritogenic *Escherichia coli* of human origin. *Infect Immun* **40:**273–283.

83. Kadurugamuwa JL, Modi K, Yu J, Francis KP, Purchio T, Contag PR. 2005. Noninvasive biophotonic imaging for monitoring of catheter-associated urinary tract infections and therapy in mice. *Infect Immun* **73:**3878–3887.

84. Conover MS, Flores-Mireles AL, Hibbing ME, Dodson K, Hultgren SJ. 2015. Establishment and characterization of UTI and CAUTI in a mouse model. *J Vis Exp* **(100):**e52892. doi:10.3791/52892.

85. Thai KH, Thathireddy A, Hsieh MH. 2010. Transurethral induction of mouse urinary tract infection. *J Vis Exp* **(42):**2070. doi:10.3791/2070.

86. Johnson DE, Lockatell CV, Hall-Craigs M, Mobley HL, Warren JW. 1987. Uropathogenicity in rats and mice of *Providencia stuartii* from long-term catheterized patients. *J Urol* **138:**632–635.

87. Guiton PS, Hung CS, Hancock LE, Caparon MG, Hultgren SJ. 2010. Enterococcal biofilm formation and virulence in an optimized murine model of foreign body-associated urinary tract infections. *Infect Immun* **78:**4166–4175.

88. Kurosaka Y, Ishida Y, Yamamura E, Takase H, Otani T, Kumon H. 2001. A non-surgical rat model of foreign body-associated urinary tract infection with *Pseudomonas aeruginosa*. *Microbiol Immunol* **45:**9–15.

89. Janssen C, Lo J, Jäger W, Moskalev I, Law A, Chew BH, Lange D. 2014. A high throughput, minimally invasive, ultrasound guided model for the study of catheter associated urinary tract infections and device encrustation in mice. *J Urol* **192:**1856–1863.

90. Williams FD, Schwarzhoff RH. 1978. Nature of the swarming phenomenon in *Proteus*. *Annu Rev Microbiol* **32:**101–122.

91. Rózalski A, Sidorczyk Z, Kotełko K. 1997. Potential virulence factors of *Proteus* bacilli. *Microbiol Mol Biol Rev* **61:**65–89.

92. O'Hara CM, Brenner FW, Miller JM. 2000. Classification, identification, and clinical significance of *Proteus, Providencia, and Morganella*. *Clin Microbiol Rev* **13:**534–546.

93. Welch RA, Burland V, Plunkett G III, Redford P, Roesch P, Rasko D, Buckles EL, Liou SR, Boutin A, Hackett J, Stroud D, Mayhew GF, Rose DJ, Zhou S, Schwartz DC, Perna NT, Mobley HL, Donnenberg MS, Blattner FR. 2002. Extensive mosaic structure revealed by the complete genome sequence of uropathogenic *Escherichia coli*. *Proc Natl Acad Sci USA* **99:**17020–17024.

94. Touchon M, Hoede C, Tenaillon O, Barbe V, Baeriswyl S, Bidet P, Bingen E, Bonacorsi S, Bouchier C, Bouvet O, Calteau A, Chiapello H, Clermont O, Cruveiller S, Danchin A, Diard M, Dossat C, Karoui ME, Frapy E, Garry L, Ghigo JM, Gilles AM, Johnson J, Le Bouguénec C, Lescat M, Mangenot S, Martinez-Jéhanne V, Matic I, Nassif X, Oztas S, Petit MA, Pichon C, Rouy Z, Ruf CS, Schneider D, Tourret J, Vacherie B, Vallenet D, Médigue C, Rocha EP, Denamur E. 2009. Organised genome dynamics in the *Escherichia coli* species results in highly diverse adaptive paths. *PLoS Genet* **5:**e1000344. doi:10.1371/journal.pgen.1000344.

95. Mobley HL, Chippendale GR. 1990. Hemagglutinin, urease, and hemolysin production by *Proteus mirabilis* from clinical sources. *J Infect Dis* **161:**525–530.

96. Sosa V, Schlapp G, Zunino P. 2006. *Proteus mirabilis* isolates of different origins do not show correlation with virulence attributes and can colonize the urinary tract of mice. *Microbiology* **152:**2149–2157.

97. Swihart KG, Welch RA. 1990. The HpmA hemolysin is more common than HlyA among *Proteus* isolates. *Infect Immun* **58:**1853–1860.

98. Cestari SE, Ludovico MS, Martins FH, da Rocha SP, Elias WP, Pelayo JS. 2013. Molecular detection of HpmA and HlyA hemolysin of uropathogenic *Proteus mirabilis*. *Curr Microbiol* **67:**703–707.

99. Stankowska D, Kwinkowski M, Kaca W. 2008. Quantification of *Proteus mirabilis* virulence factors and modulation by acylated homoserine lactones. *J Microbiol Immunol Infect* **41:**243–253.

100. Loomes LM, Senior BW, Kerr MA. 1992. Proteinases of *Proteus* spp.: purification, properties, and detection in urine of infected patients. *Infect Immun* **60:**2267–2273.

101. Kuan L, Schaffer JN, Zouzias CD, Pearson MM. 2014. Characterization of 17 chaperone-usher fimbriae encoded by *Proteus mirabilis* reveals strong conservation. *J Med Microbiol* **63:**911–922.

102. Flannery EL, Mody L, Mobley HLT. 2009. Identification of a modular pathogenicity island that is widespread among urease-producing uropathogens and shares features with a diverse group of mobile elements. *Infect Immun* **77:**4887–4894.

103. Burall LS, Harro JM, Li X, Lockatell CV, Himpsl SD, Hebel JR, Johnson DE, Mobley HLT. 2004. *Proteus mirabilis* genes that contribute to pathogenesis of urinary tract infection: identification of 25

signature-tagged mutants attenuated at least 100-fold. *Infect Immun* **72:**2922–2938.

104. Himpsl SD, Pearson MM, Arewång CJ, Nusca TD, Sherman DH, Mobley HLT. 2010. Proteobactin and a yersiniabactin-related siderophore mediate iron acquisition in *Proteus mirabilis*. *Mol Microbiol* **78:**138–157.

105. Alamuri P, Mobley HLT. 2008. A novel autotransporter of uropathogenic *Proteus mirabilis* is both a cytotoxin and an agglutinin. *Mol Microbiol* **68:**997–1017.

106. Flannery EL, Antczak SM, Mobley HLT. 2011. Self-transmissibility of the integrative and conjugative element ICE*Pm1* between clinical isolates requires a functional integrase, relaxase, and type IV secretion system. *J Bacteriol* **193:**4104–4112.

107. Pearson MM, Sebaihia M, Churcher C, Quail MA, Seshasayee AS, Luscombe NM, Abdellah Z, Arrosmith C, Atkin B, Chillingworth T, Hauser H, Jagels K, Moule S, Mungall K, Norbertczak H, Rabbinowitsch E, Walker D, Whithead S, Thomson NR, Rather PN, Parkhill J, Mobley HLT. 2008. Complete genome sequence of uropathogenic *Proteus mirabilis*, a master of both adherence and motility. *J Bacteriol* **190:**4027–4037.

108. Wozniak RA, Waldor MK. 2010. Integrative and conjugative elements: mosaic mobile genetic elements enabling dynamic lateral gene flow. *Nat Rev Microbiol* **8:**552–563.

109. Ceccarelli D, Daccord A, René M, Burrus V. 2008. Identification of the origin of transfer (oriT) and a new gene required for mobilization of the SXT/R391 family of integrating conjugative elements. *J Bacteriol* **190:**5328–5338.

110. Harada S, Ishii Y, Saga T, Tateda K, Yamaguchi K. 2010. Chromosomally encoded blaCMY-2 located on a novel SXT/R391-related integrating conjugative element in a *Proteus mirabilis* clinical isolate. *Antimicrob Agents Chemother* **54:**3545–3550.

111. Li X, Du Y, Du P, Dai H, Fang Y, Li Z, Lv N, Zhu B, Kan B, Wang D. 2016. SXT/R391 integrative and conjugative elements in Proteus species reveal abundant genetic diversity and multidrug resistance. *Sci Rep* **6:**37372. doi:10.1038/srep37372.

112. Bie L, Wu H, Wang XH, Wang M, Xu H. 2017. Identification and characterization of new members of the SXT/R391 family of integrative and conjugative elements (ICEs) in *Proteus mirabilis*. *Int J Antimicrob Agents* **50:**242–246.

113. Wenren LM, Sullivan NL, Cardarelli L, Septer AN, Gibbs KA. 2013. Two independent pathways for self-recognition in *Proteus mirabilis* are linked by type VI-dependent export. *MBio* **4:**e00374–e00313.

114. Alteri CJ, Himpsl SD, Pickens SR, Lindner JR, Zora JS, Miller JE, Arno PD, Straight SW, Mobley HL. 2013. Multicellular bacteria deploy the type VI secretion system to preemptively strike neighboring cells. *PLoS Pathog* **9:**e1003608. doi:10.1371/journal.ppat.1003608.

115. Alteri CJ, Mobley HL. 2016. The versatile type VI secretion system. *Microbiol Spectr* **4:**4. doi:10.1128/microbiolspec.VMBF-0026-2015.

116. Sullivan NL, Septer AN, Fields AT, Wenren LM, Gibbs KA. 2013. The complete genome sequence of *Proteus mirabilis* strain BB2000 reveals differences from the *P. mirabilis* reference strain. *Genome Announc* **1:**1. doi:10.1128/genomeA.00024-13.

117. Knirel YA, Perepelov AV, Kondakova AN, Senchenkova SN, Sidorczyk Z, Rozalski A, Kaca W. 2011. Structure and serology of O-antigens as the basis for classification of *Proteus* strains. *Innate Immun* **17:**70–96.

118. Ramos HC, Rumbo M, Sirard JC. 2004. Bacterial flagellins: mediators of pathogenicity and host immune responses in mucosa. *Trends Microbiol* **12:**509–517.

119. Murphy CA, Belas R. 1999. Genomic rearrangements in the flagellin genes of *Proteus mirabilis*. *Mol Microbiol* **31:**679–690.

120. Wattam AR, Davis JJ, Assaf R, Boisvert S, Brettin T, Bun C, Conrad N, Dietrich EM, Disz T, Gabbard JL, Gerdes S, Henry CS, Kenyon RW, Machi D, Mao C, Nordberg EK, Olsen GJ, Murphy-Olson DE, Olson R, Overbeek R, Parrello B, Pusch GD, Shukla M, Vonstein V, Warren A, Xia F, Yoo H, Stevens RL. 2017. Improvements to PATRIC, the all-bacterial Bioinformatics Database and Analysis Resource Center. *Nucleic Acids Res* **45**(D1)**:**D535–D542.

121. Pearson MM, Rasko DA, Smith SN, Mobley HLT. 2010. Transcriptome of swarming *Proteus mirabilis*. *Infect Immun* **78:**2834–2845.

122. Cusick K, Lee YY, Youchak B, Belas R. 2012. Perturbation of FliL interferes with *Proteus mirabilis* swarmer cell gene expression and differentiation. *J Bacteriol* **194:**437–447.

123. Coetzee JN. 1963. Transduction of swarming in *Proteus mirabilis*. *J Gen Microbiol* **33:**1–7.

124. Armbruster CE, Forsyth-DeOrnellas V, Johnson AO, Smith SN, Zhao L, Wu W, Mobley HLT. 2017. Genome-wide transposon mutagenesis of *Proteus mirabilis*: essential genes, fitness factors for catheter-associated urinary tract infection, and the impact of polymicrobial infection on fitness requirements. *PLoS Pathog* **13:** e1006434. doi:10.1371/journal.ppat.1006434.

125. Tatusova T. 2016. Update on genomic databases and resources at the national center for biotechnology information. *Methods Mol Biol* **1415:**3–30.

126. Pearson MM, Yep A, Smith SN, Mobley HLT. 2011. Transcriptome of *Proteus mirabilis* in the murine urinary tract: virulence and nitrogen assimilation gene expression. *Infect Immun* **79:**2619–2631.

127. Bode NJ, Debnath I, Kuan L, Schulfer A, Ty M, Pearson MM. 2015. Transcriptional analysis of the MrpJ network: modulation of diverse virulence-associated genes and direct regulation of mrp fimbrial and flhDC flagellar operons in *Proteus mirabilis*. *Infect Immun* **83:**2542–2556.

128. Allison C, Lai H-C, Hughes C. 1992. Co-ordinate expression of virulence genes during swarm-cell differentiation and population migration of *Proteus mirabilis*. *Mol Microbiol* **6:**1583–1591.

129. Walker KE, Moghaddame-Jafari S, Lockatell CV, Johnson D, Belas R. 1999. ZapA, the IgA-degrading metalloprotease of *Proteus mirabilis*, is a virulence factor expressed specifically in swarmer cells. *Mol Microbiol* **32:**825–836.

130. Armitage JP. 1981. Changes in metabolic activity of *Proteus mirabilis* during swarming. *J Gen Microbiol* **125:**445–450.

131. Snyder JA, Haugen BJ, Buckles EL, Lockatell CV, Johnson DE, Donnenberg MS, Welch RA, Mobley HL. 2004. Transcriptome of uropathogenic *Escherichia coli* during urinary tract infection. *Infect Immun* **72:**6373–6381.

132. Li X, Rasko DA, Lockatell CV, Johnson DE, Mobley HLT. 2001. Repression of bacterial motility by a novel fimbrial gene product. *EMBO J* **20:**4854–4862.

133. Pearson MM, Mobley HLT. 2008. Repression of motility during fimbrial expression: identification of 14 *mrpJ* gene paralogues in *Proteus mirabilis*. *Mol Microbiol* **69:**548–558.

134. Howery KE, Clemmer KM, Şimşek E, Kim M, Rather PN. 2015. Regulation of the Min cell division inhibition complex by the Rcs phosphorelay in *Proteus mirabilis*. *J Bacteriol* **197:**2499–2507.

135. Howery KE, Clemmer KM, Rather PN. 2016. The Rcs regulon in *Proteus mirabilis*: implications for motility, biofilm formation, and virulence. *Curr Genet* **62:**775–789.

136. Belas R, Suvanasuthi R. 2005. The ability of *Proteus mirabilis* to sense surfaces and regulate virulence gene expression involves FliL, a flagellar basal body protein. *J Bacteriol* **187:**6789–6803.

137. Belas R, Schneider R, Melch M. 1998. Characterization of *Proteus mirabilis* precocious swarming mutants: identification of *rsbA*, encoding a regulator of swarming behavior. *J Bacteriol* **180:**6126–6139.

138. Liaw SJ, Lai HC, Ho SW, Luh KT, Wang WB. 2001. Characterisation of p-nitrophenylglycerol-resistant *Proteus mirabilis* superswarming mutants. *J Med Microbiol* **50:**1039–1048.

139. Clemmer KM, Rather PN. 2008. The Lon protease regulates swarming motility and virulence gene expression in *Proteus mirabilis*. *J Med Microbiol* **57:**931–937.

140. Miller VL, Mekalanos JJ. 1988. A novel suicide vector and its use in construction of insertion mutations: osmoregulation of outer membrane proteins and virulence determinants in Vibrio cholerae requires toxR. *J Bacteriol* **170:**2575–2583.

141. Li X, Zhao H, Geymonat L, Bahrani F, Johnson DE, Mobley HL. 1997. *Proteus mirabilis* mannose-resistant, Proteus-like fimbriae: MrpG is located at the fimbrial tip and is required for fimbrial assembly. *Infect Immun* **65:**1327–1334.

142. Karberg M, Guo H, Zhong J, Coon R, Perutka J, Lambowitz AM. 2001. Group II introns as controllable gene targeting vectors for genetic manipulation of bacteria. *Nat Biotechnol* **19:**1162–1167.

143. Pearson MM, Mobley HLT. 2007. The type III secretion system of *Proteus mirabilis* HI4320 does not contribute to virulence in the mouse model of ascending urinary tract infection. *J Med Microbiol* **56:**1277–1283.

144. Belas R, Erskine D, Flaherty D. 1991. Transposon mutagenesis in *Proteus mirabilis*. *J Bacteriol* **173:**6289–6293.

145. de Lorenzo V, Herrero M, Jakubzik U, Timmis KN. 1990. Mini-Tn5 transposon derivatives for insertion mutagenesis, promoter probing, and chromosomal insertion of cloned DNA in gram-negative eubacteria. *J Bacteriol* **172:**6568–6572.

146. Belas R, Erskine D, Flaherty D. 1991. *Proteus mirabilis* mutants defective in swarmer cell differentiation and multicellular behavior. *J Bacteriol* **173:**6279–6288.

147. Belas R, Goldman M, Ashliman K. 1995. Genetic analysis of *Proteus mirabilis* mutants defective in swarmer cell elongation. *J Bacteriol* **177:**823–828.

148. Hay NA, Tipper DJ, Gygi D, Hughes C. 1997. A nonswarming mutant of *Proteus mirabilis lacks* the Lrp global transcriptional regulator. *J Bacteriol* **179:**4741–4746.

149. Alteri CJ, Himpsl SD, Engstrom MD, Mobley HL. 2012. Anaerobic respiration using a complete oxidative TCA cycle drives multicellular swarming in *Proteus mirabilis*. *MBio* **3:**3. doi:10.1128/mBio.00365-12.

150. Gibbs KA, Urbanowski ML, Greenberg EP. 2008. Genetic determinants of self identity and social recognition in bacteria. *Science* **321:**256–259.

151. Jiang S-S, Lin T-Y, Wang W-B, Liu M-C, Hsueh P-R, Liaw S-J. 2010. Characterization of UDP-glucose dehydrogenase and UDP-glucose pyrophosphorylase mutants of *Proteus mirabilis*: defectiveness in polymyxin B resistance, swarming, and virulence. *Antimicrob Agents Chemother* **54:**2000–2009.

152. Holling N, Lednor D, Tsang S, Bissell A, Campbell L, Nzakizwanayo J, Dedi C, Hawthorne JA, Hanlon G, Ogilvie LA, Salvage JP, Patel BA, Barnes LM, Jones BV. 2014. Elucidating the genetic basis of crystalline biofilm formation in *Proteus mirabilis*. *Infect Immun* **82:**1616–1626.

153. Hensel M, Shea JE, Gleeson C, Jones MD, Dalton E, Holden DW. 1995. Simultaneous identification of bacterial virulence genes by negative selection. *Science* **269:**400–403.

154. Himpsl SD, Lockatell CV, Hebel JR, Johnson DE, Mobley HLT. 2008. Identification of virulence determinants in uropathogenic *Proteus mirabilis* using signature-tagged mutagenesis. *J Med Microbiol* **57:**1068–1078.

155. Zhao H, Li X, Johnson DE, Mobley HLT. 1999. Identification of protease and *rpoN*-associated genes of uropathogenic *Proteus mirabilis* by negative selection in a mouse model of ascending urinary tract infection. *Microbiology* **145:**185–195.

156. Goodman AL, McNulty NP, Zhao Y, Leip D, Mitra RD, Lozupone CA, Knight R, Gordon JI. 2009. Identifying genetic determinants needed to establish a human gut symbiont in its habitat. *Cell Host Microbe* **6:**279–289.

157. Langridge GC, Phan MD, Turner DJ, Perkins TT, Parts L, Haase J, Charles I, Maskell DJ, Peters SE, Dougan G, Wain J, Parkhill J, Turner AK. 2009. Simultaneous assay of every Salmonella Typhi gene using one million transposon mutants. *Genome Res* **19:**2308–2316.

158. Gallagher LA, Shendure J, Manoil C. 2011. Genome-scale identification of resistance functions in *Pseudomonas aeruginosa* using Tn-seq. *MBio* **2:**e00315-10. doi:10.1128/mBio.00315-10.

159. van Opijnen T, Bodi KL, Camilli A. 2009. Tn-seq: high-throughput parallel sequencing for fitness and genetic interaction studies in microorganisms. *Nat Methods* **6:**767–772.

160. Gawronski JD, Wong SMS, Giannoukos G, Ward DV, Akerley BJ. 2009. Tracking insertion mutants within libraries by deep sequencing and a genome-wide screen for *Haemophilus* genes required in the lung. *Proc Natl Acad Sci USA* **106:**16422–16427.

161. Mobley HL, Island MD, Hausinger RP. 1995. Molecular biology of microbial ureases. *Microbiol Rev* **59:**451–480.

162. Mobley HL, Hausinger RP. 1989. Microbial ureases: significance, regulation, and molecular characterization. *Microbiol Rev* **53:**85–108.

163. Heimer SR, Mobley HLT. 2001. Interaction of *Proteus mirabilis* urease apoenzyme and accessory proteins identified with yeast two-hybrid technology. *J Bacteriol* **183:**1423–1433.

164. Jones BD, Mobley HL. 1987. Genetic and biochemical diversity of ureases of *Proteus, Providencia, and Morganella* species isolated from urinary tract infection. *Infect Immun* **55:**2198–2203.

165. Jones BD, Mobley HL. 1989. *Proteus mirabilis* urease: nucleotide sequence determination and comparison with jack bean urease. *J Bacteriol* **171:**6414–6422.

166. Sriwanthana B, Island MD, Mobley HL. 1993. Sequence of the *Proteus mirabilis* urease accessory gene *ureG*. *Gene* **129:**103–106.

167. Nicholson EB, Concaugh EA, Foxall PA, Island MD, Mobley HL. 1993. *Proteus mirabilis* urease: transcriptional regulation by UreR. *J Bacteriol* **175:**465–473.

168. Thomas VJ, Collins CM. 1999. Identification of UreR binding sites in the *Enterobacteriaceae* plasmid-encoded and *Proteus mirabilis* urease gene operons. *Mol Microbiol* **31:**1417–1428.

169. Coker C, Bakare OO, Mobley HL. 2000. H-NS is a repressor of the *Proteus mirabilis* urease transcriptional activator gene *ureR*. *J Bacteriol* **182:**2649–2653.

170. D'Orazio SE, Thomas V, Collins CM. 1996. Activation of transcription at divergent urea-dependent promoters by the urease gene regulator UreR. *Mol Microbiol* **21:**643–655.

171. Poore CA, Mobley HLT. 2003. Differential regulation of the *Proteus mirabilis* urease gene cluster by UreR and H-NS. *Microbiology* **149:**3383–3394.

172. Dattelbaum JD, Lockatell CV, Johnson DE, Mobley HLT. 2003. UreR, the transcriptional activator of the *Proteus mirabilis* urease gene cluster, is required for urease activity and virulence in experimental urinary tract infections. *Infect Immun* **71:**1026–1030.

173. Follmer C. 2010. Ureases as a target for the treatment of gastric and urinary infections. *J Clin Pathol* **63:**424–430.

174. Griffith DP, Gleeson MJ, Lee H, Longuet R, Deman E, Earle N. 1991. Randomized, double-blind trial of Lithostat (acetohydroxamic acid) in the palliative treatment of infection-induced urinary calculi. *Eur Urol* **20:**243–247.

175. Williams JJ, Rodman JS, Peterson CM. 1984. A randomized double-blind study of acetohydroxamic acid in struvite nephrolithiasis. *N Engl J Med* **311:**760–764.

176. Griffith DP, Khonsari F, Skurnick JH, James KE. 1988. A randomized trial of acetohydroxamic acid for the treatment and prevention of infection-induced urinary stones in spinal cord injury patients. *J Urol* **140:**318–324.

177. Zisman AL. 2017. Effectiveness of treatment modalities on kidney stone recurrence. *Clin J Am Soc Nephrol* **12:**1699–1708.

178. Nicholson EB, Concaugh EA, Mobley HL. 1991. *Proteus mirabilis* urease: use of a *ureA-lacZ* fusion demonstrates that induction is highly specific for urea. *Infect Immun* **59:**3360–3365.

179. Kanehisa M, Furumichi M, Tanabe M, Sato Y, Morishima K. 2017. KEGG: new perspectives on genomes, pathways, diseases and drugs. *Nucleic Acids Res* **45**(D1)**:**D353–D361.

180. Senior BW. 1999. Investigation of the types and characteristics of the proteolytic enzymes formed by diverse strains of *Proteus* species. *J Med Microbiol* **48:**623–628.

181. Henderson IR, Navarro-Garcia F, Desvaux M, Fernandez RC, Ala'Aldeen D. 2004. Type V protein secretion pathway: the autotransporter story. *Microbiol Mol Biol Rev* **68:**692–744.

182. Leyton DL, Rossiter AE, Henderson IR. 2012. From self sufficiency to dependence: mechanisms and factors important for autotransporter biogenesis. *Nat Rev Microbiol* **10:**213–225.

183. Nielubowicz GR, Smith SN, Mobley HLT. 2008. Outer membrane antigens of the uropathogen *Proteus mirabilis* recognized by the humoral response during experimental murine urinary tract infection. *Infect Immun* **76:**4222–4231.

184. Wimmer MR, Woods CN, Adamczak KJ, Glasgow EM, Novak WR, Grilley DP, Weaver TM. 2015. Sequential unfolding of the hemolysin two-partner secretion domain from Proteus mirabilis. *Protein Sci* **24:**1841–1855.

185. Weaver TM, Smith JA, Hocking JM, Bailey LJ, Wawrzyn GT, Howard DR, Sikkink LA, Ramirez-Alvarado M, Thompson JR. 2009. Structural and functional studies of truncated hemolysin A from *Proteus mirabilis*. *J Biol Chem* **284:**22297–22309.

186. Uphoff TS, Welch RA. 1990. Nucleotide sequencing of the *Proteus mirabilis* calcium-independent hemolysin genes (hpmA and hpmB) reveals sequence similarity with the *Serratia marcescens* hemolysin genes (shlA and shlB). *J Bacteriol* **172:**1206–1216.

187. Dienes L. 1946. Reproductive processes in *Proteus* cultures. *Proc Soc Exp Biol Med* **63:**265–270.

188. Budding AE, Ingham CJ, Bitter W, Vandenbroucke-Grauls CM, Schneeberger PM. 2009. The Dienes phenomenon: competition and territoriality in Swarming *Proteus mirabilis*. *J Bacteriol* **191:**3892–3900.

189. Gibbs KA, Wenren LM, Greenberg EP. 2011. Identity gene expression in *Proteus mirabilis*. *J Bacteriol* **193:**3286–3292.

190. Braun V, Focareta T. 1991. Pore-forming bacterial protein hemolysins (cytolysins). *Crit Rev Microbiol* **18:**115–158.

191. Welch RA. 1987. Identification of two different hemolysin determinants in uropathogenic Proteus isolates. *Infect Immun* **55:**2183–2190.

192. Swihart KG, Welch RA. 1990. Cytotoxic activity of the *Proteus* hemolysin HpmA. *Infect Immun* **58:**1861–1869.

193. Senior BW, Albrechtsen M, Kerr MA. 1987. Proteus mirabilis strains of diverse type have IgA protease activity. *J Med Microbiol* **24:**175–180.

194. Senior BW, Albrechtsen M, Kerr MA. 1988. A survey of IgA protease production among clinical isolates of Proteeae. *J Med Microbiol* **25:**27–31.

195. Loomes LM, Senior BW, Kerr MA. 1990. A proteolytic enzyme secreted by *Proteus mirabilis* degrades immunoglobulins of the immunoglobulin A1 (IgA1), IgA2, and IgG isotypes. *Infect Immun* **58:**1979–1985.

196. Almogren A, Senior BW, Loomes LM, Kerr MA. 2003. Structural and functional consequences of cleavage of human secretory and human serum immunoglobulin A1 by proteinases from *Proteus mirabilis* and *Neisseria meningitidis*. *Infect Immun* **71:**3349–3356.

197. Belas R, Manos J, Suvanasuthi R. 2004. *Proteus mirabilis* ZapA metalloprotease degrades a broad spectrum of substrates, including antimicrobial peptides. *Infect Immun* **72:**5159–5167.

198. Wassif C, Cheek D, Belas R. 1995. Molecular analysis of a metalloprotease from *Proteus mirabilis*. *J Bacteriol* **177:**5790–5798.

199. Phan V, Belas R, Gilmore BF, Ceri H. 2008. ZapA, a virulence factor in a rat model of *Proteus mirabilis*-induced acute and chronic prostatitis. *Infect Immun* **76:**4859–4864.

200. Hacker J, Knapp S, Goebel W. 1983. Spontaneous deletions and flanking regions of the chromosomally inherited hemolysin determinant of an *Escherichia coli* O6 strain. *J Bacteriol* **154:**1145–1152.

201. Knapp S, Then I, Wels W, Michel G, Tschäpe H, Hacker J, Goebel W. 1985. Analysis of the flanking regions from different haemolysin determinants of *Escherichia coli*. *Mol Gen Genet* **200:**385–392.

202. Burrus V, Waldor MK. 2004. Shaping bacterial genomes with integrative and conjugative elements. *Res Microbiol* **155:**376–386.

203. Seth-Smith H, Croucher NJ. 2009. Genome watch: breaking the ICE. *Nat Rev Microbiol* **7:**328–329.

204. Hospenthal MK, Costa TRD, Waksman G. 2017. A comprehensive guide to pilus biogenesis in Gram-negative bacteria. *Nat Rev Microbiol* **15:**365–379.

205. Thanassi DG, Nuccio SP, Shu Kin So S, Bäumler AJ. 2007. Fimbriae: classification and biochemistry. *Ecosal Plus* **2:**2. doi:10.1128/ecosalplus.2.4.2.1.

206. Nuccio SP, Bäumler AJ. 2007. Evolution of the chaperone/usher assembly pathway: fimbrial classification goes Greek. *Microbiol Mol Biol Rev* **71:**551–575.

207. Old DC, Adegbola RA. 1982. Haemagglutinins and fimbriae of *Morganella, Proteus* and *Providencia*. *J Med Microbiol* **15:**551–564.

208. Adegbola RA, Old DC, Senior BW. 1983. The adhesins and fimbriae of *Proteus mirabilis* strains associated with high and low affinity for the urinary tract. *J Med Microbiol* **16:**427–431.

209. Snyder JA, Haugen BJ, Lockatell CV, Maroncle N, Hagan EC, Johnson DE, Welch RA, Mobley HL. 2005. Coordinate expression of fimbriae in uropathogenic *Escherichia coli*. *Infect Immun* **73:**7588–7596.

210. Rocha SPD, Pelayo JS, Elias WP. 2007. Fimbriae of uropathogenic *Proteus mirabilis*. *FEMS Immunol Med Microbiol* **51:**1–7.

211. Edén CS, Larsson P, Lomberg H. 1980. Attachment of *Proteus mirabilis* to human urinary sediment epithelial cells in vitro is different from that of *Escherichia coli*. *Infect Immun* **27:**804–807.

212. Massad G, Bahrani FK, Mobley HL. 1994. *Proteus mirabilis* fimbriae: identification, isolation, and characterization of a new ambient-temperature fimbria. *Infect Immun* **62:**1989–1994.

213. Massad G, Lockatell CV, Johnson DE, Mobley HL. 1994. *Proteus mirabilis* fimbriae: construction of an isogenic *pmfA* mutant and analysis of virulence in a CBA mouse model of ascending urinary tract infection. *Infect Immun* **62:**536–542.

214. Zunino P, Sosa V, Schlapp G, Allen AG, Preston A, Maskell DJ. 2007. Mannose-resistant *Proteus*-like and *P. mirabilis fimbriae* have specific and additive roles in *P. mirabilis* urinary tract infections. *FEMS Immunol Med Microbiol* **51:**125–133.

215. Li X, Mobley HLT. 2002. Vaccines for *Proteus mirabilis* in urinary tract infection. *Int J Antimicrob Agents* **19:**461–465.

216. Pellegrino R, Galvalisi U, Scavone P, Sosa V, Zunino P. 2003. Evaluation of *Proteus mirabilis* structural fimbrial proteins as antigens against urinary tract infections. *FEMS Immunol Med Microbiol* **36:**103–110.

217. Li X, Lockatell CV, Johnson DE, Lane MC, Warren JW, Mobley HLT. 2004. Development of an intranasal vaccine to prevent urinary tract infection by *Proteus mirabilis*. *Infect Immun* **72:**66–75.

218. Li X, Erbe JL, Lockatell CV, Johnson DE, Jobling MG, Holmes RK, Mobley HLT. 2004. Use of translational fusion of the MrpH fimbrial adhesin-binding domain with the cholera toxin A2 domain, coexpressed with the cholera toxin B subunit, as an intranasal vaccine to prevent experimental urinary tract infection by *Proteus mirabilis*. *Infect Immun* **72:**7306–7310.

219. Scavone P, Sosa V, Pellegrino R, Galvalisi U, Zunino P. 2004. Mucosal vaccination of mice with recombinant *Proteus mirabilis* structural fimbrial proteins. *Microbes Infect* **6:**853–860.

220. Duguid JP. 1959. Fimbriae and adhesive properties in Klebsiella strains. *J Gen Microbiol* **21:**271–286.

221. Li X, Johnson DE, Mobley HLT. 1999. Requirement of MrpH for mannose-resistant Proteus-like fimbria-mediated hemagglutination by *Proteus mirabilis*. *Infect Immun* **67:**2822–2833.

222. Zhao H, Li X, Johnson DE, Blomfield I, Mobley HL. 1997. In vivo phase variation of MR/P fimbrial gene expression in *Proteus mirabilis* infecting the urinary tract. *Mol Microbiol* **23:**1009–1019.

223. Li X, Lockatell CV, Johnson DE, Mobley HLT. 2002. Identification of MrpI as the sole recombinase that regulates the phase variation of MR/P fimbria, a bladder colonization factor of uropathogenic *Proteus mirabilis*. *Mol Microbiol* **45:**865–874.

224. Bahrani FK, Mobley HL. 1993. *Proteus mirabilis* MR/P fimbriae: molecular cloning, expression, and nucleotide sequence of the major fimbrial subunit gene. *J Bacteriol* **175:**457–464.

225. Latta RK, Schur MJ, Tolson DL, Altman E. 1998. The effect of growth conditions on in vitro adherence, invasion, and NAF expression by Proteus mirabilis 7570. *Can J Microbiol* **44:**896–904.

226. Lane MC, Li X, Pearson MM, Simms AN, Mobley HLT. 2009. Oxygen-limiting conditions enrich for fimbriate cells of uropathogenic *Proteus mirabilis* and *Escherichia coli*. *J Bacteriol* **191:** 1382–1392.

227. Jansen AM, Lockatell V, Johnson DE, Mobley HLT. 2004. Mannose-resistant *Proteus*-like fimbriae are produced by most *Proteus mirabilis* strains infecting the urinary tract, dictate the in vivo localization of bacteria, and contribute to biofilm formation. *Infect Immun* **72:**7294–7305.

228. Scavone P, Iribarnegaray V, Caetano AL, Schlapp G, Härtel S, Zunino P. 2016. Fimbriae have distinguishable roles in *Proteus mirabilis* biofilm formation. *Pathog Dis* **74:**74. doi:10.1093/femspd/ftw033.

229. Zunino P, Geymonat L, Allen AG, Preston A, Sosa V, Maskell DJ. 2001. New aspects of the role of MR/P fimbriae in *Proteus mirabilis* urinary tract infection. *FEMS Immunol Med Microbiol* **31:** 113–120.

230. Scavone P, Villar S, Umpiérrez A, Zunino P. 2015. Role of *Proteus mirabilis* MR/P fimbriae and flagella in adhesion, cytotoxicity and genotoxicity induction in T24 and Vero cells. *Pathog Dis* **73:**73. doi:10.1093/femspd/ftv017.

231. Sareneva T, Holthöfer H, Korhonen TK. 1990. Tissue-binding affinity of *Proteus mirabilis* fimbriae in the human urinary tract. *Infect Immun* **58:**3330–3336.

232. Bahrani FK, Massad G, Lockatell CV, Johnson DE, Russell RG, Warren JW, Mobley HL. 1994. Construction of an MR/P fimbrial mutant of *Proteus mirabilis:* role in virulence in a mouse model of ascending urinary tract infection. *Infect Immun* **62:**3363–3371.

233. Wray SK, Hull SI, Cook RG, Barrish J, Hull RA. 1986. Identification and characterization of a uroepithelial cell adhesin from a uropathogenic isolate of *Proteus mirabilis*. *Infect Immun* **54:**43–49.

234. Pellegrino R, Scavone P, Umpiérrez A, Maskell DJ, Zunino P. 2013. *Proteus mirabilis* uroepithelial cell adhesin (UCA) fimbria plays a role in the colonization of the urinary tract. *Pathog Dis* **67:**104–107.

235. Tolson DL, Barrigar DL, McLean RJ, Altman E. 1995. Expression of a nonagglutinating fimbria by *Proteus mirabilis*. *Infect Immun* **63:**1127–1129.

236. Cook SW, Mody N, Valle J, Hull R. 1995. Molecular cloning of *Proteus mirabilis* uroepithelial cell adherence (*uca*) genes. *Infect Immun* **63:**2082–2086.

237. Altman E, Harrison BA, Latta RK, Lee KK, Kelly JF, Thibault P. 2001. Galectin-3-mediated adherence of Proteus mirabilis to Madin-Darby canine kidney cells. *Biochem Cell Biol* **79:**783–788.

238. Lee KK, Harrison BA, Latta R, Altman E. 2000. The binding of *Proteus mirabilis* nonagglutinating fimbriae to ganglio-series asialoglycolipids and lactosyl ceramide. *Can J Microbiol* **46:**961–966.

239. Canesin G, Gonzalez-Peramato P, Palou J, Urrutia M, Cordón-Cardo C, Sánchez-Carbayo M. 2010. Galectin-3 expression is associated with bladder cancer progression and clinical outcome. *Tumour Biol* **31:**277–285.

240. Massad G, Mobley HL. 1994. Genetic organization and complete sequence of the *Proteus mirabilis pmf* fimbrial operon. *Gene* **150:**101–104.

241. Zunino P, Sosa V, Allen AG, Preston A, Schlapp G, Maskell DJ. 2003. *Proteus mirabilis* fimbriae (PMF) are important for both bladder and kidney colonization in mice. *Microbiology* **149:**3231–3237.

242. Johnson DE, Bahrani FK, Lockatell CV, Drachenberg CB, Hebel JR, Belas R, Warren JW, Mobley HLT. 1999. Serum immunoglobulin response and protection from homologous challenge by *Proteus mirabilis* in a mouse model of ascending urinary tract infection. *Infect Immun* **67:**6683–6687.

243. Massad G, Fulkerson JF Jr, Watson DC, Mobley HL. 1996. *Proteus mirabilis* ambient-temperature fimbriae: cloning and nucleotide sequence of the aft gene cluster. *Infect Immun* **64:**4390–4395.

244. Zunino P, Geymonat L, Allen AG, Legnani-Fajardo C, Maskell DJ. 2000. Virulence of a *Proteus mirabilis* ATF isogenic mutant is not impaired in a mouse model of ascending urinary tract infection. *FEMS Immunol Med Microbiol* **29:**137–143.

245. Bijlsma IG, van Dijk L, Kusters JG, Gaastra W. 1995. Nucleotide sequences of two fimbrial major subunit genes, pmpA and ucaA, from canine-uropathogenic *Proteus mirabilis* strains. *Microbiology* **141:**1349–1357.

246. Tsai YL, Chien HF, Huang KT, Lin WY, Liaw SJ. 2017. cAMP receptor protein regulates mouse colonization, motility, fimbria-mediated adhesion, and stress tolerance in uropathogenic Proteus mirabilis. *Sci Rep* **7:**7282. doi:10.1038/s41598-017-07304-7

247. Yakubu DE, Old DC, Senior BW. 1989. The haemagglutinins and fimbriae of *Proteus penneri*. *J Med Microbiol* **30:**279–284.

248. Bahrani FK, Cook S, Hull RA, Massad G, Mobley HL. 1993. *Proteus mirabilis* fimbriae: n-terminal amino acid sequence of a major fimbrial subunit and nucleotide sequences of the genes from two strains. *Infect Immun* **61:**884–891.

249. Mobley HL, Chippendale GR, Tenney JH, Mayrer AR, Crisp LJ, Penner JL, Warren JW. 1988. MR/K hemagglutination of *Providencia stuartii* correlates with adherence to catheters and with persistence in catheter-associated bacteriuria. *J Infect Dis* **157:**264–271.

250. Collado-Vides J, Magasanik B, Gralla JD. 1991. Control site location and transcriptional regulation in Escherichia coli. *Microbiol Rev* **55:**371–394.

251. Meslet-Cladiere LM, Pimenta A, Duchaud E, Holland IB, Blight MA. 2004. In vivo expression of the mannose-resistant fimbriae of *Photorhabdus temperata* K122 during insect infection. *J Bacteriol* **186:**611–622.

252. He H, Snyder HA, Forst S. 2004. Unique organization and regulation of the mrx fimbrial operon in *Xenorhabdus nematophila*. *Microbiology* **150:**1439–1446.

253. Chen YT, Peng HL, Shia WC, Hsu FR, Ken CF, Tsao YM, Chen CH, Liu CE, Hsieh MF, Chen HC, Tang CY, Ku TH. 2012. Whole-genome sequencing and identification of *Morganella morganii* KT pathogenicity-related genes. *BMC Genomics* **13**(Suppl 7)**:**S4. doi:10.1186/1471-2164-13-S7-S4.

254. Bode NJ, Chan KW, Kong XP, Pearson MM. 2016. Distinct residues contribute to motility repression and autoregulation in the *Proteus mirabilis* fimbria-associated transcriptional regulator AtfJ. *J Bacteriol* **198:**2100–2112.

255. Morris NS, Stickler DJ, McLean RJ. 1999. The development of bacterial biofilms on indwelling urethral catheters. *World J Urol* **17:**345–350.

256. Stickler D, Young R, Jones G, Sabbuba N, Morris N. 2003. Why are Foley catheters so vulnerable to encrustation and blockage by crystalline bacterial biofilm? *Urol Res* **31:**306–311.

257. Stickler DJ. 2014. Clinical complications of urinary catheters caused by crystalline biofilms: something needs to be done. *J Intern Med* **276:**120–129.

258. Davey ME, O'toole GA. 2000. Microbial biofilms: from ecology to molecular genetics. *Microbiol Mol Biol Rev* **64:**847–867.

259. Jones BV, Young R, Mahenthiralingam E, Stickler DJ. 2004. Ultrastructure of *Proteus mirabilis* swarmer cell rafts and role of swarming in catheter-associated urinary tract infection. *Infect Immun* **72:**3941–3950.

260. Jones SM, Yerly J, Hu Y, Ceri H, Martinuzzi R. 2007. Structure of *Proteus mirabilis* biofilms grown in artificial urine and standard laboratory media. *FEMS Microbiol Lett* **268:**16–21.

261. Jones BV, Mahenthiralingam E, Sabbuba NA, Stickler DJ. 2005. Role of swarming in the formation of crystalline *Proteus mirabilis* biofilms on urinary catheters. *J Med Microbiol* **54:**807–813.

262. Rocha SPD, Elias WP, Cianciarullo AM, Menezes MA, Nara JM, Piazza RMF, Silva MRL, Moreira CG, Pelayo JS. 2007. Aggregative adherence of uropathogenic *Proteus mirabilis* to cultured epithelial cells. *FEMS Immunol Med Microbiol* **51:**319–326.

263. Sabbuba NA, Stickler DJ, Mahenthiralingam E, Painter DJ, Parkin J, Feneley RC. 2004. Genotyping demonstrates that the strains of *Proteus mirabilis* from bladder stones and catheter encrustations of patients undergoing long-term bladder catheterization are identical. *J Urol* **171:**1925–1928.

264. Winters C, Stickler DJ, Howe TJ, Wilkinson N, Buckley CJ. 1995. Some observations on the structure of encrusting biofilms of *Proteus mirabilis* on urethral catheters. *Cells Mater* **5:**245–253.

265. Jacobsen SM, Shirtliff ME. 2011. *Proteus mirabilis* biofilms and catheter-associated urinary tract infections. *Virulence* **2:**460–465.

266. Liaw S-J, Lai H-C, Wang W-B. 2004. Modulation of swarming and virulence by fatty acids through the RsbA protein in *Proteus mirabilis*. *Infect Immun* **72:**6836–6845.

267. Wang MC, Chien HF, Tsai YL, Liu MC, Liaw SJ. 2014. The RNA chaperone Hfq is involved in stress tolerance and virulence in uropathogenic *Proteus mirabilis*. *PLoS One* **9:**e85626. doi:10.1371/journal.pone.0085626.

268. Izquierdo L, Abitiu N, Coderch N, Hita B, Merino S, Gavin R, Tomás JM, Regué M. 2002. The inner-core lipopolysaccharide biosynthetic waaE gene: function and genetic distribution among some *Enterobacteriaceae*. *Microbiology* **148:**3485–3496.

269. Jiang SS, Liu MC, Teng LJ, Wang WB, Hsueh PR, Liaw SJ. 2010. *Proteus mirabilis pmrI*, an RppA-regulated gene necessary for polymyxin B resistance, biofilm formation, and urothelial cell invasion. *Antimicrob Agents Chemother* **54:**1564–1571.

270. Czerwonka G, Guzy A, Kałuża K, Grosicka M, Dańczuk M, Lechowicz Ł, Gmiter D, Kowalczyk P, Kaca W. 2016. The role of *Proteus mirabilis* cell wall features in biofilm formation. *Arch Microbiol* **198:**877–884.

271. Dumanski AJ, Hedelin H, Edin-Liljegren A, Beauchemin D, McLean RJ. 1994. Unique ability of the *Proteus mirabilis* capsule to enhance mineral growth in infectious urinary calculi. *Infect Immun* **62:**2998–3003.

272. Wilks SA, Fader MJ, Keevil CW. 2015. Novel insights into the *Proteus mirabilis* crystalline biofilm using real-time imaging. *PLoS One* **10:**e0141711. doi:10.1371/journal.pone.0141711.

273. Moryl M, Kaleta A, Strzelecki K, Różalska S, Różalski A. 2014. Effect of nutrient and stress factors on polysaccharides synthesis in *Proteus mirabilis* biofilm. *Acta Biochim Pol* **61:**133–139.

274. Hamill TM, Gilmore BF, Jones DS, Gorman SP. 2007. Strategies for the development of the urinary catheter. *Expert Rev Med Devices* **4:**215–225.

275. Soto SM. 2014. Importance of biofilms in urinary tract infections: new therapeutic approaches. *Adv Bryol* **2014:**13.

276. Levering V, Wang Q, Shivapooja P, Zhao X, López GP. 2014. Soft robotic concepts in catheter design: an on-demand fouling-release urinary catheter. *Adv Healthc Mater* **3:**1588–1596.

277. Morgan SD, Rigby D, Stickler DJ. 2009. A study of the structure of the crystalline bacterial biofilms that can encrust and block silver Foley catheters. *Urol Res* **37:**89–93.

278. Stickler DJ, Jones GL, Russell AD. 2003. Control of encrustation and blockage of Foley catheters. *Lancet* **361:**1435–1437.

279. Jones GL, Muller CT, O'Reilly M, Stickler DJ. 2006. Effect of triclosan on the development of bacterial biofilms by urinary tract pathogens on urinary catheters. *J Antimicrob Chemother* **57:**266–272.

280. Stickler DJ, Jones GL. 2008. Reduced susceptibility of *Proteus mirabilis* to triclosan. *Antimicrob Agents Chemother* **52:**991–994.

281. Azeredo J, Azevedo NF, Briandet R, Cerca N, Coenye T, Costa AR, Desvaux M, Di Bonaventura G, Hébraud M, Jaglic Z, Kačániová M, Knøchel S, Lourenço A, Mergulhão F, Meyer RL, Nychas G, Simões M, Tresse O, Sternberg C. 2017. Critical review on biofilm methods. *Crit Rev Microbiol* **43:**313–351.

282. Hola V, Peroutkova T, Ruzicka F. 2012. Virulence factors in *Proteus* bacteria from biofilm communities of catheter-associated urinary tract infections. *FEMS Immunol Med Microbiol* **65:**343–349.

283. Kwiecinska-Piróg J, Bogiel T, Skowron K, Wieckowska E, Gospodarek E. 2015. *Proteus mirabilis* biofilm – qualitative and quantitative colorimetric methods-based evaluation. *Braz J Microbiol* **45:**1423–1431.

284. Schlapp G, Scavone P, Zunino P, Härtel S. 2011. Development of 3D architecture of uropathogenic Proteus mirabilis batch culture biofilms-a quantitative confocal microscopy approach. *J Microbiol Methods* **87:**234–240.

285. Czerwonka G, Arabski M, Wąsik S, Jabłońska-Wawrzycka A, Rogala P, Kaca W. 2014. Morphological changes in *Proteus mirabilis* O18 biofilm under the influence of a urease inhibitor and a homoserine lactone derivative. *Arch Microbiol* **196:**169–177.

286. O'May GA, Jacobsen SM, Longwell M, Stoodley P, Mobley HLT, Shirtliff ME. 2009. The high-affinity phosphate transporter Pst in *Proteus mirabilis* HI4320 and its importance in biofilm formation. *Microbiology* **155:**1523–1535.

287. Stickler D, Hughes G. 1999. Ability of *Proteus mirabilis* to swarm over urethral catheters. *Eur J Clin Microbiol Infect Dis* **18:**206–208.

288. Brooks T, Keevil CW. 1997. A simple artificial urine for the growth of urinary pathogens. *Lett Appl Microbiol* **24:**203–206.

289. Macleod SM, Stickler DJ. 2007. Species interactions in mixed-community crystalline biofilms on urinary catheters. *J Med Microbiol* **56:**1549–1557.

290. Moryl M, Torzewska A, Jałmuzna P, Rózalski A. 2013. Analysis of *Proteus mirabilis* distribution in multi-species biofilms on urinary catheters and determination of bacteria resistance to antimicrobial agents. *Pol J Microbiol* **62:**377–384.

291. Holá V, Ruzicka F, Horka M. 2010. Microbial diversity in biofilm infections of the urinary tract with the use of sonication techniques. *FEMS Immunol Med Microbiol* **59:**525–528.

292. Li X, Lu N, Brady HR, Packman AI. 2016. Biomineralization strongly modulates the formation of *Proteus mirabilis* and *Pseudomonas aeruginosa* dual-species biofilms. *FEMS Microbiol Ecol* **92:** fiw189. doi:10.1093/femsec/fiw189.

293. Williams GJ, Stickler DJ. 2008. Some observations on the migration of *Proteus mirabilis* and other urinary tract pathogens over foley catheters. *Infect Control Hosp Epidemiol* **29:**443–445.

294. Galván EM, Mateyca C, Ielpi L. 2016. Role of interspecies interactions in dual-species biofilms developed in vitro by uropathogens isolated from polymicrobial urinary catheter-associated bacteriuria. *Biofouling* **32:**1067–1077.

295. Hoeniger JFM. 1965. Development of Flagella by *Proteus mirabilis*. *J Gen Microbiol* **40:**29–42.

296. Williams FD, Anderson DM, Hoffman PS, Schwarzhoff RH, Leonard S. 1976. Evidence against the involvement of chemotaxis in swarming of *Proteus mirabilis*. *J Bacteriol* **127:**237–248.

297. Harshey RM, Partridge JD. 2015. Shelter in a Swarm. *J Mol Biol* **427:**3683–3694.

298. Belas R, Flaherty D. 1994. Sequence and genetic analysis of multiple flagellin-encoding genes from *Proteus mirabilis*. *Gene* **148:** 33–41.

299. Belas R. 1994. Expression of multiple flagellin-encoding genes of *Proteus mirabilis*. *J Bacteriol* **176:**7169–7181.

300. Manos J, Belas R. 2004. Transcription of *Proteus mirabilis flaAB*. *Microbiology* **150:**2857–2863.

301. Zunino P, Piccini C, Legnani-Fajardo C. 1994. Flagellate and non-flagellate *Proteus mirabilis* in the development of experimental urinary tract infection. *Microb Pathog* **16:**379–385.

302. Legnani-Fajardo C, Zunino P, Piccini C, Allen A, Maskell D. 1996. Defined mutants of *Proteus mirabilis* lacking flagella cause ascending urinary tract infection in mice. *Microb Pathog* **21:**395–405.

303. Sabbuba N, Hughes G, Stickler DJ. 2002. The migration of *Proteus mirabilis* and other urinary tract pathogens over Foley catheters. *BJU Int* **89:**55–60.

304. Allison C, Emödy L, Coleman N, Hughes C. 1994. The role of swarm cell differentiation and multicellular migration in the uropathogenicity of *Proteus mirabilis*. *J Infect Dis* **169:**1155–1158.

305. Jansen AM, Lockatell CV, Johnson DE, Mobley HLT. 2003. Visualization of *Proteus mirabilis* morphotypes in the urinary tract: the elongated swarmer cell is rarely observed in ascending urinary tract infection. *Infect Immun* **71:**3607–3613.

306. Cassat JE, Skaar EP. 2013. Iron in infection and immunity. *Cell Host Microbe* **13:**509–519.

307. Subashchandrabose S, Mobley HL. 2015. Back to the metal age: battle for metals at the host-pathogen interface during urinary tract infection. *Metallomics* **7:**935–942.

308. Pazin GJ, Braude AI. 1974. Immobilizing antibodies in urine. II. Prevention of ascending spread of *Proteus mirabilis*. *Invest Urol* **12:**129–133.

309. Shand GH, Anwar H, Kadurugamuwa J, Brown MR, Silverman SH, Melling J. 1985. In vivo evidence that bacteria in urinary tract infection grow under iron-restricted conditions. *Infect Immun* **48:**35–39.

310. Miles AA, Khimji PL. 1975. Enterobacterial chelators of iron: their occurrence, detection, and relation to pathogenicity. *J Med Microbiol* **8:**477–490.

311. Evanylo LP, Kadis S, Maudsley JR. 1984. Siderophore production by *Proteus mirabilis*. *Can J Microbiol* **30:**1046–1051.

312. Hart RC, Kadis S, Chapman WL Jr. 1982. Nutritional iron status and susceptibility to *Proteus mirabilis* pyelonephritis in the rat. *Can J Microbiol* **28:**713–717.

313. Gaisser S, Hughes C. 1997. A locus coding for putative non-ribosomal peptide/polyketide synthase functions is mutated in a swarming-defective Proteus mirabilis strain. *Mol Gen Genet* **253:**415–427.

314. Drechsel H, Thieken A, Reissbrodt R, Jung G, Winkelmann G. 1993. Alpha-keto acids are novel siderophores in the genera *Proteus, Providencia*, and *Morganella* and are produced by amino acid deaminases. *J Bacteriol* **175:**2727–2733.

315. Massad G, Zhao H, Mobley HL. 1995. *Proteus mirabilis* amino acid deaminase: cloning, nucleotide sequence, and characterization of *aad*. *J Bacteriol* **177:**5878–5883.

316. Piccini CD, Barbé FM, Legnani-Fajardo CL. 1998. Identification of iron-regulated outer membrane proteins in uropathogenic *Proteus mirabilis* and its relationship with heme uptake. *FEMS Microbiol Lett* **166:**243–248.

317. Lima A, Zunino P, D'Alessandro B, Piccini C. 2007. An iron-regulated outer-membrane protein of *Proteus mirabilis* is a haem receptor that plays an important role in urinary tract infection and in in vivo growth. *J Med Microbiol* **56:**1600–1607.

318. D'Alessandro B, Lery LM, von Krüger WM, Lima A, Piccini C, Zunino P, Oswald E. 2011. Proteomic analysis of *Proteus mirabilis* outer membrane proteins reveals differential expression in vivo vs. in vitro conditions. *FEMS Immunol Med Microbiol* **63:**174–182.

319. Nielubowicz GR, Smith SN, Mobley HLT. 2010. Zinc uptake contributes to motility and provides a competitive advantage to *Proteus mirabilis* during experimental urinary tract infection. *Infect Immun* **78:**2823–2833.

320. Bode W, Gomis-Rüth FX, Stöckler W. 1993. Astacins, serralysins, snake venom and matrix metalloproteinases exhibit identical zinc-binding environments (HEXXHXXGXXH and Met-turn) and topologies and should be grouped into a common family, the 'metzincins'. *FEBS Lett* **331:**134–140.

321. Wang S, Fleming RT, Westbrook EM, Matsumura P, McKay DB. 2006. Structure of the *Escherichia coli* FlhDC complex, a prokaryotic heteromeric regulator of transcription. *J Mol Biol* **355:**798–808.

322. Lai H-C, Gygi D, Fraser GM, Hughes C. 1998. A swarming-defective mutant of *Proteus mirabilis* lacking a putative cation-transporting membrane P-type ATPase. *Microbiology* **144:**1957–1961.

323. Nakashige TG, Zygiel EM, Drennan CL, Nolan EM. 2017. Nickel sequestration by the host-defense protein human calprotectin. *J Am Chem Soc* **139:**8828–8836.

324. Lamarche MG, Wanner BL, Crépin S, Harel J. 2008. The phosphate regulon and bacterial virulence: a regulatory network connecting phosphate homeostasis and pathogenesis. *FEMS Microbiol Rev* **32:**461–473.

325. Jacobsen SM, Lane MC, Harro JM, Shirtliff ME, Mobley HLT. 2008. The high-affinity phosphate transporter Pst is a virulence factor for *Proteus mirabilis* during complicated urinary tract infection. *FEMS Immunol Med Microbiol* **52:**180–193.

326. Liu L, Mo H, Wei S, Raftery D. 2012. Quantitative analysis of urea in human urine and serum by 1H nuclear magnetic resonance. *Analyst (Lond)* **137:**595–600.

327. Shaykhutdinov RA, MacInnis GD, Dowlatabadi R, Weljie AM, Vogel HJ. 2009. Quantitative analysis of metabolite concentrations in human urine samples using 13C{1H} NMR spectroscopy. *Metabolomics* **5:**307–317.

328. Bouatra S, Aziat F, Mandal R, Guo AC, Wilson MR, Knox C, Bjorndahl TC, Krishnamurthy R, Saleem F, Liu P, Dame ZT, Poelzer J, Huynh J, Yallou FS, Psychogios N, Dong E, Bogumil R, Roehring C, Wishart DS. 2013. The human urine metabolome. *PLoS One* **8:**e73076. doi:10.1371/journal.pone.0073076.

329. Simpson DP. 1983. Citrate excretion: a window on renal metabolism. *Am J Physiol* **244:**F223–F234.

330. Hess B. 2011. Urinary citrate and citrate metabolism, p 181–184. *In* Rao NP, Preminger GM, Kavanagh JP (ed), *Urinary Tract Stone Disease*. Springer London, London. doi:10.1007/978-1-84800-362-0_14.

331. Alteri CJ, Himpsl SD, Mobley HL. 2015. Preferential use of central metabolism in vivo reveals a nutritional basis for polymicrobial infection. *PLoS Pathog* **11:**e1004601. doi:10.1371/journal.ppat.1004601.

332. Huang Y, Nishikawa T, Satoh K, Iwata T, Fukushima T, Santa T, Homma H, Imai K. 1998. Urinary excretion of D-serine in human: comparison of different ages and species. *Biol Pharm Bull* **21:**156–162.

333. Roesch PL, Redford P, Batchelet S, Moritz RL, Pellett S, Haugen BJ, Blattner FR, Welch RA. 2003. Uropathogenic *Escherichia coli* use d-serine deaminase to modulate infection of the murine urinary tract. *Mol Microbiol* **49:**55–67.

334. Helling RB. 1994. Why does *Escherichia coli* have two primary pathways for synthesis of glutamate? *J Bacteriol* **176:**4664–4668.

335. Scavone P, Miyoshi A, Rial A, Chabalgoity A, Langella P, Azevedo V, Zunino P. 2007. Intranasal immunisation with recombinant Lactococcus lactis displaying either anchored or secreted forms of *Proteus mirabilis* MrpA fimbrial protein confers specific immune response and induces a significant reduction of kidney bacterial colonisation in mice. *Microbes Infect* **9:**821–828.

336. Scavone P, Rial A, Umpierrez A, Chabalgoity A, Zunino P. 2009. Effects of the administration of cholera toxin as a mucosal adjuvant on the immune and protective response induced by *Proteus mirabilis* MrpA fimbrial protein in the urinary tract. *Microbiol Immunol* **53:**233–240.

337. Scavone P, Umpiérrez A, Maskell DJ, Zunino P. 2011. Nasal immunization with attenuated *Salmonella Typhimurium* expressing an MrpA-TetC fusion protein significantly reduces *Proteus mirabilis* colonization in the mouse urinary tract. *J Med Microbiol* **60:**899–904.

338. Scavone P, Umpiérrez A, Rial A, Chabalgoity JA, Zunino P. 2014. Native flagellin does not protect mice against an experimental *Proteus mirabilis* ascending urinary tract infection and neutralizes the protective effect of MrpA fimbrial protein. *Antonie van Leeuwenhoek* **105:**1139–1148.

339. Habibi M, Asadi Karam MR, Bouzari S. 2016. Transurethral instillation with fusion protein MrpH.FimH induces protective innate immune responses against uropathogenic *Escherichia coli* and *Proteus mirabilis*. *APMIS* **124:**444–452.

340. Habibi M, Asadi Karam MR, Shokrgozar MA, Oloomi M, Jafari A, Bouzari S. 2015. Intranasal immunization with fusion protein MrpH·FimH and MPL adjuvant confers protection against urinary tract infections caused by uropathogenic *Escherichia coli* and *Proteus mirabilis*. *Mol Immunol* **64:**285–294.

341. Uehling DT, Hopkins WJ, Beierle LM, Kryger JV, Heisey DM. 2001. Vaginal mucosal immunization for recurrent urinary tract infection: extended phase II clinical trial. *J Infect Dis* **183**(Suppl 1)**:**S81–S83.

342. Hopkins WJ, Elkahwaji J, Beierle LM, Leverson GE, Uehling DT. 2007. Vaginal mucosal vaccine for recurrent urinary tract infections in women: results of a phase 2 clinical trial. *J Urol* **177:**1349–1353, quiz 1591.

343. Kochiashvili D, Khuskivadze A, Kochiashvili G, Koberidze G, Kvakhajelidze V. 2014. Role of the bacterial vaccine Solco-Urovac® in treatment and prevention of recurrent urinary tract infections of bacterial origin. *Georgian Med News* **Jun**(231)**:**11–16.

344. Mathur S, Suller MT, Stickler DJ, Feneley RC. 2006. Prospective study of individuals with long-term urinary catheters colonized with *Proteus* species. *BJU Int* **97:**121–128.

345. Chew R, Thomas S, Mantha ML, Killen JP, Cho Y, Baer RA. 2012. Large urate cystolith associated with *Proteus* urinary tract infection. *Kidney Int* **81:**802. doi:10.1038/ki.2011.506.

346. Carver TJ, Rutherford KM, Berriman M, Rajandream MA, Barrell BG, Parkhill J. 2005. ACT: the Artemis Comparison Tool. *Bioinformatics* **21:**3422–3423.

347. Stickler DJ. 2008. Bacterial biofilms in patients with indwelling urinary catheters. *Nat Clin Pract Urol* **5:**598–608.

348. Armbruster CE, Hodges SA, Mobley HL. 2013. Initiation of swarming motility by *Proteus mirabilis* occurs in response to specific cues present in urine and requires excess L-glutamine. *J Bacteriol* **195:**1305–1319.

349. Torzewska A, Budzyńska A, Białczak-Kokot M, Różalski A. 2014. In vitro studies of epithelium-associated crystallization caused by uropathogens during urinary calculi development. *Microb Pathog* **71-72:**25–31.

350. Kurihara S, Sakai Y, Suzuki H, Muth A, Phanstiel O IV, Rather PN. 2013. Putrescine importer PlaP contributes to swarming motility and urothelial cell invasion in *Proteus mirabilis*. *J Biol Chem* **288:**15668–15676.

351. Wang WB, Lai HC, Hsueh PR, Chiou RY, Lin SB, Liaw SJ. 2006. Inhibition of swarming and virulence factor expression in *Proteus mirabilis* by resveratrol. *J Med Microbiol* **55:**1313–1321.

352. Schneider R, Lockatell CV, Johnson D, Belas R. 2002. Detection and mutation of a *luxS*-encoded autoinducer in *Proteus mirabilis*. *Microbiology* **148:**773–782.

353. Armbruster CE, Hodges SA, Smith SN, Alteri CJ, Mobley HL. 2014. Arginine promotes *Proteus mirabilis* motility and fitness by contributing to conservation of the proton gradient and proton motive force. *MicrobiologyOpen* **3:**630–641.

354. Liu MC, Kuo KT, Chien HF, Tsai YL, Liaw SJ. 2015. New aspects of RpoE in uropathogenic *Proteus mirabilis*. *Infect Immun* **83:**966–977.

355. Li X, Mobley HL. 1998. MrpB functions as the terminator for assembly of *Proteus mirabilis* mannose-resistant *Proteus*-like fimbriae. *Infect Immun* **66:**1759–1763.

356. Stickler D, Morris N, Moreno MC, Sabbuba N. 1998. Studies on the formation of crystalline bacterial biofilms on urethral catheters. *Eur J Clin Microbiol Infect Dis* **17:**649–652.

357. Liaw S-J, Lai H-C, Ho S-W, Luh K-T, Wang W-B. 2003. Role of RsmA in the regulation of swarming motility and virulence factor expression in *Proteus mirabilis*. *J Med Microbiol* **52:**19–28.

358. Allison C, Lai HC, Gygi D, Hughes C. 1993. Cell differentiation of Proteus mirabilis is initiated by glutamine, a specific chemoattractant for swarming cells. *Mol Microbiol* **8:**53–60.